NTNU

Norwegian University of
Science and Technology

Cristobalite formation on quartz crucibles inner surface for CZ solar cell ingot production

Helene Elisabeth J Hendrickx

Materials Technology
Submission date: June 2017
Supervisor: Marisa Di Sabatino, IMA

Norwegian University of Science and Technology
Department of Materials Science and Engineering

Abstract

Cristobalite, the stable high temperature polymorph of quartz, is formed on the surface of fused quartz crucibles used for the growth of monocrystalline silicon ingots by the Czochralski process. When not controlled and occurring locally, cristobalite can flocculate and enter the melt introducing possible defects and structure losses at the solidification front. This is detrimental to the quality of the silicon ingot. One way to suppress the release of cristobalite particles in the silicon melt is to promote the formation of a homogeneously distributed cristobalite layer on the crucible surface. This protective shell is obtained by coating or doping the crucible surface with a devitrification agent.

This work aims to understand the growth of cristobalite and the factors influencing it. Three different crucible types (A, B and Std) have been investigated. They differ by their quartz sand properties. Crucible pieces before their use in the CZ process and after their use, respectively coated by the crucible manufacturer or non coated have been studied.

Some new non coated crucible pieces have been covered with a barium based devitrification agent by different techniques. Heat treatments in a vertical gradient freeze (VGF) furnace and a CZ puller have been performed on new crucible rods (non coated, coated by the industry and coated at NTNU) as an attempt to reproduce industrial conditions and study the influences of the heat treatment type, the holding time at high temperature, the crucible sand quality and the presence and type of the coating. Samples of the resulting crucible pieces have been analysed by optical microscopy, scanning electron microscopy and X-ray diffraction in order to obtain informations about the cristobalite occurrence (e.g. layer thickness, crystal composition and orientation, morphology). A comparison with the results from the used crucible pieces has been made.

The results suggest that the cristobalite formation is influenced by many factors such as the coating pattern, homogeneity and thickness, the holding time at high temperature and the interactions at the melt/crucible surface interface. The spray coating technique is more suitable to obtain a homogeneous coating on the crucible surface even if the coating is easily removed by the handling procedures. Cristobalite nucleates faster on coated crucibles pieces and the layer formed is thicker and more homogeneous. The coating also seems to influence the orientation of the cristobalite growth. The longer the holding time at high temperature, the thicker and more homogeneously spread the cristobalite layer is, independently of the coating presence. In addition, the cristobalite layer nucleated tends to end up with the orientation {200} when enough time at high temperature is given. The contact with the melt during the heat treatment induces a dissolution of the quartz material and once formed, of the cristobalite layer as well. The cristobalite nucleation direction is also influenced by the contact with the melt. Std crucible shows non conclusive results while B crucible has the most coherent ones and seems to be the most suitable choice of crucible materials for the CZ process.

Acknowledgements

This Master's Thesis is the evaluation basis for the course TMT4900 at the Norwegian University of Science and Technology (NTNU) and has been performed at the Department of Materials Science and Engineering. The work is a part of a project supervised by NTNU, The QUARTZ Corp and SINTEF.

I would like to thank the many people that helped me during the past 5 months. First of all, my main supervisor Marisa Di Sabatino Lundberg and my co-supervisors Astrid Marie Flattum Muggerud (The QUARTZ Corp) and Mari Juel (SINTEF) for their availability and guidance and the many precious advices provided during the whole working process. I am also very grateful for the help given by the different engineers and members of the technical staff at the Department, especially Mrs. Birgite Karlsen (SINTEF), for showing me the basis of sample preparation and Mr. Jonas Einan Gjovik for his help with the different heat treatments and his patience with all the problems encountered. I would also like to thank Magnus Rothan that trained me for the use of the XRD and explained to me how to analyse the spectra obtained, Yingda Wu that helped me with all the features of the SEM and John Atle Bones (SINTEF) that performed the temperature simulations and helped, along with Pal Tetlie (SINTEF) and Eivind Johannes Ovrelid (SINTEF), with the CZ furnace experiment. I am also very grateful to Mr. Ove Paulsen (SINTEF) for sharing his previous experience with cristobalite study and barium coating and Mrs. Sidsel Meli Hanetho and Mr. Paul Inge Dahl for teaching me the different coating techniques. In addition, I would like to thank my student co-worker Sebastian Holand Hansen for his substantial help with the many tasks we had to perform. It was a pleasure working with such a productive and dedicated person. Finally, I would like to thank my family for their support even with the 2000km standing between us and Brice for his invaluable presence, especially in the most stressful moments.

Nivelles, 22nd of June 2017
Helene Elisabeth J. Hendrickx

Contents

List of Abbreviations

ρ Density of quartz

CZ Czochralski

e-Si Electronical Grade Silicon

EDS Energy-Dispersive Spectroscopy

EELS Electron Energy Loss Spectroscopy

FBR Fluidised Bed Reactor

HPQ High Purity Quartz

HT1 Heat Treatment in the VGF furnace

HT2 Heat Treatment in the CZ puller

HT3 Industrial Heat Treatment of the used crucibles

Liquinert Liquid in an inert state

LM Light Microscope/Microscopy

m_{diss} Dissolved mass of crucible

MCZ Magnetic-field applied Czochralski

MG-Si Metallurgical Grade Silicon

ppm Parts per million

ppma Parts per million

PV Photovoltaic

S_{in} Inner surface of a crucible

SEM Scanning Electron Microscope/Microscopy

SoG-Si Solar Grade Silicon

$thickness_{avg}$ Average thickness of crucible dissolved

V_{diss} Dissolved volume of a crucible

VGF Vertical Gradient Freeze

X_{nc} New coated crucible piece

X_n New non coated crucible piece

X_{uc} Used coated crucible piece

X_u Used non coated crucible piece

XRD X-ray diffraction

1 Introduction

1.1 Motivation

The gap between energy production and demand in the world keeps growing. One of the current biggest challenge is to fill this gap with clean, widely available and cost-efficient energies. At the end of 2015, roughly 85% of the energy consumed by the population was still based on oil, natural gas and coal. [1] Those energy resources start depleting and bring many concerns in terms of environmental impacts.

One attractive, high potential but challenging alternative to those fossil fuels is solar power. Exploiting solar energy requires overcoming many difficulties from capturing the sun's energy, converting it into a usable form and storing it to mitigate the intermittence. Many of those concerns are investigated in industries and at universities. Particularly, the technology device that converts the sunlight into electricity, called solar photovoltaic cell, requires a certain level of expertise, extremely high quality materials and meticulous control over the many steps of the production process. [2]

Currently, solar cells are mainly based on silicon, one of the most abundant materials in the Earth crust. In fact, silicon solar cells represent about 90% of the current solar cell market and are based on either mono or multicrystalline silicon ingots. [3] The highest cell efficiency is obtained with monocrystalline silicon wafers whose ingots are grown by a process called the Czochralski process consisting basically in stacking the silicon feedstock in a quartz crucible, melting it at high temperature then solidifying it slowly by pulling an oriented seed out of the melt. [4]

In the solar cell industry, all the production steps can introduce impurities and defects in the silicon material which reduce its efficiency as a cell and bring extra costs for the final module. To make solar cells economically competitive, it is crucial to avoid the spreading of defects and impurities at the beginning of the value chain. [5] Therefore, there is a need for a high purity crucible material with high thermal and mechanical resistances and a relatively low price. The most suitable material that currently meets those requirements is amorphous quartz (SiO_2). [6]

Quartz is the stable ambient polymorph of silica. The high temperatures (typically as high as 1550°C) experienced during the ingot growth induce successive phase transitions and deformations of the silica structure until the cubic β-cristobalite, the stable high-temperature polymorph of silica, forms on the inner and outer surfaces of the crucible. [7] It is known that the localised occurrence of cristobalite on the inner surface of the crucible can be a precursor of structure losses in the Si crystal. This has an important effect on the productivity and yield of the Czochralski process. [8]

It has been proven that the addition of a devitrification agent in the form of coating or doping on the inner and outer surface of the crucible promotes the formation of a homogeneous layer of cristobalite on both surfaces. The inner layer mainly acts as a shell, preventing the cristobalite particles from floculating into the melt while the outer layer enhances the stiffness and allows a better structural resistance of the crucible. [9]

1.2 Aim of this work

This work focuses on the properties of the cristobalite layer formed on the inner surface of crucibles made of different sand qualities after their exposure to high temperature and tries to understand the transitions experienced by the crucible pieces during those heat treatments. The work is performed in parallel to a study about the bubble content evolution in the same crucible materials subjected to the same heat treatments.

First of all, new crucible pieces, coated and non coated by the crucible producer have been observed and two different coating routines have been established and used on some of the non coated new pieces. The pieces have then been subjected to several heat treatments in a Vertical Gradient Freeze (VGF) furnace and a Czochralski (CZ) puller in order to reproduce the industrial conditions and observe the resulting cristobalite presence. This cristobalite occurrence has been characterised in terms of the crucible sand quality, the coating applied and the heat treatment duration and type, and compared to the occurrence observed on crucible pieces that have been used in the CZ process also provided by the industry. The analyses have been conducted by light microscopy, scanning electron microscopy and X-ray diffraction spectroscopy.

The goal of this thesis is to highlight the following characteristics of the cristobalite:

- Average thickness of the layer;
- Morphology of the layer;
- Crystalline composition;
- Crystal orientations.

The work will be organised as follows: a theoretical background about the solar cell production, the crucible characteristics, the cristobalite formation and the characterisation methods used in this thesis will first be presented. Then, the experimental procedure will be explained and the results will be shown and discussed. Finally, a conclusion will be drawn and possible further works will be proposed.

2 Theory

2.1 Silicon feedstock and casting

The solar value chain, presented in Figure 1 below, shows the successive steps from the raw polysilicon material feedstock to the final solar modules. From the value chain, five processes can be highlighted:

- The extraction and refining of the raw material giving the silicon feedstock;
- The crystallisation process, stacking the silicon feedstock in a quartz crucible and casting mono or multicrystalline ingots;
- The wafering process to form the silicon wafers;
- The processing of the wafers to obtain the so-called solar cells;
- The assembling of the cells to obtain the PV modules arranged together into PV arrays.

The final efficiency of a solar cell depends on the control of the quality of each step of the value chain. In this subchapter, only the feedstock characteristics and the casting process will be presented due to their direct relationship with the crucible properties studied in this work. The crucible features and the cristobalite occurrence will be detailed just after.

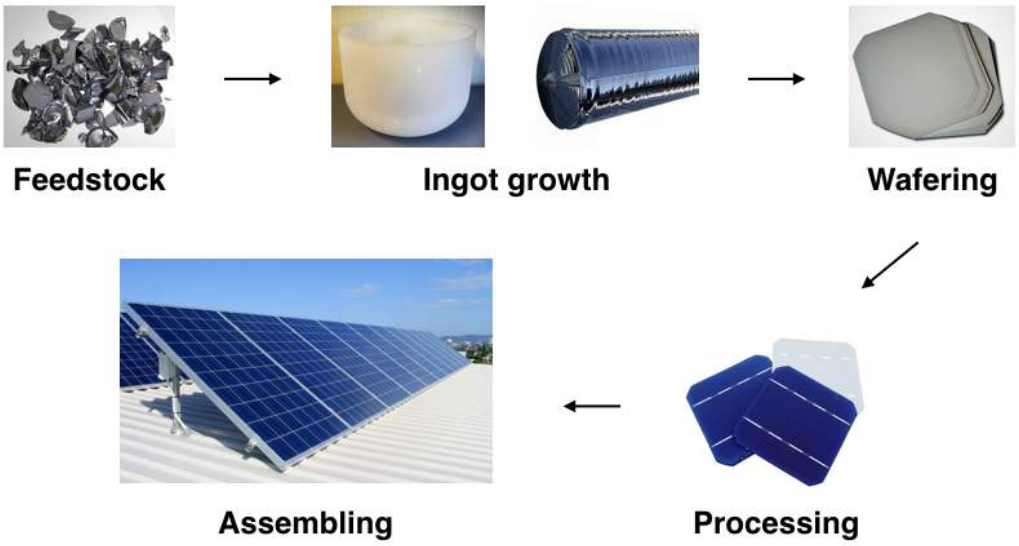

Figure 1: Solar value chain

2.1.1 Polysilicon feedstock material

In its natural state on Earth, silicon is found in sand or rocks as silicon dioxide SiO_2 (quartz). The process that removes the oxygen to isolate the Si used for industrial applications is called the carbothermal reduction process and is represented in Figure 2.

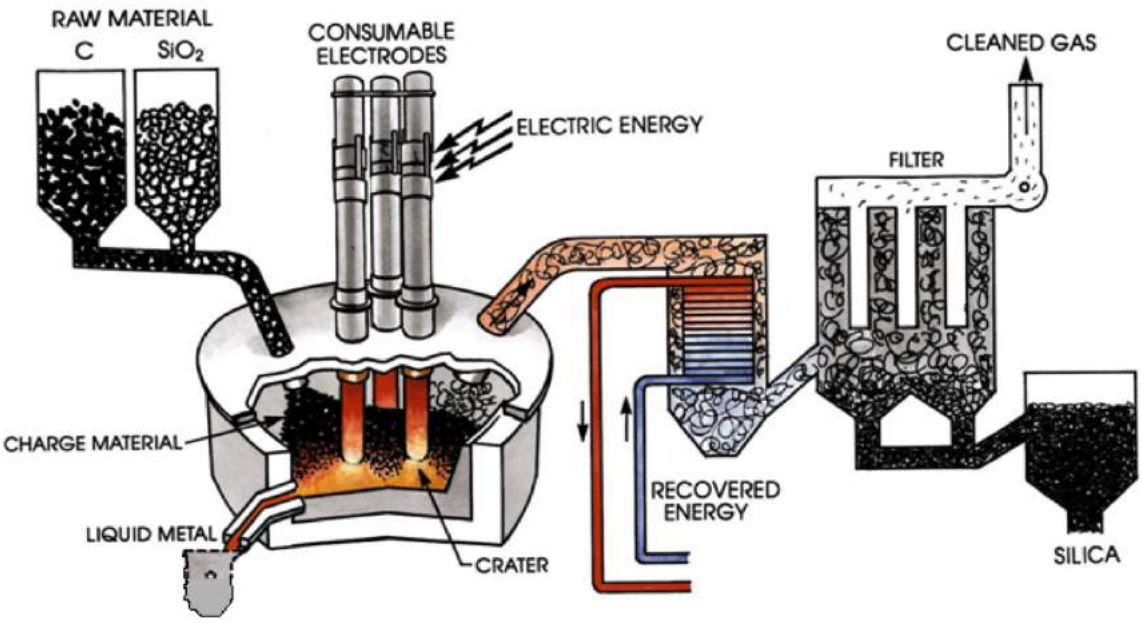

Figure 2: Carbothermal reduction process where raw silicon dioxide and carbon source materials react in an arc furnace with the produced silicon collected at the bottom [10]

The quartz reacts in the furnace with carbon, typically from coal, coke or wood-chips, through a carbothermal reduction reaction represented by the following equation:

$$SiO_2 + 2C \longrightarrow Si + 2CO \tag{1}$$

The furnace is heated up to about 2000°C by submerged electric arcs produced by consumable carbon electrodes. Tapped liquid Si is obtained from the tap-hole at the bottom of the furnace while carbon monoxide and microsilica are collected in the fumes. Those two compounds can be respectively used for energy recovery and material recovery. [10]

From this process, a so-called Metallurgical Grade Silicon (MG-Si) is obtained and characterised by a purity of about 98-99%.

The silicon quality required by the solar cell industry is called Solar Grade Silicon (SoG-Si) and is defined by a purity of 99.9999% or "6N" quality with impurities concentrations typically lower than 5 ppm. In order to obtain SoG-Si, MG-Si must be refined.

There are two main methods to produce SoG-Si: the "chemical route" and the "metallurgical route".

Chemical route

The chemical route consists in either the Siemens process or an improvement of it where a fluidised bed reactor (FBR) is used. Those two processes are illustrated on Figure 3.

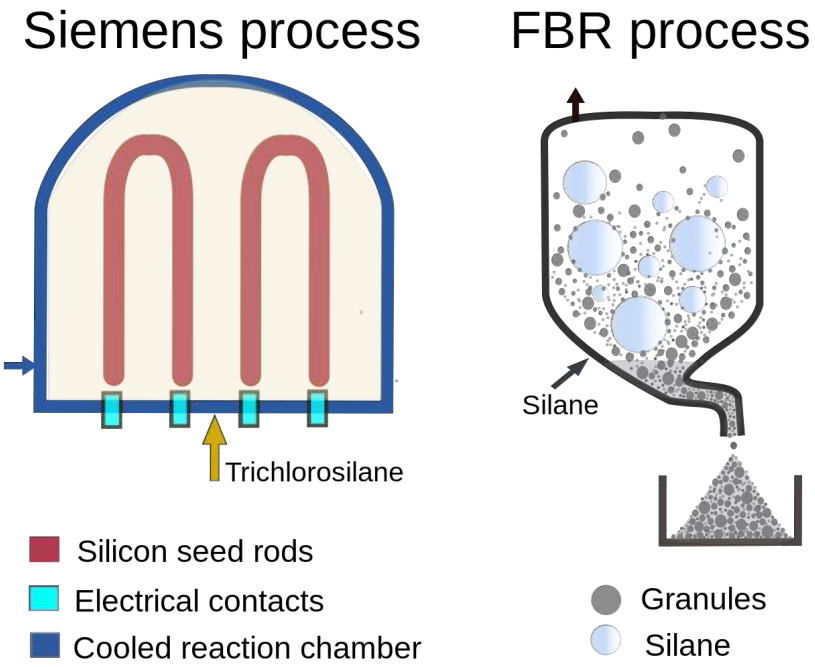

Figure 3: Siemens and FBR processes used in the chemical route [11]

Both are based on the same successive steps. First, MG-Si, used as feedstock, is either chlorinated to form chlorosilanes (liquid compound, e.g. $SiHCl_3$) or volatilised into silane gas (SiH_4). $SiHCl_3$ is purified by multiple distillations leading to a vapour compound that is deposited in solid form by chemical vapour deposition (CVD) while SiH_4 can be directly deposited. The deposition reactions are the following:

$$SiHCl_3 + H_2 \longrightarrow Si(s) + 3HCl \tag{2}$$

$$SiH_4 \longrightarrow Si + 2H_2 \tag{3}$$

In the Siemens process, the decomposition of the chlorosilanes occurs on an U-shaped hot silicon filament resulting in the production of polysilicon rods that are broken into

Si chunks. On the other hand, in the FBR, the decomposition surface is increased by using Si grains that will grow with the decomposition of silane then fall to the bottom of the reactor to be collected in the form of granules. The FBR process has been proven to be a more efficient process in terms of energy consumption and capital costs. However, the Siemens process still remains the most common production process for high purity polysilicon. [10]

In both those processes, the output is a so-called electronic grade silicon (e-Si) also called the "9N" purity, a 99.999999% pure silicon commonly used in specific electronic applications. Typical Si chunks obtained from the Siemens process and Si granules obtained via the FBR process are shown in Figure 4.

Figure 4: Pictures of Si chunks from the Siemens process (left) and Si granules from the FBR process (right), both from NTNU ressources

Some major problems with the chemical route are the production of chlorosilanes (toxic, corrosive compounds), the safety issues related with their handling and the relatively high energy consumption leading to high production costs associated with the process. This explains why there has been a keen interest in the recent years in developing the alternative metallurgical route.

Metallurgical route

In the metallurgical route, SoG-Si is produced through the use of a combination of metallurgical techniques to refine MG-Si. One key process step is directional solidification due to its ability to remove a wide range of impurities. Many additional refining techniques exist such as slag refining, vacuum refining, plasma refining, solvent refining and leaching. Different combinations of some of them are used prior to directional solidification to remove specific impurities difficult or impossible to remove efficiently with directional solidification (e.g. Boron and phosphorous). In Norway, the common metallurgical route is the Elkem Solar process where MG-Si is refined through slag treatment followed by acid leaching and directional solidification. [12] Those techniques will not be detailed here.

Table 1 shows the typical acceptable levels of impurities for MG-Si, SoG-Si and e-Si. The values are given in parts per million atoms with 1 ppma being a fraction of 1 in 10^6 atoms.

Table 1: Acceptable ranges for the significant impurities in silicon grades [13]

Impurity	**MG-Si [ppma]**	**SoG-Si (p-type) [ppma]**	**e-Si [ppma]**
Al	1200-4000	0.08-0.5	0.0008
B	10-50	0.1-3	0.0002
C	700	60	0.5
Ca	590	0.1	0.003
Cr	50-140	0.006-0.05	0.003
Cu	24-90	0.3	0.003
Fe	1600-3000	0.02-0.3	0.010
Mn	70-80	0.015-0.05	0.003
Mo	<10	1.5×10^{-5}	0.003
Ni	40-80	0.1-0.2	0.010
P	15-50	0.1-1.0	0.0008
Ti	140-200	0.1	0.003
V	100-200	5×10^{-5}	0.003

2.1.2 Single crystal growth by the CZ process

Production of single crystalline silicon is one key technology in photovoltaics due to the fact that it provides grown materials with higher quality and efficiency than those based on multicrystalline silicon even if higher costs and a lower throughput are the main drawbacks associated. [6]

This thesis investigates crucibles used in the production of monocrystalline silicon by the Czochralski (CZ) process thus the focus will be on this production process, while the details about the float zone (FZ) process, an alternative monocrystalline silicon production process, and multicrystalline silicon production processes are found in literature. [14], [15]

The Czochralski growth process, named after the Polish scientist Jan Czochralski who established the basis of it, is the most widely used process in the monocrystalline solar cell industry. The basic successive steps of the CZ process are represented in Figure 5.

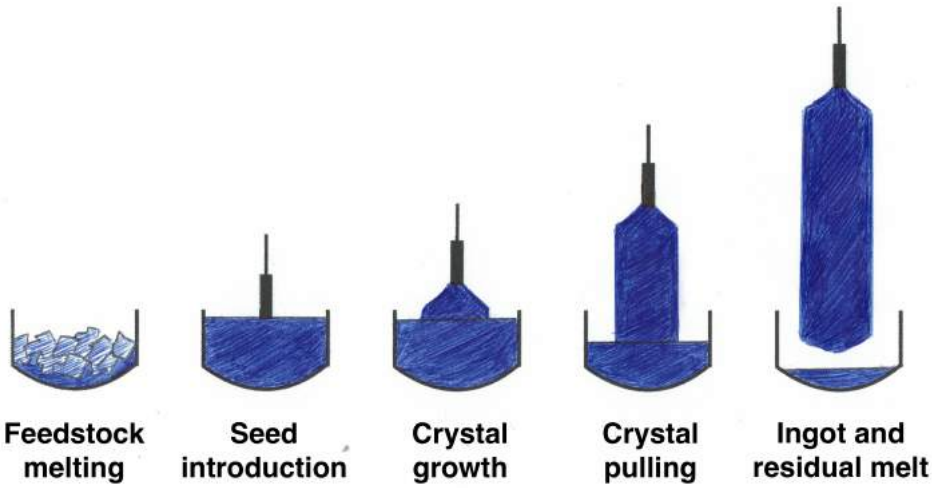

Figure 5: Czochralski (CZ) process steps [16]

First of all, the purified silicon feedstock is stacked in a quartz crucible that is placed into a graphite susceptor in a furnace where the silicon is melted at temperatures higher than its melting point (1414°C), typically 1500°C. The heat is provided by an inductive hot-zone created by a graphite electrode surrounding the crucible. The heating process is conducted in an inert atmosphere with the crucible rotating to ensure homogeneous mixing and heating and to evacuate small gas bubbles trapped in the melt. [17], [18]

Once the melt is stable, an oriented mono-crystal seed (common orientations {111} or {100}) mounted on a rod is dipped into the melt then slowly pulled out with a reverse rotation to that of the crucible. The contact between the seed and the melt creates a thermal shock generating dislocations in the growing crystal. The first pulling steps are fast and the resulting ingot diameter is of only a few mm so that the dislocations are concentrated in this thin part. This procedure is called "Dash-necking": the generated dislocations have glide planes that are oriented in the pulling direction so that they will simply move out of the crystal and disappear after few centimetres of the neck part has been grown. This part will be removed from the ingot afterwards. [19]

Once the neck has been generated, the pulling speed is reduced (usually until a range of 2 to 5 mm/min) and the diameter of the ingot increases to form the crown part. The body of the ingot is obtained once the desired diameter (up to 300 mm) is reached and kept constant through the rest of the growth while controlling the temperature, the pulling rate and the impacts of the reduction of the melt level. [20]

When the desired length or weight (respectively 1-2 m or 50-100 kg) of the ingot has been reached, the last step consists in forming a tail by increasing the pulling rate and controlling the temperature to decrease the rod diameter and minimise again the thermal shock created when the ingot pops out of the melt. This concentrates the slip dislocations out of the body. When the ingot is freed from the melt, it is cooled down in a receiving chamber. [4], [21], [22]

The typical furnace assembly for CZ monocrystalline silicon production is shown in Figure 6.

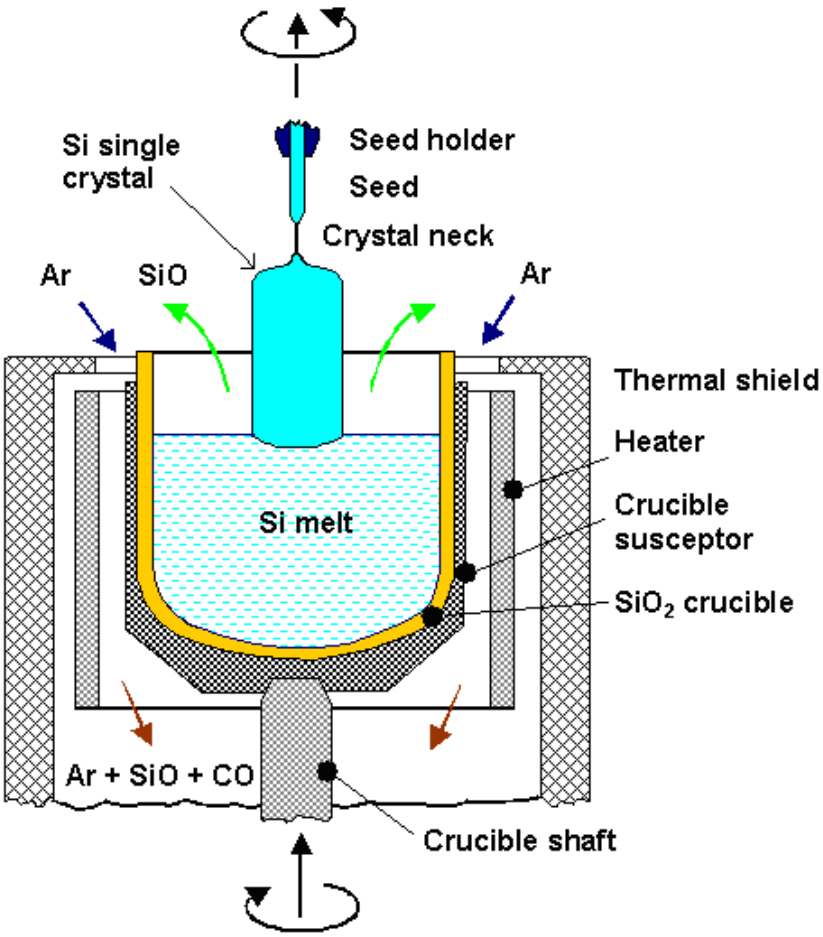

Figure 6: Czochralski (CZ) Furnace [23]

2.2 Quartz crucibles production and interactions during silicon ingot growth

In the CZ process, the first step consists in melting the feedstock in a quartz crucible. Amorphous silicon dioxide (SiO_2), or quartz, is a suitable choice of material because it resists the high melting temperature of silicon (1414°C), has a low expansion coefficient and stays relatively inert in contact with the highly reactive molten silicon without introducing detrimental amounts of impurities in the melt.

2.2.1 Crucible production

2.2.1.1 Quartz feedstock

The raw material used to produce the crucibles for the solar cell industry is high purity quartz (HPQ) sand. This sand has a reduced impurity level of about 30 ppm, thus the purity of SiO_2 is about 99.997%. The nature of the impurities in the remaining 0.003% plays a critical role in the end-use of the HPQ, especially if there is a high content in alkalis and transition metals. [24] Even small traces of impurities in the final crucible can have an important impacts if they enter the melt. In fact, during a CZ process, about 1-2 mm of the crucible inner surface dissolve when in contact with the molten silicon. Considering a crucible with approximate dimensions 53 cm in inner diameter (26.5 cm in radius) and 25 cm of height in contact with the melt during the CZ process, the inner surface of a truncated cylinder (approximate shape of a crucible) is about;

$$S_{in} = \pi r^2 + 2\pi rh \approx 6369\ cm^2 \tag{4}$$

So that the volume dissolved accounts for;

$$V_{diss} = S_{in} * thickness_{avg} = 6369 * 0.15 \approx 955\ cm^3 \tag{5}$$

With quartz having an approximate density of 2.203 g/cm^3 [25], the mass of crucible dissolved is;

$$m_{diss} = V_{diss} * \rho = 955 * 2.203 \approx 2103g \approx 2.1\ kg \tag{6}$$

Since approximately 2.1 kg of quartz from the crucible dissolve into the melt, it is important to controlling its quality.

High purity quartz sand has only been found in few locations around the world. It needs to be processed in order to be used for crucible production. A typical multiple step refining procedure can be summarised as [26]:

- Mechanical pre-processing
- Physical processing
- Chemical leaching
- Thermal treatment

Mechanical pre-processing

The pre-processing steps depend on the quartz deposit characteristics. Most of the time, large cubes of sand material are extracted from the source by blasting or similar methods. Then, several mechanical treatments such as jaw crushing and grinding are applied. In order to furthermore separate the quartz (constituting approximately 20% of the sand source) from the other components, sorting (optical, size separation, etc.) is conducted.

Physical processing

Once the material contains mainly quartz, it is processed continuously until reaching a desired quality. Firstly, physical processing is performed to liberate and eliminate the impurities from the quartz surface by, for example, attrition, magnetic separation, high tension separation and flotation. Flotation is a key process to separate spar, myca and iron from the quartz material.

Chemical treatment

Subsequently, chemical treatments including acid washing and leaching are applied to liberate the impurities contained even further within the quartz grains (e.g. in micro fissures or dislocations). Hot chlorination is also sometimes performed to reduce the level of alkali metal impurities.

Thermal treatment

Finally, once a certain quality of quartz has been reached (after several rounds of physical and chemical treatments typically), a thermal treatment is applied to the material. It is a drying step followed by a calcination step that improves the melting behaviour of quartz by removing fluid inclusions.

At the end of those steps, the quartz has reached the required purity to be processed into a crucible for solar applications. A typical HPQ sand content is shown in Table 2. If the HPQ content is compared to the impurity contents accepted in SoG-Si (Table 1), it can be seen that introduction of Fe, Ca, Cr, Mn, Ti from the crucible in the melt might impact the Si quality but it seems obvious that Al constitutes the biggest treat.

Table 2: Typical and maximum values for elements content in High Purity Quartz sand [27]

Chemical Content	Typical value [ppm]	Maximum [ppm]
Al	13	18.0
B	≤ 0.1	0.1
Ca	0.5	1.0
Co	≤ 0.01	0.01
Cr	≤ 0.01	0.03
Cu	≤ 0.01	0.03
Fe	0.2	0.6
K	0.5	0.9
Li	0.4	1.0
Mg	≤ 0.1	0.1
Mn	≤ 0.1	0.2
Na	0.8	1.2
Ni	≤ 0.01	0.03
Ti	1.2	1.5

2.2.1.2 Crucible manufacturing

There are two main crucible production processes: slip cast crucibles and fused crucibles.

Slip cast crucibles

The slip cast crucible production method uses a lower grade quartz than HPQ. It has been observed that crucibles with lower density and higher impurity content are obtained. Therefore, they are mainly used for the production of multicrystalline silicon and will not be detailed more in this work. [28], [29]

Fused crucibles

Fused crucibles are used in the CZ process. The manufacturers tend to keep their process confidential so that the specific route used to produce the crucibles investigated in this thesis is unknown but several patents can be found to get an idea of the different steps followed to obtain such fused crucibles.

The general procedure consists in pouring the HPQ sand continuously or discontinuously into a hollow mould rotating around its vertical axis. The centrifugal forces keep the material against the mould walls ensuring the growth of a layer of homogeneous thickness. An electric arc is used to generate heat from inside the mould to the outer wall so that the sand particles sinter then gradually fuse into an amorphous glass. The process continues until the desired thickness is achieved while a vacuum treatment is applied through holes or pores in the mould to suck out gases that create bubbles in the crucible wall. It is suggested in different patents to use two successive layers of quartz material, a fine one and a coarse one, in order to reduce even more the presence of bubbles close to the inner surface of the crucible. [30], [31] In fact, most of the process energy is used to build the continuous, homogeneous and bubble free inner surface while the bubbles are packed in the outer surface to ensure good thermal properties and stiffness of the resulting crucible. The final step is the removal of the crucible from the mould with the help of compressed air flows through the holes. [32]

Moulds used in this process are typically made of graphite due to its low price, good conduction properties, easy shaping and relative inertia. [33] During the crucible manufacturing, it is important to avoid interactions between the mould and the silica material in order to minimise the introduction of impurities. In addition, graphite constitutes a good choice due to its resistance to deformation, reducing then the risks of stresses and cracks in the manufactured crucible that could weaken its structure. While carbon contamination might still be introduced into the crucible (carbon presenting risks if it enters the melt afterwards during the CZ process), it is considered momentarily as the best option for mould material. The general set-up used to produce fused quartz crucibles can be seen in Figure 7, where an example of a quartz crucible produced by a Chinese supplier is also shown.

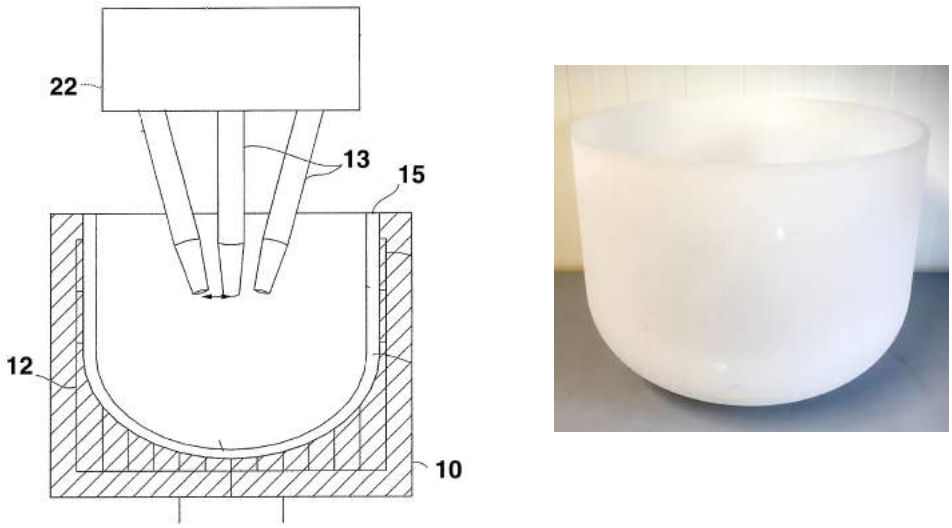

Figure 7: Left: Fused quartz crucible production process: Set-up with (22) the heater and (13) the graphite rods associated, (15) the growing crucible, (10) and (12) the outer and inner surfaces of the mold respectively [32]; Right: Industrial crucible

2.2.2 Interactions crucible-melt during crystal growth

2.2.2.1 Influence of impurities

When growing monocrystalline silicon ingots, the crucible is in direct contact with the Si melt and constitutes a major source of impurities.

There are several impurities that can affect the solar cell efficiency. They can be classified as follows:

- Dopant (e.g. B, P, Al, Sb, As): Active and most of the time wanted impurities that affect mainly the resistivity in the final material.
- Atmospheric (e.g. O, C, H, N): Impurities that may form complexes (e.g. CO, BO) and are difficult to eliminate.
- Metallic (e.g. Fe, Cu, Ni, Ti, Cr): Impurities that, even in small concentrations, can have a detrimental effect on the cell efficiency.

Most of the metallic impurities are eliminated from the silicon feedstock by the different refining processes along with the different dopants to avoid compensation that occurs in the presence of both acceptor and donor species, like B and P. In the crucible, there are some inherent impurities present even when using high purity quartz. Mainly metals remain in the quartz material but they are found in low quantities, typically a few ppm or less (see Table 2). They do not tend to be considered as a threat for the cell efficiency due to their small segregation coefficient that prevents the growth of metals in the solidified silicon. [10], [34] Transition metals, on the other hand, can be quickly transported in the vapour phase to the solidification interface and diffuse in the bulk crystal. Some sources of transition metals are, e.g., the crucible shaft, the seed cable, and the furnace walls.

However, the most likely impurity to diffuse in the melt from the crucible is oxygen, coming directly from the SiO_2 material. Typically, oxygen is present in a range of 10^{18} atoms/cm^3 (i.e. 20 ppma) in the crystal produced, a value higher than its solubility in Si. Oxygen is incorporated in the melt in the form of SiO gas, following the reaction:

$$Si(l) + SiO_2(s) \rightleftharpoons 2SiO(g) \tag{7}$$

The SiO gas will most likely evaporate from the melt surface and can be removed up to 99% through low pressure argon flushing. The remaining oxygen is found in dissolved state, it is mainly present as interstitial oxygen allowing the formation of oxide precipitates. Oxygen impurities provide gettering sites for metallic impurities, improving the minority carrier lifetime and thus the device efficiency but they can also create centres for carriers recombination and constitute extrinsic defects that enhance stresses, decrease mechanical properties and reduce lifetime by introducing dislocations at the solidification front. [34]

Due to the use of graphite supports in the furnace, carbon is another impurity often encountered in the CZ process that can affect significantly the properties of the silicon material. Carbon reacts with the quartz crucible and the silicon monoxide evaporating from the melt through the following reactions:

$$C(s) + SiO_2(s) \rightleftharpoons SiO(g) + CO(g) \tag{8}$$

$$2C(s) + SiO(g) \rightleftharpoons SiC(s) + CO(g) \tag{9}$$

It leads to silicon carbides and carbon monoxide which can both diffuse at the melt-crystal interface and end up in the solidified crystal, directly affecting its lifetime. [34]

In order to control the gas formations and the diffusion of the main impurities, some solutions are:

- The MCZ "Magnetic-field applied Czochralski" method where a horizontal or vertical magnetic field is applied to control the silicon flow and reduce the mixing between the edge of the melt in contact with the crucible and the centre that has highest purity and that will constitute the final ingot.
- The use of liquinert (i.e. "liquid in an inert state") crucibles where the silicon melt does not wet the crucible wall, avoiding direct contact. [35]

Those methods are not common, under developments, still too expensive for large scale applications and will not be detailed in this thesis.

2.2.2.2 Crucible structure and inner surface characteristics

From the observation of a crucible section like the one shown on Figure 8, the crucible can be divided into two layers: the inner surface, in contact with the melt during the CZ process, is the transparent layer commonly called the "bubble free layer" while the opaque outer layer is called the "bubble containing layer". When fusing the quartz particles during the manufacturing process of the crucible presented before, bubbles are produced and trapped by the viscous fused SiO_2 before cooling. The bubble free layer is obtained after a high temperature and high vacuum treatment. The presence of both those layers represents a good compromise for the crucible properties.

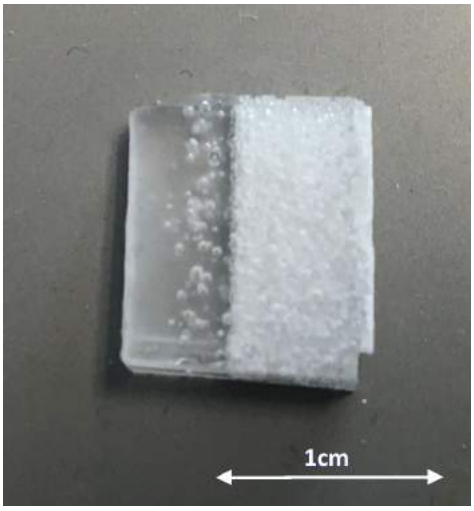

Figure 8: Cross section of a crucible piece : bubble free (BF) layer (left) and bubble containing (BC) layer (right)

First of all, it is important for the layer in contact with the melt to have a very low bubble content. In fact, due to the high temperature at the interface, the quartz can experience a lowering in viscosity that can cause creeping and it is known that this phenomenon is enhanced by the presence of bubbles. In addition, as already mentioned before, due to the induced movements of the highly reactive silicon melt during the ingot growth, a part of the inner layer of the crucible, typically about 0.5-2 mm, dissolves in the melt so that if bubbles are present in this layer, they may enter the melt or explode at the interface and allow for gases and impurities to diffuse into the melt causing, for example, dislocations or cavities in the growing crystal and leading to inherent structural losses. [36]

However, the external bubble containing layer also has its advantages: as mentioned earlier, the presence of air bubbles makes the crucible a good insulator for heat and participates to the softening of the quartz structure by increasing its viscosity hence enabling easier small deformation during ingot pulling and preventing crack formation that would also affect the ingot quality. In other words, this layer constitutes a good skeleton for the crucible.

In conclusion, the complete structure of the crucible and its intrinsic quality, especially at the interface with the melt, play an important role in the final crystal quality and solar cell efficiency.

The properties of the two layers building the crucible, their sensitivity to experimental parameters and their impact on the ingot quality have been investigated in other studies [37], [38] and will be investigated in another work parallel to this study, on the same crucible materials. In the following parts of this thesis, it is the cristobalite formation, phenomenon occurring during the ingot growth at the melt-crucible interface that might influence the crystal characteristics considerably, that is investigated more in details.

2.3 Cristobalite formation

2.3.1 Silica phase transitions

Amorphous quartz, the building material of crucibles used in the CZ process, is one of the many polymorphs of SiO_2. A polymorph of a substance has the same chemical formula but a different crystal structure. In the case of silica, several polymorphs are observed in function of the temperature and pressure and quartz is the stable form at ambient conditions. [7] The phase diagram of silicon dioxide, showing the different phase transitions in function of temperature and pressure, is represented in Figure 9.

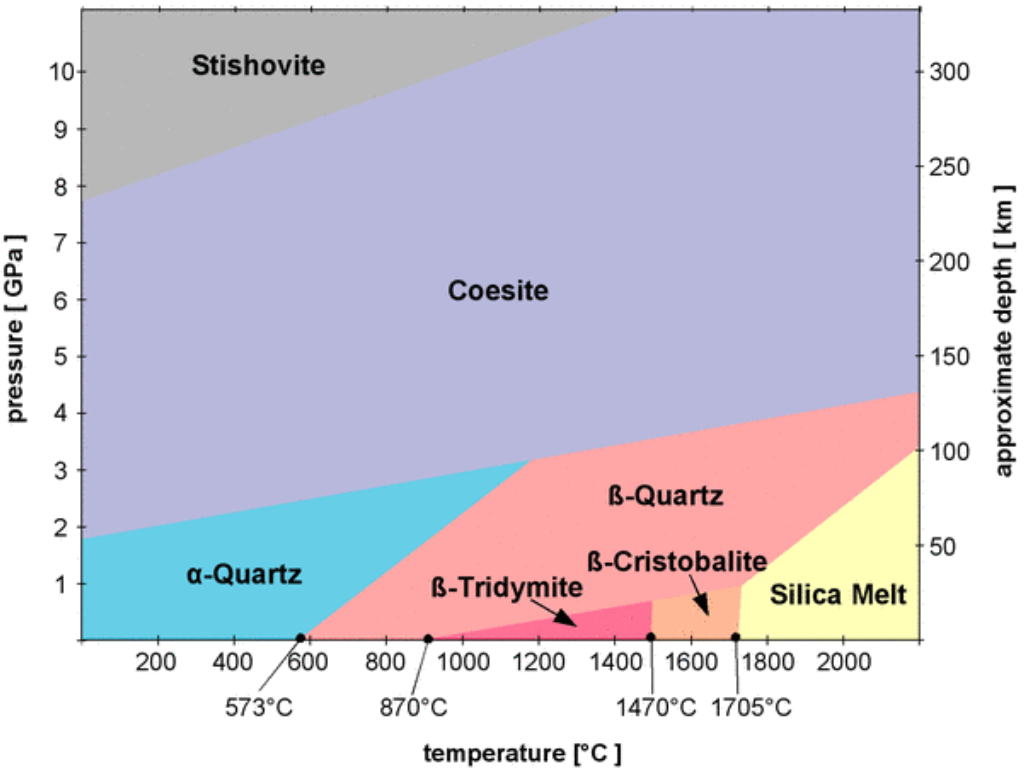

Figure 9: Phase diagram of silica [7]

During the CZ process, the crucible can be subjected to temperatures up to 1500°C. Under those conditions, the successive phase transitions can be summarised as in Figure 10.

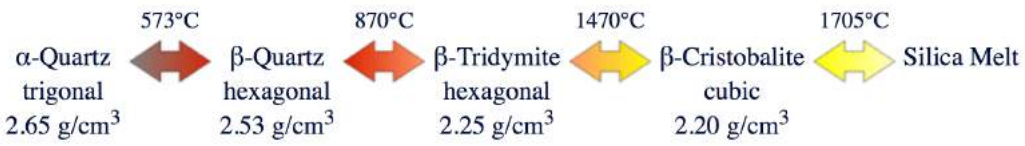

Figure 10: Successive phase transitions of α-quartz with increasing temperature [7]

However, when using HPQ, the most likely transitions that occur when the quartz is heated are the following : the α-quartz (trigonal crystal system) first shifts to β-quartz (hexagonal crystal system) around 573°C then it devitrifies spontaneously to cristobalite in the beta form (cubic crystal system) that is the stable silica polymorph at high temperatures. [7] If the temperature is furthermore increased silica would melt at 1705°C. In fact, one study relates that β-tridymite does not form from pure quartz so that cristobalite can be observed from 1050°C and not 1470°C as the phase diagram suggests. [39]

When considering quartz crucible, the transitions observed are once again different. It has been explained in section 2.2.1.2 that when producing quartz crucibles from HPQ sand, the sand is fused into amorphous glass. At ambient temperature, the silica glass remains so that the structure of a quartz crucible is highly amorphous. When the crucible is subjected to high temperatures in the CZ process, it has been observed that the transitions to β-quartz and β-tridymite are skipped and the surfaces of the crucible, made of silica glass, just experience a transition to β-cristobalite before melting if the temperature was brought to 1705°C. The transitions observed on high purity fused quartz crucibles are represented in Figure 11.

Figure 11: Successive phase transitions of high purity fused quartz crucibles made of silica glass with increasing temperature [7]

Those transitions are highly dependent on the heating rate. If the quartz crucibles are heated very quickly they can soften earlier than expected and melt at 1550°C, which would of course be detrimental for the process knowing that the molten silicon in contact with the crucible is kept for hours at temperatures as high as 1550°C. After cooling, the remaining phases on the crucible will be amorphous quartz and α-cristobalite (tetragonal crystal structure) that is stable under 270°C.

All those phase transitions induce the breakage of chemical bonds between the different polymorphs and changes of length of chemical bonds and angles between the alpha and beta forms of the polymorphs. Those changes lead to differences in specific density and, in the case of crucibles, it introduces constrains having repercussions on the macrostructure, e.g. cracks in the cristobalite layer upon cooling.

In addition, while there is no macroscopic difference between β-cristobalite and glassy silica, the transition to α-cristobalite at low temperature is noticeable by the change in refractive index that gives alpha cristobalite a white colour while silica glass stays relatively transparent. [40]

2.3.2 Effect of the presence of cristobalite on the crucible inner surface

The formation of cristobalite on the crucible inner surface is inevitable in the CZ process and has different impacts on the melt it is in contact with.

First of all, once cristobalite is formed at high temperature, the crucible is altered and will deform when the transition alpha-beta occurs during the cooling. Since this transformation is irreversible, it prevents the reuse of the crucible, which is an important cost factor for the solar cell industry.

Two possible ways to reuse the crucible are either to continuously refill it at high temperature by the so-called "continuous Czochralski growth" or to keep the crucibles at high temperature between each pulling and recharge feedstock in it (batch process). The second method is more encountered for solar cell silicon production with the use of SoG-Si while the continuous CZ growth is often implemented when using e-Si for semiconductors applications. The reuse of the crucible reduces the costs and the time lost during the successive heating and cooling steps but some residual melt stays during a long time in the process and it rises concerns about the purity of the final ingot. In the continuous CZ, the implementation of the continuous feed complicates the control of the process itself and the equipment required. [41] Nevertheless, both those solutions induce longer time of use for the crucible so that it is more and more important to get precise knowledge about how the crucible behaves during the whole process.

The transition from quartz to cristobalite is supposed to occur freely when the crucible is heated in the CZ process. Upon cooling, a white, brittle cristobalite layer is expected to cover the whole surface of the crucible. However, when the crucible inner surface is in contact with the melt at high temperatures, different occurrences have been observed. In that case, cristobalite tends to grow locally i.e. in the form of islands that are mainly nucleated due to the lack of purity on the crucible surface. Those islands, who take the macroscopic form of brownish rings, roughen the inner surface and generate small cristobalite particles resulting from pitting corrosion between the cristobalite and the silicon melt. Those particles can separate from the crucible surface, enter the melt and cause structural losses if they reach the solidification front before being dissolved. [42] This is an unwanted effect of the cristobalite formation.

From what is explained above it seems obvious that controlling the cristobalite formation is important. In fact, it is desired to form cristobalite on the inner surface of the crucible when it is uniformly spread on the crucible surface, forming a continuous protective layer.

Firstly, a uniform layer provides a shell between the melt and the crucible, being an armour for the diffusion of impurities and SiO gas. In fact, the dissolution rate of cristobalite is smaller than the one of amorphous quartz so that it resists better to the dissolution induced by the contact between the molten silicon and the crucible surface. [43], [44]

Secondly, this layer acts as a mould that maintains the shape of the silica crucible even when it softens due to high temperature processing, preventing large structure losses. In fact, cristobalite only melts at a temperature higher than 1713°C while amorphous silica commonly softens around 1544°C. The cristobalite layer then helps to withstand the operating conditions in the CZ furnace. Finally, this skin also reacts less easily with the melt hence producing less SiO gas.

Different types of cristobalite occurrence can be observed on Figure 12 on the inner surface of crucible samples used in the CZ process. On Figure 13, an unused crucible piece is shown in comparison.

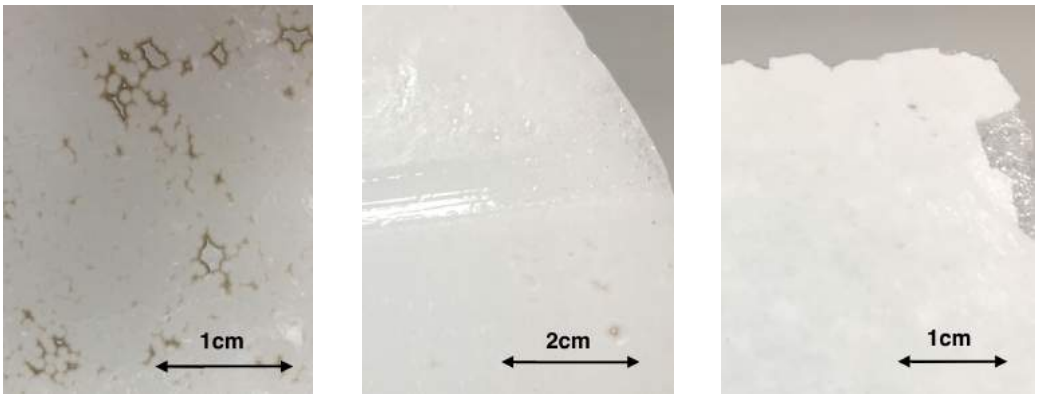

Figure 12: Different cristobalite occurrences : Brownish rings (left), brown and white spots (center), white crystalline layer (right)

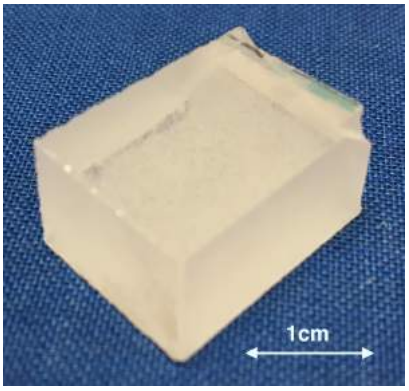

Figure 13: New crucible piece with no cristobalite occurrence

2.3.3 Control of the cristobalite formation

One way to control the cristobalite formation to obtain an even crystalline protective layer on the crucible, is to coat or doped the surface of the crucible with a devitrification agent. The devitrification agent reacts at high temperature with the amorphous silica and creates nucleation sites that promote the phase transition from quartz to cristobalite by lowering the activation energy of the quartz surface. It has been observed that the layer grows radially to form a uniformly spread skin. [8], [9]

Devitrification agents are mostly based on alkaline-earth metals elements or ions in the form of oxides, carbonates, hydroxides and silicates. When doping or coating the inner surface of the crucible, one has to be sure that the agent will not alter the silicon melt purity. The alkaline-earth metals beryllium, magnesium, calcium, and strontium, have large segregation coefficients so that they can easily enter the silicon ingot during the growth which is not desirable. In the solar industry, the most used agent is barium. In fact, relatively high concentrations of barium, typically until 100 ppm, are used to avoid the localised formation of cristobalite while the low segregation coefficient of barium prevents quantities as large as 100 ppm to enter the solid crystal. However, barium poses problems in terms of handling due to its high toxicity so that the coating or doping procedure must be performed with care.

Most coating techniques include dip coating the material or spray coating it.

Dip coating

Dip coating consists in dipping a substrate into the coating solution then withdrawing it from the liquid at a specific speed with constant temperature and atmospheric conditions. The lifting speed must be controlled carefully to be smooth and ensure uniform spreading of the solution on the surface. Once the substrate is out of the liquid, it is kept stable for the solvent to evaporate. The thickness of the film deposited on the substrate is mainly influenced by the angle of the inclination between the liquid and the substrate, the lifting speed, the viscosity of the solution, its density and the surface tension. [45] The stages of the dip coating process are represented on Figure 14.

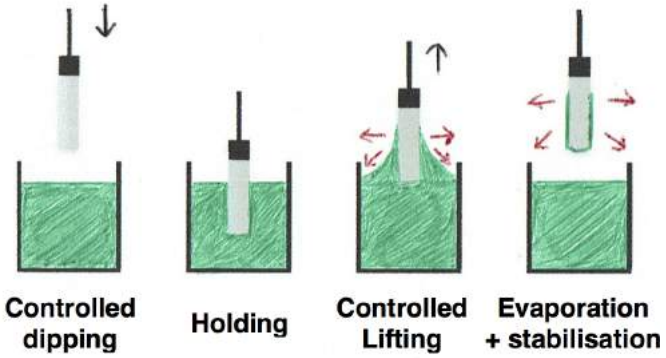

Figure 14: Schematic view of the dip coating process [46]

Spray coating

In spray coating, the solution is atomised in a nozzle by the use of a pressurised gas (e.g. nitrogen). It generates a flow of droplets that is spread on the surface in a certain pattern by a mobile head. The main parameters influencing the spray characteristics are fluid viscosity and density, surface tension, gas flow properties and liquid speed withdrawal. The homogeneity and thickness of the layer depend on numerous factors : the droplet sizes, their kinetics, the interactions between the fluid and the surface, the surface temperature, etc. [47]

In the case of crucibles for the CZ process, spray coating is the most used technique. The crucible is placed in a rotating support while an atomising nozzle is introduced vertically through a mounting rod, at the centre of the crucible. The nozzle has a reciprocate movement to the crucible and sprays a high purity barium hydroxide solution with nitrogen as carrier gas. The substrate is heated at elevated temperatures before and during the spraying in order to increase the adherence of the devitrification agent. [48] The typical set-up for crucible coating in the industry can be observed in Figure 15 and a lab spray coater set-up shown in Figure 16. It should be noted that in most industrial applications, the outer surface of the crucible is also coated in order to take advantage of the cristobalite formation acting as a shell for the crucible shape.

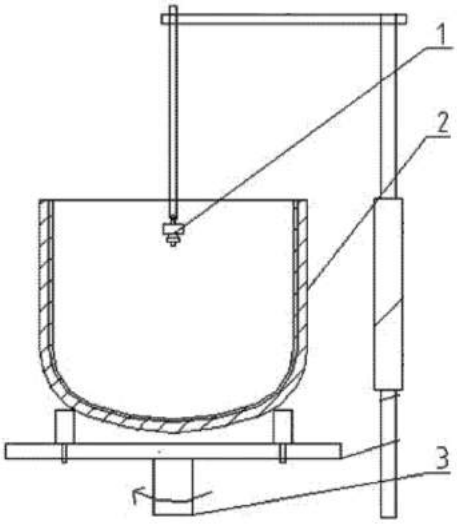

Figure 15: Spray coating set-up in the industry: nozzle (1), crucible (2), rotating support (3) [48]

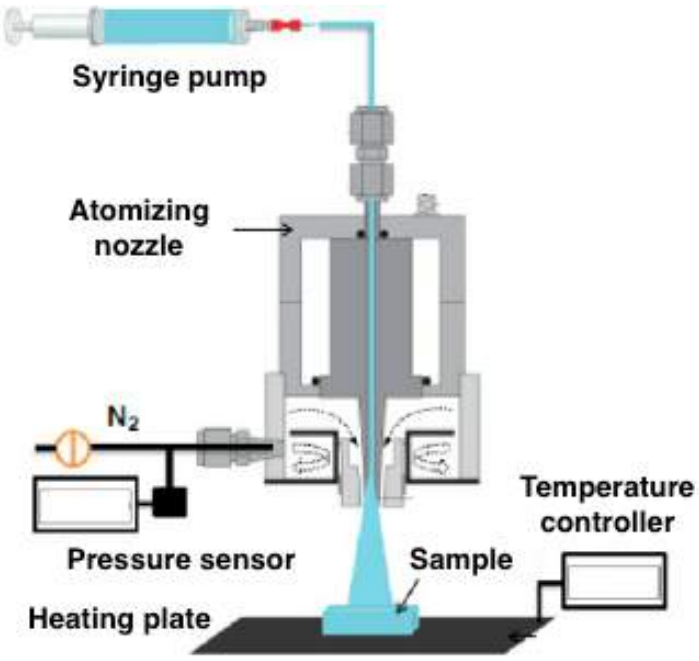

Figure 16: Typical lab spray coater set-up [49]

As said before, the most encountered solutions of devitrification agent are based on barium, more specially barium hydroxide. Once coated on the surface, $Ba(OH)_2$ reacts with carbon dioxide in air to precipitate as barium carbonate $BaCO_3$ on the surface of the crucible. The barium carbonate powder on the inner surface of the crucible is not fixed with any binder so that its adhesion strength is very weak and it can be easily detached from the surface when the crucible in handled. One consequence of that possible abrasion it that the coating is non-uniformly spread on the surface and the number of nucleation sites for cristobalite formation is then reduced. The low adherence also induces that the crucible cannot be washed or the coating would be washed away and the transport of it would also lead to easy removal of the layer. In addition, since barium powder can constitute a threat to health, it should not be so easily removable from the surface. It is why several alternative methods suggest to dip in a silica sol liquid that has a higher wettability on the crucible surface. [50]

After coating, during the CZ process, at high temperature (about 600°C), barium carbonate becomes unstable and converts to barium oxide which can react readily with silica to form barium silicates that will serve as nucleation sites for the quartz to crystallise into a dense, white cristobalite layer. [51], [52]

Surface doping

While coating the crucible seems like a good solution for the generation of a uniform cristobalite layer, the thickness of the layer formed is not easily controlled. In fact, the quartz crucible inner surface experiences a volume change when the cristobalite forms and this change can cause stresses between the quartz and the cristobalite layer and if the layer is too thick, the crucible surface is more susceptible to cracks. This drawback, in addition to the problem of the non homogeneity of the coating or its lack of resistance to handling has led to another technique consideration : doping of the crucible inner surface. [53], [54]

Doping of the crucible inner surface is made during the manufacturing of the crucible itself. As presented in section 2.2.1.2, when a fused crucible in manufactured, the silica grains are heated and fused in a rotating mould. To dope the crucible inner surface, the same process is conducted but the bulk layer of the crucible is first manufactured then the inner layer is made with silica grains doped with barium. Typical doping concentrations are in the range of about 5-150 ppm (often between 15-75 ppm). The barium-containing compound mixed in the silica feedstock for the inner layer can be of different forms : liquid (e.g. aqueous solution of barium hydroxide ($Ba(OH)_2$) or barium chloride ($BaCl_2$)), solid (e.g. barium carbonate $BaCO_3$), ionic, etc. The common solution is to dope silica grain with Ba before the fusing and mix those grains with pure silica feedstock. In most cases, an outer doped layer is also build during the process to promote the cristobalite formation on the outer surface of the crucible. The layer is often Al-doped and in this case, presence of aluminium in the outer surface would not represent a risk for the melt quality. [53]

Doping the crucible inner surface enables the barium concentration in the inner layer to be controlled. The doped inner layer thickness can also be controlled by variating the doped grain flow rate or flow time. Substantially all of the introduced dopant ends up fixed in the inner layer. With that, the thickness of the crystallised layer is also controlled. It has been observed that only the doped regions crystallise while the regions not doped do not. Finally, since the dopant is fused in the quartz glass, the crucible can be handled, cleaned, even etched without a risk of altering the doping and the probability of forming the uniform cristobalite layer. [53]

A doping set-up is illustrated on Figure 17. It is not often encountered in the CZ industry supposedly because it involves an extra step in the crucible manufacturing that does not always depend on the same companies that the one pulling the ingots. This extra step needs to be carefully controlled and this induces a large energy consumption and additional costs in comparison to coating that is easy to implement and cheaper.

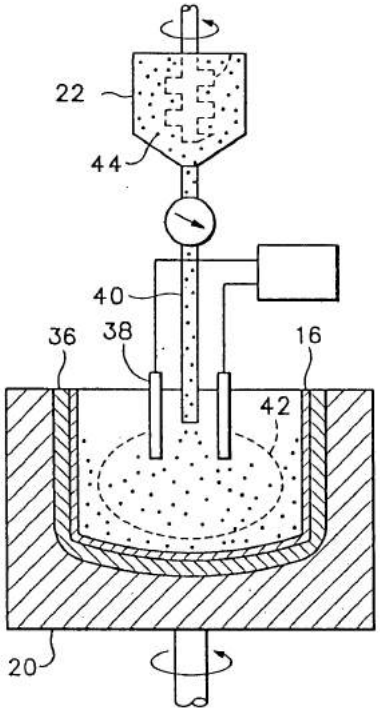

Figure 17: Doping set-up: inner layer of the crucible (16), graphite mold (20), grain hopper (22), bulk layer of the crucible (36), electrode (38), feed tube (40), heat region (42) and inner layer grain (44) [54]

2.4 Characterisation techniques

2.4.1 Optical microscopy

One of the basic but nonetheless important technique that will be used in this thesis is light microscopy. An optical microscope or light microscope employs visible light to detect small objects by the use of successive lenses. Its typical set-up is represented in Figure 18.

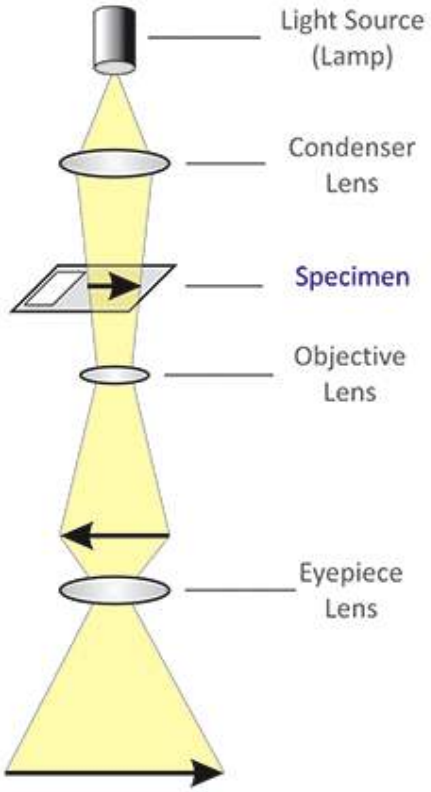

Figure 18: General set-up of a light microscope [55]

Light from an incandescent source is concentrated on the condenser lens then aimed at the specimen. The eye receives an image due to the collection of the light scattered by the sample on the objective lens and the magnification from the set of lenses called the eyepiece. The pattern creating the image from this set-up comes from the light absorbed by the sample due to natural pigmentation, contrast, etc. and appears enlarged in the eye, allowing to see at a smaller scale than the human eye. [56]

Advantages of the optical microscope are plenty: it is an easy tool to use, the analysing time is short, the sample preparation is relatively simple and fast, no specific observation conditions are required (e.g. vacuum, cooling, radiations).

The limitations come from the quality and number of the lenses in addition to the limited resolving power and magnification coming from the diffraction limit of visible light. In fact, white light has wavelengths from 400 to 700 nm with an average wavelength of 550nm resulting in a maximum theoretical resolution between 0.2 and 0.3 microns. [57], [58] In practice, it is hard to observe features smaller than 1 micron.

2.4.2 Scanning Electron Microscopy

In order to counter the limitations of the light microscope and be able to collect data at a smaller scale along with additional information, scanning electron microscopy, or SEM, constitutes a good complementary characterisation technique.

SEM uses electrons that have shorter wavelengths than the photons from visible light, enabling better magnifications.

The main SEM components include [59]:

- A source of electrons
- A set of condenser lenses
- A scanning coil
- A sample chamber
- An electron detector
- A Computer and display

An ordinary SEM set-up is shown in Figure 19.

Electrons are typically produced by resistive heating, of a tungsten (W) filament for example, then accelerated and condensed into a narrow beam by a set of focusing lenses. The scanning coil is used to deflect the beam around the surface to scan it in a raster fashion. The sample is mounted and placed into a vacuum chamber. It can be translated, rotated and tilted to modify its orientation while observed.

The electrons from the beam interact with the sample onto a depth of approximately one micron producing various signals that can be used to obtain information mainly about the surface topography, morphology, the crystalline structure and orientation and the composition of the material. The main signals used to obtain those information are obtained from secondary and backscattered electrons (image topography production and contrast), diffracted backscattered electrons (crystal structure and orientation) and characteristic X-rays (qualitative and quantitative elemental analysis). [60] The main interactions electron-sample are represented in Figure 20.

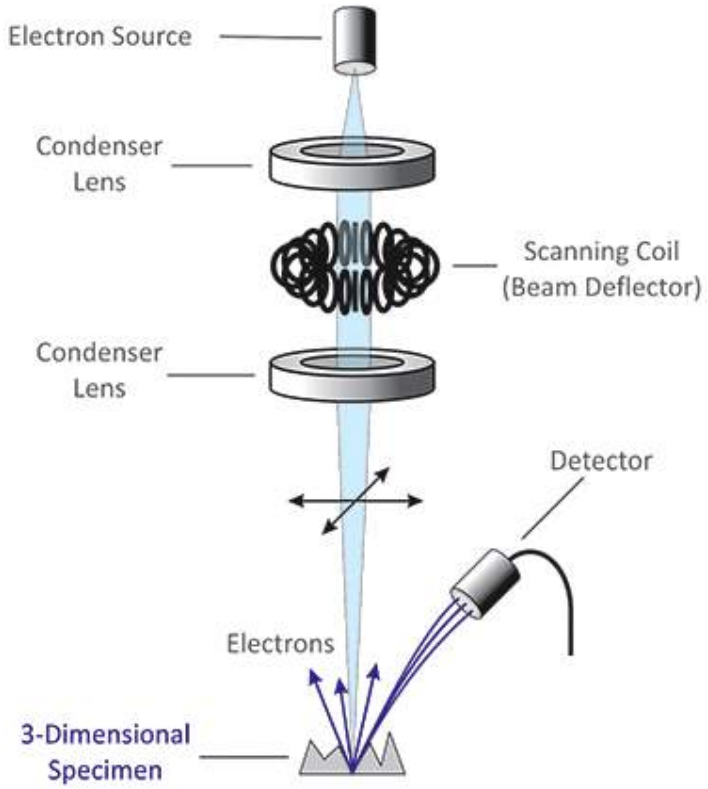

Figure 19: General Set-up of a scanning electron microscope [55]

After collection of the signals on different detectors, the computer processes the information from the detectors and displays the two dimensional images in black and white. [61]

The main advantages of the SEM in addition to the large range of information it provides, are its user-friendly interface, the data acquisition that is relatively fast, its high resolution, typically between 1-20 nm, and the fact that it is a non-destructive analysis.

However, there are some inherent disadvantages : SEM's are expensive and volumetric. They must be placed in isolated areas to avoid any vibrations, electric or magnetic interferences. The sample preparation is important and can be time consuming in function of the nature of the sample. In fact, the sample must be solid and fit into the SEM chamber and in addition, it must be a conducting material to prevent charge build-up. Most electrically insulating samples need to be coated with a thin layer of conducting material like carbon or gold among the most common ones: carbon is most suitable for a precise elemental analysis, while metal coatings like gold are most effective when a high resolution image is desired. The coating process is easy to conduct but it can affect the morphology of the coated surface.

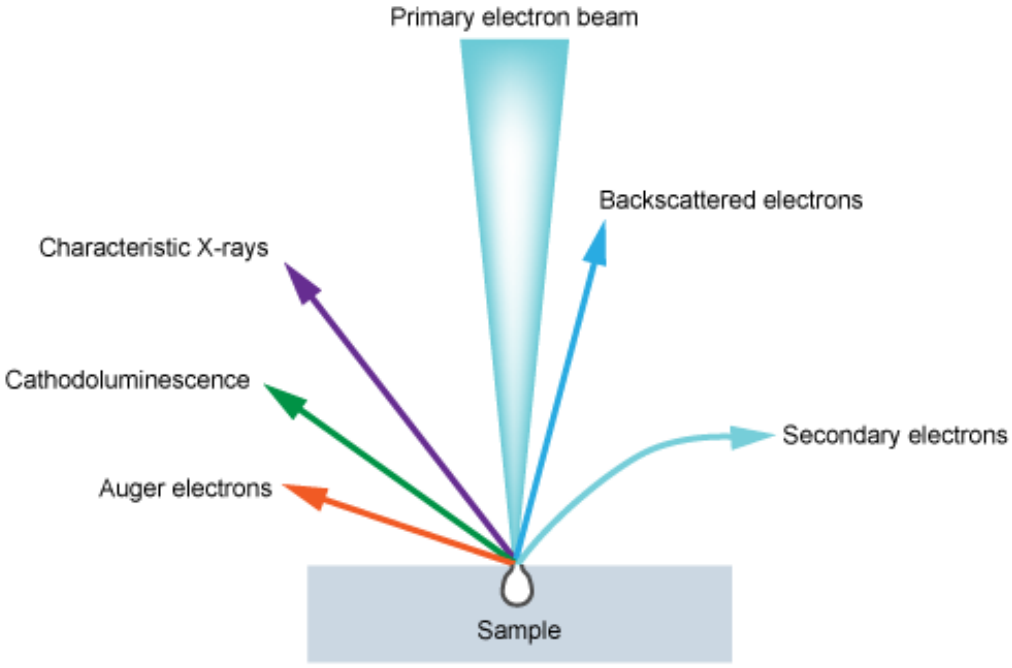

Figure 20: Main interactions electron-sample in SEM [60]

It is possible to analyse non-conducting materials without coating if the microscope can work with a low energy electron beam and additional specific features but the resulting pictures are less clear and precise than with a coating and it is not reconcilable with the features required for the chemical analysis, for example. [62]

2.4.2.1 Energy-dispersive X-ray spectroscopy

An energy-dispersive detector can be found on a SEM and uses the characteristic X-rays emitted by the sample (see Figure 19) to map the elements composition. The EDS X-ray detector measures the relative abundance of emitted X-rays in comparison to their specific energy that is characteristic of each specific atom. The analysis is easily conducted and fast and provides reliable qualitative measurements. Features as small as 1 micrometer or less can be analysed. Semi-quantitative analysis can be done by observing the peak-height ratio compared to a standard. [63]

One limitation of the EDS is that it cannot detect light elements, typically those with an atomic number < 10, and that several peaks may overlap and being interpreted as other compounds but this can be overcome by the use of an EELS apparatus for the light elements and by selective analysis for the overlaps.

2.4.3 X-ray diffraction

X-ray diffraction analysis or XRD is a simple and widely used characterisation technique for crystalline materials. It is based on the interactions between an X-ray beam and the surface of a crystalline object.

When a X-ray beam is focused on a sample, it interacts with the different phases in the material leading to parts transmitted, absorbed, refracted and diffracted. If a constructive interference occurs between the beam and the sample, the diffracted part of the X-ray is characteristic of the d spacing of plans in the crystal lattice of a specific arrangement of atoms. In fact, the distance travelled by the X-ray wave in the sample surface depends on the separation of the layers of atoms and the angle at which the X-ray entered the material. It is the Bragg's Law that allows to identify the plans of atoms in function of the constructive interference measured and it can be illustrated by:

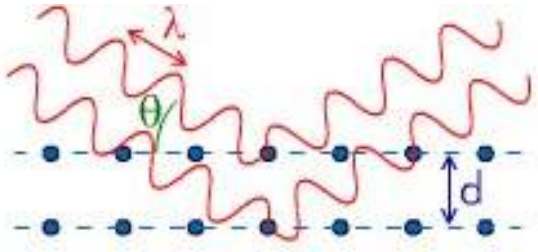

Figure 21: Schematic illustration of the Bragg's Law [64]

With

- λ, the wavelength of the rays;
- θ, the angle between the incident rays and the surface of the crystal studied;
- d, the spacing between the plans of atoms.

A constructive interference occurs when n is an integer (whole number).

To examine the reflection of X-rays from crystals, X-ray spectrometers or X-ray diffractometer have been developed. A monochromatic X-ray beam is generated from targeting a metal (commonly, copper, iron, molybdenum or chromium) with electrons and filtering the resulting signal by a monochromator. The narrowed X-ray is concentrated toward the sample material while the detector and sometimes the sample rotate in order to vary the angle in the whole 2θ range and measure the reflections from constructive interferences in all possible directions in the randomly oriented crystal sample. The reflexions are detected then processed and analysed as counts in function of the angle, corresponding to a peak in intensity for each plane arrangement. Each set of peak constitutes a unique pattern characteristic of the minerals present in the sample. It is possible to identify the phases present by comparing the pattern to standard references. [64]

A simplified set-up of an X-ray spectrometer is shown on Figure 22. It consists mainly of three elements: an X-ray tube, a sample holder and an X-ray detector.

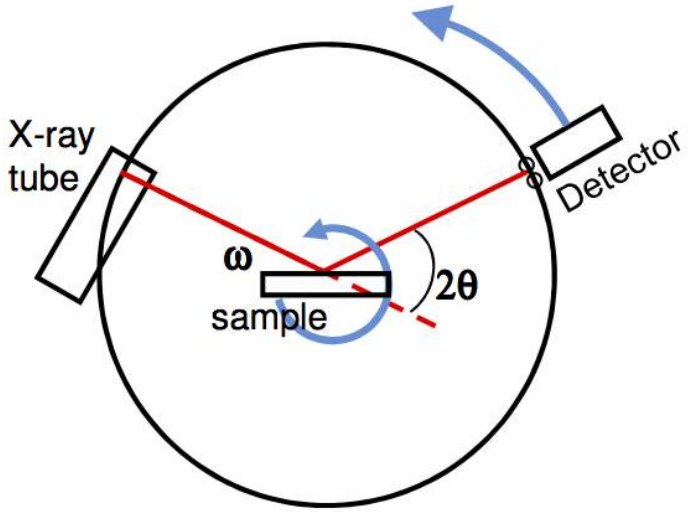

Figure 22: X-ray diffractometer set-up [65]

In addition to the qualitative analysis of the XRD, a semi quantitative determination of the material and its crystal structure can be obtained by Rietveld refinement and numerical methods that will not be covered here.

Some main advantages of the XRD is that it identifies unknown mineral in a simple, powerful, rapid, non-destructive way with an easy sample preparation and large data bases available for straightforward identification. The main limitations come from the interpretation of the pattern with sometimes peak overlays and demanding analytical techniques for quantification. [65]

3 Experimental

3.1 Investigation method

Three crucible types are investigated in this work. They differ by the sand quality used for their manufacturing. From each type of crucible, sets of used and new and respectively coated and non-coated pieces are available. From each used piece, cubes of approximate dimensions 1x1x1 cm and slides of approximate dimensions 1x1.5x0.3 cm are cut while for new crucible pieces, rods of approximate dimensions 1x1x4 cm and cubes of approximate dimensions 1x1x1 cm are cut. All of the samples are cut from a large piece selected at 12 cm below the top of the crucible. This is represented in Figure 23.

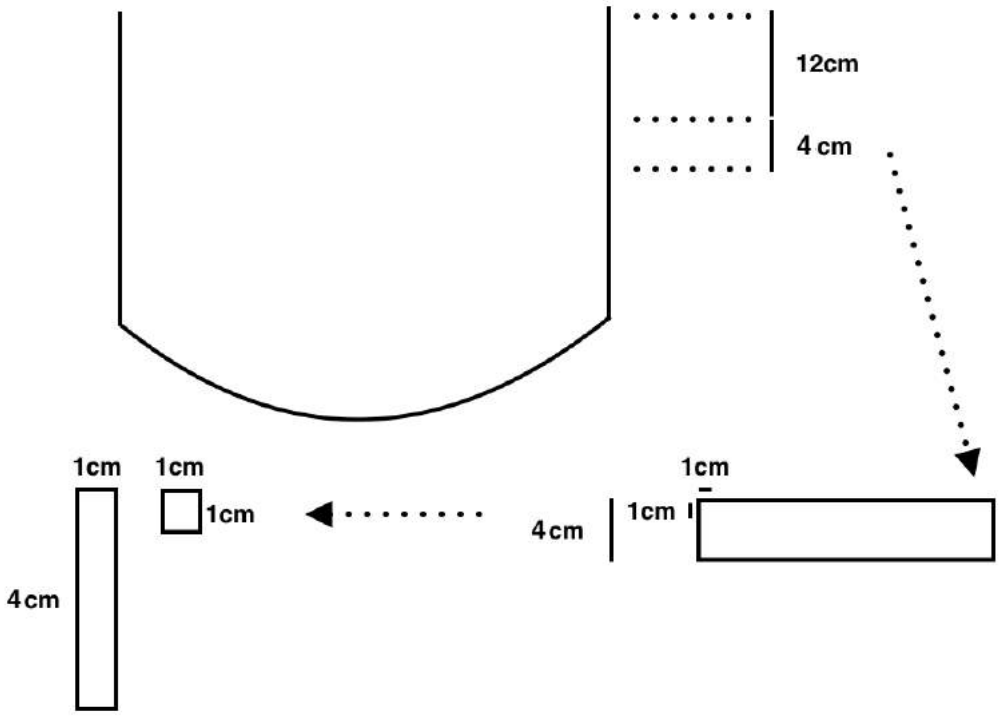

Figure 23: Sampling of cubes and rods from a 4 cm wide piece cut at 12 cm below the top of the crucible

Table 3 summarises the different materials studied in this work and the codes used to differentiate them. Coarse and fine relate to the sand quality while the chemistry is defined by the company sand purification process which is kept secret. One information available is that Standard+ means that the sand has a higher quality due to the fact that it has a finer particle size distribution (larger surface area) which allows for a better removal of impurities.

Table 3: Materials investigated and their code

	Sand quality and Chemistry	**New/used**	**Industrial coating**
A	Coarse - Standard		
$\mathbf{A}_n$		New	No
$\mathbf{A}_{nc}$		New	Yes
$\mathbf{A}_u$		Used	No
$\mathbf{A}_{uc}$		Used	Yes
B	Fine - Standard +		
$\mathbf{B}_n$		New	No
$\mathbf{B}_{nc}$		New	Yes
$\mathbf{B}_u$		Used	No
$\mathbf{B}_{uc}$		Used	Yes
Std	Coarse - Standard		
$\mathbf{Std}_{nc}$		New	Yes
$\mathbf{Std}_{uc}$		Used	Yes

In order to characterise the cristobalite occurrence, the samples are investigated as follows:

- The new crucible pieces are cut in cubes and rods. A_{nc}, B_{nc} and Std_{nc} cubes are studied by SEM in order to characterise the coating morphology. Part of the A_n and B_n rods are coated with a devitrification agent in a NTNU lab. This coating is also studied by SEM and compared to the one from the industry. Then, all the new crucible rods are heat treated in order to observe the cristobalite layer produced under different conditions. This layer is observed from the rods after heat treatment by light microscopy, SEM and XRD to obtain information respectively about the thickness of the cristobalite layer formed, its morphology and the nature of the crystalline phases present.

- From all the used crucibles pieces, cubes and top surface slides are cut. They are analysed by light microscopy, SEM and XRD to study the same features as for the unused heat treated crucibles pieces.

3.2 Sampling

Large pieces of the different crucibles are provided by the industry. Most of the characterisation techniques and the heat treatments set-up require specifically sized samples so that they need to be cut.

First, a rough and fast cutting is performed with a coarse circular diamond blade saw in order to obtain the rods and the pieces whose sizes fit the more accurate saw, a high precision diamond blade saw. Pictures of the two machines used in this work are shown in Figures 24 and 25.

Figure 24: Rough diamond saw: Side view with the rough blade and the mobile sample holder

Figure 25: Precise diamond saw: Cutting chamber with mobile sample holder and fine blade

While the rough cutting of the large pieces and the rods is done quite approximately and manually, the precise cutting is performed at a speed of 0.06 mm/s in order to have a good compromise between the time spent for the cutting, the precision of the cutting and the preservation of the brittle cristobalite layer on the heat treated and used pieces. Examples of an unused quartz crucible rod and a cube of used quartz crucible investigated are shown on Figure 26.

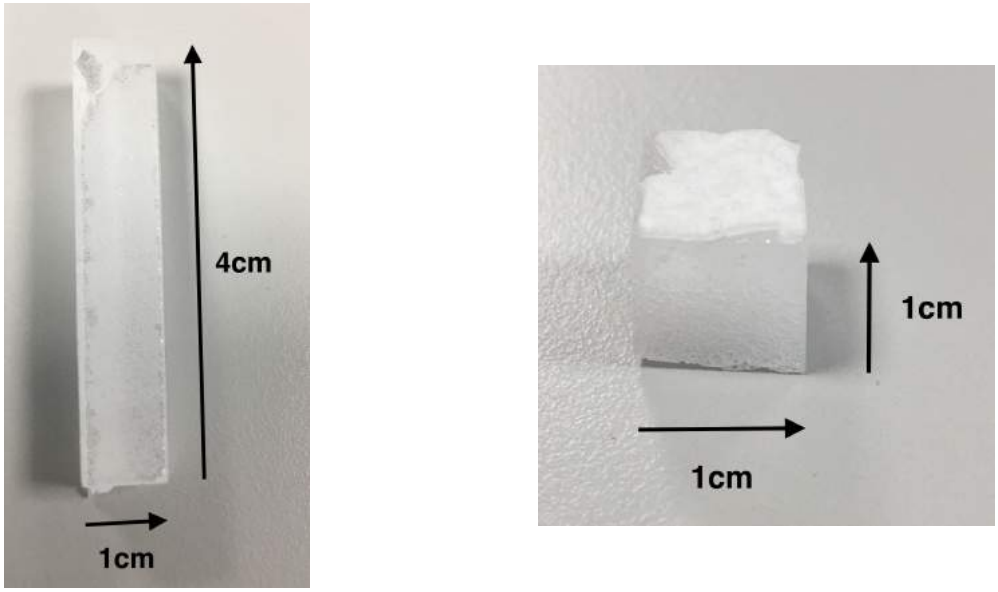

Figure 26: Example of an unused crucible rod and a used crucible cube investigated with their respective dimensions

3.2.1 Limitations

When cutting the rods with the rough saw, the measurements are made with a ruler on the sample then cut as precisely as the eye can see with a blade of about 1 mm thick so that induces inherent deviations resulting in rods of 4x1x1 cm with variations from 1 to 3 mm in length and width observed.

When cutting the cubes with the precise saw, the measurements can be made automatically and are verified with a ruler as well. It gives more precise results but the blade is still 0.4 mm thick, which can lead to small deviations in the cubic shape. In addition, if the pieces introduced in the holder are long, their shape will not be straight in the machine due to an unavoidable curvature and this can lead to additional inaccuracies.

3.3 New samples

3.3.1 Coating

In order to have an insight about the influence of the coating process with a devitrification agent, in this case barium, on the cristobalite layer that forms on the quartz crucibles, some of the A_n and B_n rods are coated before being heat treated.

3.3.1.1 Coating procedures

The coating routines followed in this work are inspired by an US Patent and a research paper from SINTEF. [48], [66] This choice results from a compromise between ease of solution preparation, coating apparatus available and data provided in these reports to reproduce the experiment. The two coating techniques investigated are the dip coating and the spray coating.

Dip coating

First, a barium hydroxide ($Ba(OH)_2$) solution of 0.3 M is prepared. The crucible rod sample is heated on a plate at 80°C for about 30 min then it is attached to the holder of the dip coater with glue on an aluminium foil and dipped one time in the solution with a dipping speed of 171.38 mm/min, a holding time in the solution of 15 s and a retrieval speed of 171.38 mm/min. This is performed automatically by the machine presented in Figure 27. Once it has been dipped, the rod is placed back on the heating plate for another 30 min at 80°C.

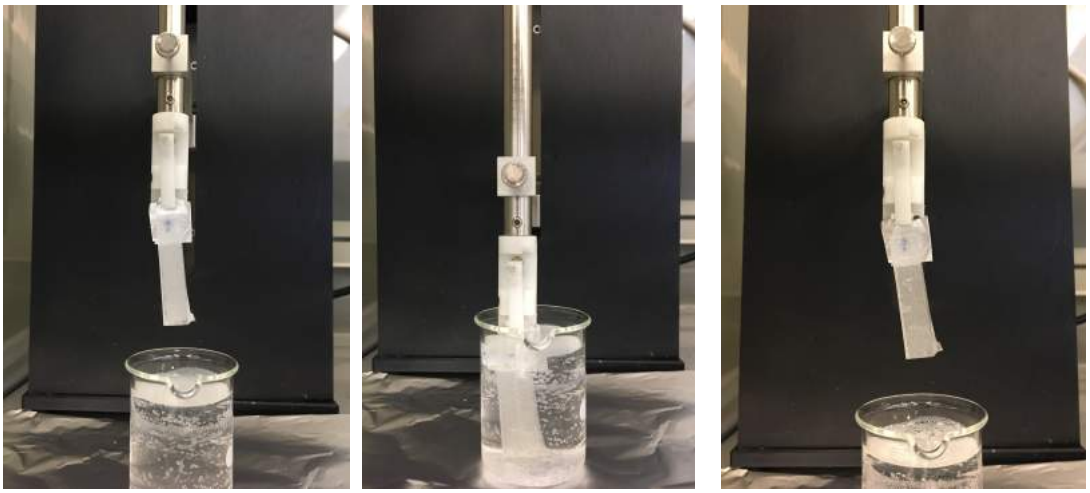

Figure 27: Dip coating of a new non-coated crucible rod in a $Ba(OH)_2$ solution

Spray coating

The coating method used by the industry on the crucible pieces provided is based on a barium solution that is spray coated on the crucible inner surface. The general set-up was presented in section 2.3.3 of this work. No information about the precise steps of this routine is available but some patents give general information that allows to execute a similar spray coating routine. The solution used for dip coating is also used to spray coat some of the A_n and B_n rods.

The spray coating is done with the machine shown in Figure 28 with nitrogen as gas carrier. The rod is placed in a closed chamber on a heating plate with an aluminium foil under it and is heated at 80°C during 30 min. The nozzle at the end of the mobile arm sprays the coating solution while being moved in a zigzag pattern also represented on Figure 28, in blue. The parameters used for the spraying are an infuse rate of 0.7 ml/min and an area spacing of 2 mm. Those parameters have been established after 4 different tests in order to best reproduce the coating pattern of the industrial coating. In addition, similarly as for the dip coating, once the rod is coated, it is kept on the heating plate at 80°C for an extra 30 min.

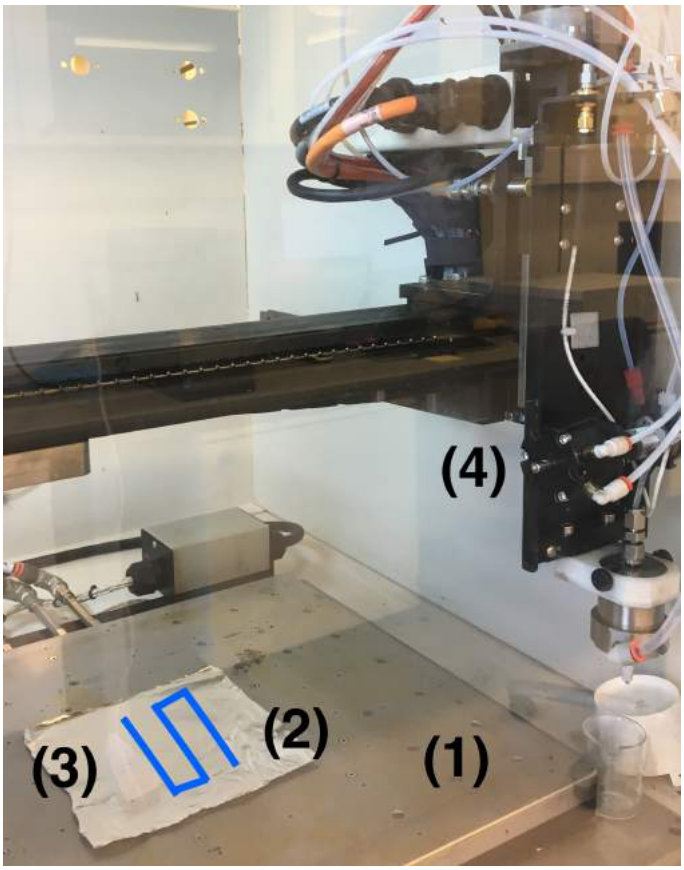

Figure 28: Spray coater set-up: Heating plate (1), aluminium foil (2), quartz sample (3), mobile arm (4), simplified spray pattern (blue)

After the 30 min drying, all the rods are left in a fire hood overnight for the barium hydroxide to completely react with carbon dioxide on the surface of the quartz. [50]

3.3.1.2 Limitations

Both coatings applied might not be completely homogeneously spread on the surface of the rods. In addition, the coating is very fragile and might be brushed away easily by any kind of handling.

3.3.2 Heat treatment 1

Heat treatments are performed to study the influence on the cristobalite layer of the holding time of the crucible piece at high temperature. A_n, A_{nc} (industrial, dip and spray), B_n, B_{nc} (industrial and spray) and Std_{nc} rods are subjected to heat treatment 1.

3.3.2.1 Samples preparation

Small high purity silica crucibles produced at NTNU are filled with high purity silicon feedstock. Si chunks (Siemens process) or granules (FBR process) were available to fill the crucibles but after a first melting test was conducted, the chunks were chosen as feedstock due to the results that showed a better homogeneity and distribution of the Si around the rod after melting and solidification. Approximately 40 g of feedstock is filled in each crucible. A rod of new crucible piece coated, non coated or coated at NTNU is placed in the middle of the feedstock. The rod dimensions are 4x1x1 cm approximately while the crucible is a cylinder of 2.5cm diameter and 6 cm height so that the rods are placed in the feedstock in a way that they do not exceed the crucible height. The typical set-up of the samples is presented in Figure 29.

Figure 29: Sample set-up for HT1: 4 cm long quartz rod in 40 g Si chunks

3.3.2.2 Furnace equipment and experimental procedure

The heat treatments are conducted in a vertical gradient freeze (VGF) furnace used for directional solidification. The main principles of this type of furnace can be found in literature. [15] Basically, two heating elements, one on top of the set-up, one at the bottom, are used to melt then solidify the silicon following a temperature profile that will be presented in the next section.

Crucibles are placed in graphite insulation parts. Those ensure homogeneous heating. Four small crucibles at a time can be processed as shown on Figure 30. Once the furnace is closed, a vacuum pump brings the pressure until 10^{-2} mbar. When this value is reached, the vacuum is broken by applying a constant flow of argon via an air flowmeter. After that, the furnace temperature is brought manually to about 1000°C then the temperature profile is run automatically. The furnace elements can be seen on Figure 31.

Figure 30: Furnace set-up for HT1: The 4 crucibles placed in the insulation parts

3.3.2.3 Temperature profiles

The influence of the contact time at high temperature between the crucible rod and the melt is studied with three different temperature profiles. Both the top and bottom temperatures have profiles that will differ in terms of the high temperature dwell and the cooling ramp. The holding times studied are 90 minutes (1 hour 30), 600 minutes (10 hours) and 1440 minutes (24 hours) for the top temperature profile with the bottom temperature profile adjusted in consequence. In general, in the industry, the process takes place during about 100 hours but it was practically impossible to reproduce those conditions at a laboratory scale.

Figure 31: VGF elements: Sealed furnace (a); open furnace with graphite parts and sample holder (b); manometers (c); argon flowmeter (d); vacuum pump (e)

The different temperature profiles are presented in Tables 4, 5 and 6 with the variable dwell times shown in red. The curves representative of the profiles for both the top and bottom temperatures can be seen on Figure 32 for the 90min holding time as an example while the two others can be found in Appendix A.1.

Table 4: Temperature profile data for 90 min holding time (dwell) at 1550°C with T1 the top temperature and T2 the bottom temperature

T1

Step #	**Set point [°C]**	**Ramp [°C/h]**	**Dwell [min]**
0	1550	1200	2
1	1550	600	**90**
2	1483	10	2
3	1	250	1
4	2	250	6000

T2

Step #	**Set point [°C]**	**Ramp [°C/h]**	**Dwell [min]**
0	1550	1200	2
1	1450	1200	**72**
2	750	75	166
3	1	250	1
4	2	250	6000

Table 5: Temperature profile data for 10 h holding time (dwell) at 1550°C with T1 the top temperature and T2 the bottom temperature

T1

Step #	**Set point [°C]**	**Ramp [°C/h]**	**Dwell [min]**
0	1550	1200	2
1	1550	600	**600**
2	1483	10	2
3	1	250	1
4	2	250	6000

T2

Step #	**Set point [°C]**	**Ramp [°C/h]**	**Dwell [min]**
0	1550	1200	2
1	1450	1200	**550**
2	750	75	166
3	1	250	1
4	2	250	6000

Table 6: Temperature profile data for 24 h holding time (dwell) at 1550°C with T1 the top temperature and T2 the bottom temperature

T1

Step #	**Set point [°C]**	**Ramp [°C/h]**	**Dwell [min]**
0	1550	1200	2
1	1550	600	**1440**
2	1483	10	2
3	1	250	1
4	2	250	6000

T2

Step #	**Set point [°C]**	**Ramp [°C/h]**	**Dwell [min]**
0	1550	1200	2
1	1450	1200	**1325**
2	750	75	166
3	1	250	1
4	2	250	6000

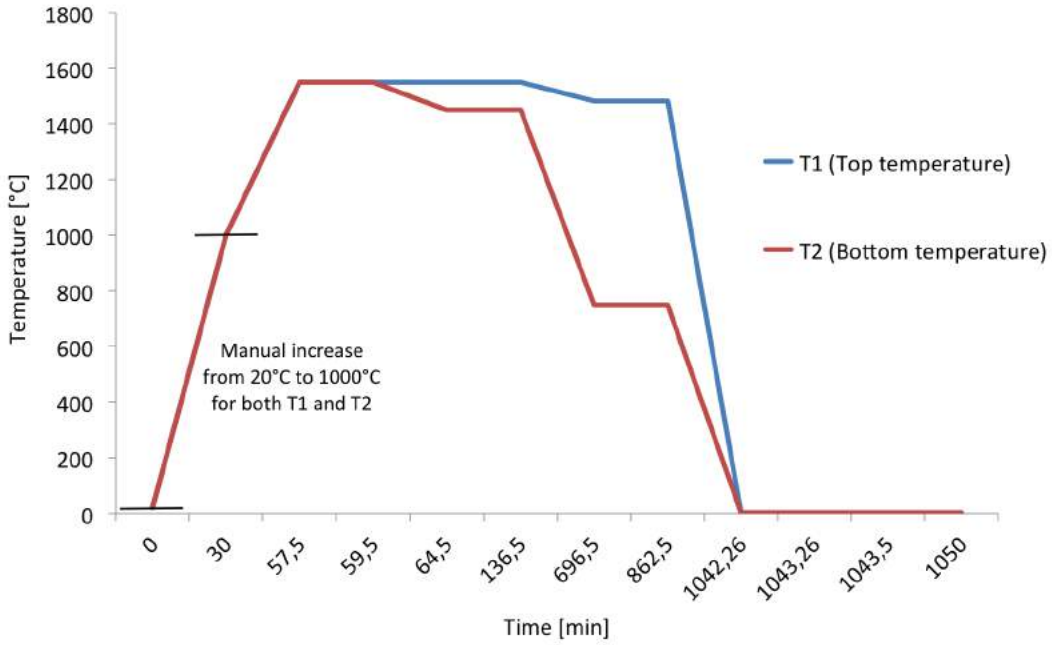

Figure 32: Temperature profile for HT1 in function of the time for the 90 min holding time and total experiment time of 1050 min or 17 h and 30 min

A summary of each experiment conducted with the type of crucible rods used, the weight of the feedstock and the holding time at high temperature can be found in Appendix A.1 in Table 13.

It is the part of the rod just above the solidified melt that is investigated. In order to collect it without breaking it, the part in Si is covered with epoxy that is solidified overnight under a fire hood then the part of the rod outside of Si is cut off from the epoxy with the rough saw. From this crucible part, only a piece of about 1 cm is available to be studied while the rest is used in the parallel study about the bubble content.

3.3.3 Heat treatment 2

An additional heat treatment has been performed in a Ferrotec CZ puller for monocrystalline silicon ingot growth.

3.3.3.1 Samples preparation

3 rods of A_{nc} crucible and 3 rods of Std_{nc} of approximate dimensions 10x1x1 cm have been cut with the rough saw.

3.3.3.2 Samples set-up and experimental procedure

The 6 rods are attached with a molybdenum wire around a graphite holder connected to the seeder of the CZ puller. This set-up can be seen on Figure 33.

Figure 33: HT2 rods set-up on the Ferrotec seeder

High purity silicon feedstock is fed into a large crucible and melted, in the mean time, the rods are brought slowly at about 20 cm above the melt level to start a progressive heating. Once the melt is stable, the rods are dipped in it. A 2.8 cm length is dipped and kept for 10 hours into the molten silicon (see Figure 34). After 10 hours, the rods are carefully lifted up and kept close to the melt for 1 hour to start a relatively slow cooling. After that time, the rods are lifted up at about 1 metre from the melt to finish cooling.

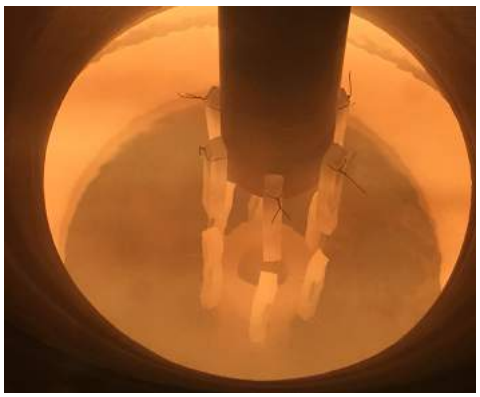

Figure 34: Furnace set-up HT2: Immersion of the 6 rods in the molten silicon

Two pieces of about 1.5x1x1 cm are collected from each rod from just above and just below the limit that the melt was reaching during the experiment. Those pieces constitute the material investigated after.

In addition to the study of the material, a temperature simulation has been conducted in order to get an insight about the temperatures experienced by the parts of the rod in the melt and right above it and the influence it might have on the cristobalite development. This modelling is performed with the logiciel CGSim taking into account the differences in the thermal conductivity of quartz and silicon, a 20 mbar argon pressure in the furnace, a turbulent flow model and a crucible rotation of 1rpm.

3.3.4 Light microscopy

As first step of cristobalite characterisation, the heat treated rods are studied by light microscopy.

3.3.4.1 Sample preparation

In order to observe the cristobalite layer precisely from the cross section of samples with the light microscope, the surface needs to be polished. For the quartz pieces and the brittle cristobalite layer to withstand the stresses induced by the polishing, it has been found that embodying each cube in epoxy was the best solution. The samples are carefully placed in the middle of a sample holder that is filled with a mixture of Epofix resin and hardener in a 25:3 mass ratio until the sample has its top surface just covered. The sample holder is then placed in a fire hood for 8 hours to let the resin harden and evacuate some of the air bubbles. A resulting embedded sample is shown on Figure 35.

Figure 35: Epoxy embedded quartz sample, cross section oriented

The polishing is performed with the help of the machine shown in Figure 36, a Struers TegraPol-31 capable of holding six samples at the same time. The polishing consists in successive steps including first grinding the samples with silicon carbide papers of different roughness then polishing with cloths of micrometer precision with addition of a water based diamond suspension. The details of this procedure are presented in Table 7. Between each running step, the samples and the sample holder are cleaned with soap, washed with water then cleaned again with ethanol. In addition, between each polishing step, the cloths are also carefully cleaned with water and soap.

Figure 36: Struers TegraPol-31 for automatic grinding and polishing of the samples

Table 7: Polishing successive steps

Silicon carbide paper roughness	**Time**
120	2 min 30
320	2 min 30
500	2 min 30
1200	2 x 2 min 30
2400	2 x 2 min 30
Polishing cloth precision	**Time**
3 μm	2 x 12 min 30
1 μm	2 x 12 min 30

3.3.4.2 Observations

The heat treated crucible rods parts (coated and non-coated) are analysed in the light microscope in order to look at the thickness of the cristobalite layer from cross section oriented cubes embedded and polished. The morphology of the cristobalite is also investigated from top surface observations of the cubes (no specific sample preparation).

The optical microscope used for this work is a Leica MEF4M model represented on Figure 37. It is connected to a camera that allows to take pictures of the sample observed with the help of a software (ProgRes CapturePro) on a linked computer. The pictures were taken at different magnifications, typically 5×, 10× and 20× even if the microscope offers magnifications up to 100×. A lower magnification allows to get overview pictures while higher magnifications are used to get the details about the cristobalite morphology. Thickness measurements were performed manually from the scale on the pictures.

Figure 37: Light microscope used in this work

3.3.4.3 Limitations

From the polishing step, if the cloths and the holder are not well cleaned, some particles may scratch the surface. Most of the scratches can be removed by repeating the polishing steps and checking the surface at the light microscope between each of them. Unfortunately, some inherent scratches tend to stay on the surface.

Concerning the cristobalite layer, since it is very brittle, all the preparation steps may remove partially or totally the layer so that its thickness might be impossible to measure on some samples. In addition, in the sample preparation steps, a lot of water and soap are used and some of it gets trapped on the quartz surface. When observed with the microscope, those liquid accumulations prevent a good focus at high magnifications.

3.3.5 SEM

3.3.5.1 Sample preparation

After being studied with the light microscope, the top surfaces of some of the heat treated samples are observed with the SEM. However, additional preparation steps must be performed.

First of all, the samples must be wrapped in an aluminium foil, leaving the area of interest uncovered. A carbon tape can be used to link the foil and the sample surface to ensure a better conductivity on the sample surface.

When using a SEM, "charging effects" are observed because of electrons accumulation on insulating samples like quartz. These effects affect the quality of the image displayed by the SEM by preventing a good focusing. One solution to this problem is to coat the sample with a conductive material as explained in Section 2.4.2. This is why a thin layer of carbon coating is deposited on the samples. The coating is obtained from graphite rods that are decomposed in a sputtering machine. The machine works under vacuum and a sputtering time of 6.8 seconds is used. Most of the time, to ensure a good covering of the coating, a second sputtering of 6.8 seconds is performed.

3.3.5.2 Observations

The SEM apparatus used in this work is shown in Figure 38. The inside of the equipment with the sample holder can be seen on Figure 39. Top surface analysis were performed in order to characterise the morphology of the cristobalite. In addition, some EDS was performed in order to identify the surface atomic composition. The main parameters used for the SEM and EDS analysis are found in Table 8.

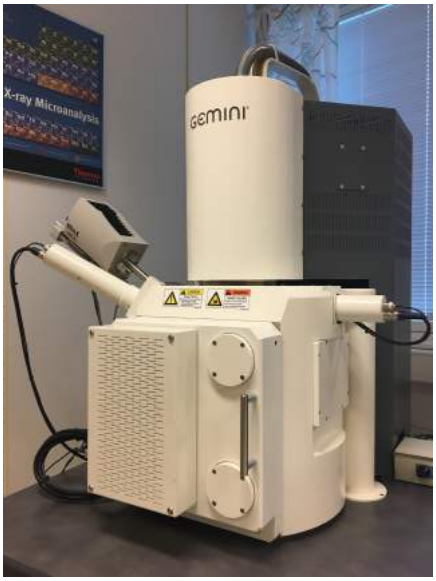

Figure 38: External view of the SEM used in this work

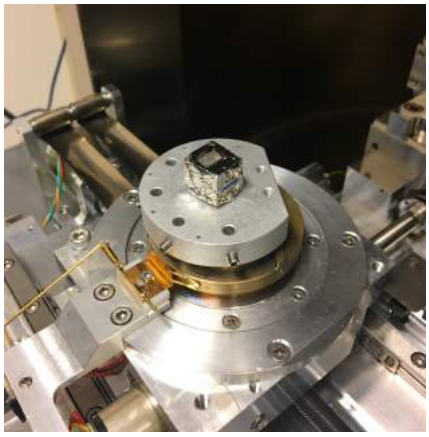

Figure 39: SEM sample holder from inside the SEM chamber with a typically prepared and coated quartz sample

3.3.5.3 Limitations

Attention must be paid to the coating of the sample during the preparation steps. Typically two runs of sputtering of carbon are conducted to have a sufficient covering. In fact, the covering must be homogeneous in order to have a good conduction all over the sample surface but by sputtering several times, the thickness of the layer also increases and that might influence the topography of the sample.

Table 8: SEM and EDS observation parameters

	Voltage (EHT)	**Current**	**Aperture**	**Working distance (WD)**
SEM	10-15 keV	Low	30 μm	10-20 mm
EDS	15-20 keV	High	60 μm	10-20 mm

3.3.6 XRD

3.3.6.1 Sample preparation

Most of the time, XRD is used on powders. When investigating the cristobalite layer on quartz sample, it is possible to observe thin slides of the surface layer like the one shown on Figure 40.

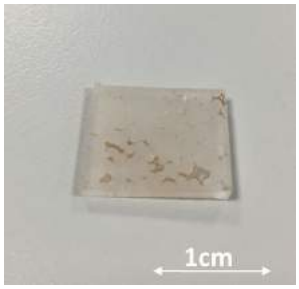

Figure 40: XRD slide

Those slides are cut with the precise diamond saw presented in section 3.2. It is important that the surface be flat and of relatively low roughness to be observed in the XRD. No polishing of the slides is performed in order to preserve the cristobalite layer. The slides are simply sticked on the sample holder with a ceramic paste. Their top surface must be placed as precisely as possible at the same height than the border of the sample holder. The set-up is shown on Figure 41.

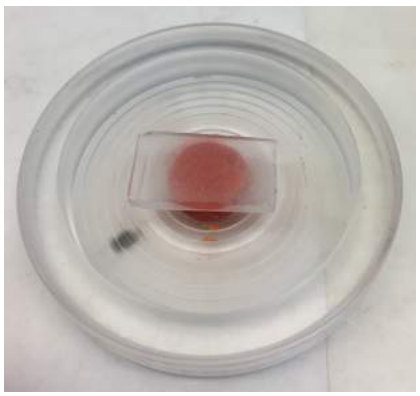

Figure 41: Sample set-up for XRD

3.3.6.2 Measurements parameters

The XRD used in this work is a Bruker D8 Advance shown on Figure 42. The parameters used for the analysis were kept constant for each sample. They are based on a pre-defined set of parameters for highly crystalline materials and are presented in Table 9. The database used to analyse the peaks is the Powder Diffraction File (PDF).

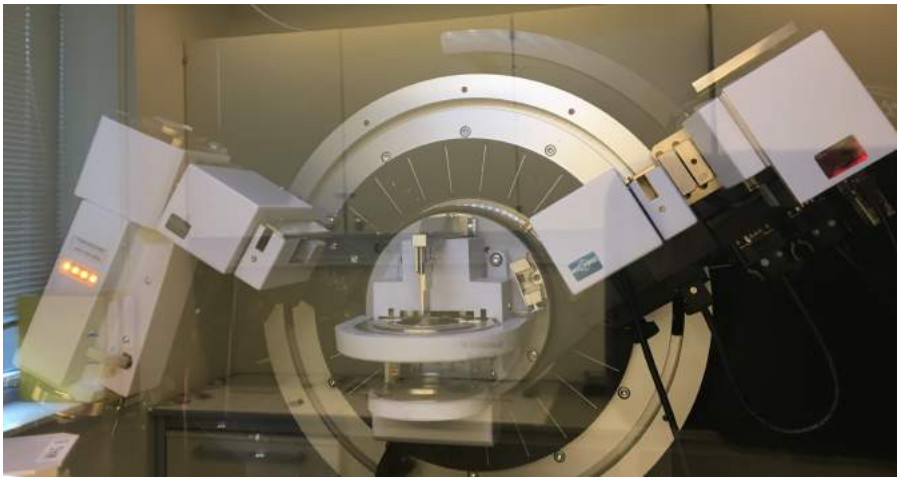

Figure 42: Bruker D8 Advance XRD used in this work

Table 9: XRD analysis parameters

Quartz-Cristobalite	
Sample type	Highly crystalline
Scan time	30 min
Angular range (2θ)	10-75
Divergence slit	V6 (6 mm illuminated at 2θ)
XRD anode	Cu (λ = 1.54 10 Å)

3.3.6.3 Limitations

Attention must be paid not to remove the brittle cristobalite layer during the preparations steps. After the heat treatments, the slides cut are of small and variable areas which means that the quantitativity (height of the peaks observed) is not reproduced. Since cutting slides from the top surface destroys the sample, this characterisation could not always be performed in order to preserve the sample for other analysis. Finally, some of the slides are covered by epoxy which is amorphous and that can affect greatly the sensibility of the method.

3.4 Used samples

The used samples are provided by the industry. They are considered as samples resulting from a "Heat treatment 3" of 100 h.

3.4.1 Light microscopy

Cubes of each used crucible are observed at the light microscope. Cross sections are observed after putting the cubes in epoxy resin and polishing as explained in section 3.3.4 while top surfaces are also observed without any specific preparation step.

3.4.2 SEM

Each sample observed in the light microscope has also its top surface observed in the SEM after the additional preparation steps presented in section 3.3.5.

3.4.3 XRD

XRD is performed on two slides of each used crucible, coated and non-coated. Since cutting the slides would destroy the cubes that need to be observed for other features and the fact that there is more material available in the case of used crucibles, it was decided to cut the XRD slides from other portions of the large pieces cut at 12 cm below the top of the crucibles provided.

The same parameters as those presented in section 3.3.6 are used for the XRD investigations of used crucibles.

3.5 Summary

Table 10 summarises the experimental analysis conducted in function of the materials investigated. "LM" stands for light microscope. As explained previously, only the top surface of the samples is investigated in the SEM and the XRD.

The samples for which the characterisation has not been conducted ("No") are the ones who were not in sufficient quantity to be observed by SEM after the HT1 so that it was kept for the XRD and the parallel study about the bubbles content. In addition, HT1 of 24 h has not been performed on 4 crucibles types (A_{nc}, A_n dip coated, A_n spray coated, B_n spray coated) due to lack of time following recurrent furnace problems.

Table 10: Summary of the samples investigated, their features and the characterisations conducted

	Coating	**Heat treatment**	**LM Cross section**	**LM Top surface**	**SEM**	**XRD**
New						
$\mathbf{A}_n$	/	HT1 : 90 min	X	X	No	X
$\mathbf{A}_n$	/	HT1 : 10 h	X	X	No	X
$\mathbf{A}_n$	/	HT1 : 24 h	X	X	No	X
$\mathbf{A}_n$	Spray	HT1 : 90 min	X	X	No	X
$\mathbf{A}_n$	Spray	HT1 : 10 h	X	X	No	X
$\mathbf{A}_n$	Spray	HT1 : 24 h	No	No	No	No
$\mathbf{A}_n$	Dip	HT1 : 90 min	X	X	No	X
$\mathbf{A}_n$	Dip	HT1 : 10 h	X	X	No	X
$\mathbf{A}_n$	Dip	HT1 : 24 h	No	X	No	X
$\mathbf{A}_{nc}$	Industry	HT1 : 90 min	X	X	No	X
$\mathbf{A}_{nc}$	Industry	HT1 : 10 h	X	X	No	X
$\mathbf{A}_{nc}$	Industry	HT1 : 24 h	No	No	No	No
$\mathbf{A}_{nc}$	Industry	HT2 : 10 h	X	X	X	X
$\mathbf{B}_n$	/	HT1 : 90 min	X	X	No	X
$\mathbf{B}_n$	/	HT1 : 10 h	X	X	No	X
$\mathbf{B}_n$	/	HT1 : 24 h	X	X	No	X
$\mathbf{B}_n$	Spray	HT1 : 90 min	X	X	No	X
$\mathbf{B}_n$	Spray	HT1 : 10 h	X	X	No	X
$\mathbf{B}_n$	Spray	HT1 : 24 h	No	No	No	No
$\mathbf{B}_{nc}$	Industry	HT1 : 90 min	X	X	No	X
$\mathbf{B}_{nc}$	Industry	HT1 : 10 h	X	X	No	X
$\mathbf{B}_{nc}$	Industry	HT1 : 24 h	X	X	No	X
$\mathbf{Std}_{nc}$	Industry	HT1 : 90 min	X	X	No	X
$\mathbf{Std}_{nc}$	Industry	HT1 : 10 h	X	X	No	X
$\mathbf{Std}_{nc}$	Industry	HT1 : 24 h	X	X	No	X
$\mathbf{Std}_{nc}$	Industry	HT2 : 10 h	X	X	X	X
Used						
$\mathbf{A}_u$	/	HT3 : 100 h	X	X	X	X
$\mathbf{A}_{uc}$	Industry	HT3 : 100 h	X	X	X	X
$\mathbf{B}_u$	/	HT3 : 100 h	X	X	X	X
$\mathbf{B}_{uc}$	Industry	HT3 : 100 h	X	X	X	X
$\mathbf{Std}_{uc}$	Industry	HT3 : 100 h	X	X	X	X

4 Results

The results of this work are presented in the following way : section 4.1 focusses on the new samples. First, the observations of the different coatings are presented then the results from each heat treatments are given and shortly commented. In section 4.2, the results concerning the used samples are shown.

4.1 New samples

4.1.1 Coatings

The industrial coating and the coatings performed at NTNU are hereafter compared from observations of the new crucible pieces at the SEM. In addition, some XRD analysis have been conducted in order to get an idea of the thickness of the coating deposited with each technique and the constituents of the coating.

Figures 43 and 44 show the industrial coating observed with the SEM on A_{nc} and Std_{nc} crucible pieces at different magnifications. The spray pattern can be seen from the white circular shapes. It looks widely spread despite a few scratches and other handling procedures that have removed the coating in some areas. This is more noticeable for Std_{nc} on Figure 44 where the coating is difficult to observe. The B_{nc} crucible pieces show the same covering and patterns as the A_{nc} crucible pieces but it is not represented here.

Figures 45 and 46 show the coating observed on A_n and B_n pieces that have been respectively spray and dip coated at NTNU. The spray coating pattern looks quite similar to the one observed on the industrially spray coated pieces. The coating seems to cover the whole surface of the piece. On the other hand, the dip coating pattern (Figure 46) shows a variable covering and is easily removed from the surface of the crucible piece. The pattern observed is completely different, in the form of elongated fibres spreading in several directions.

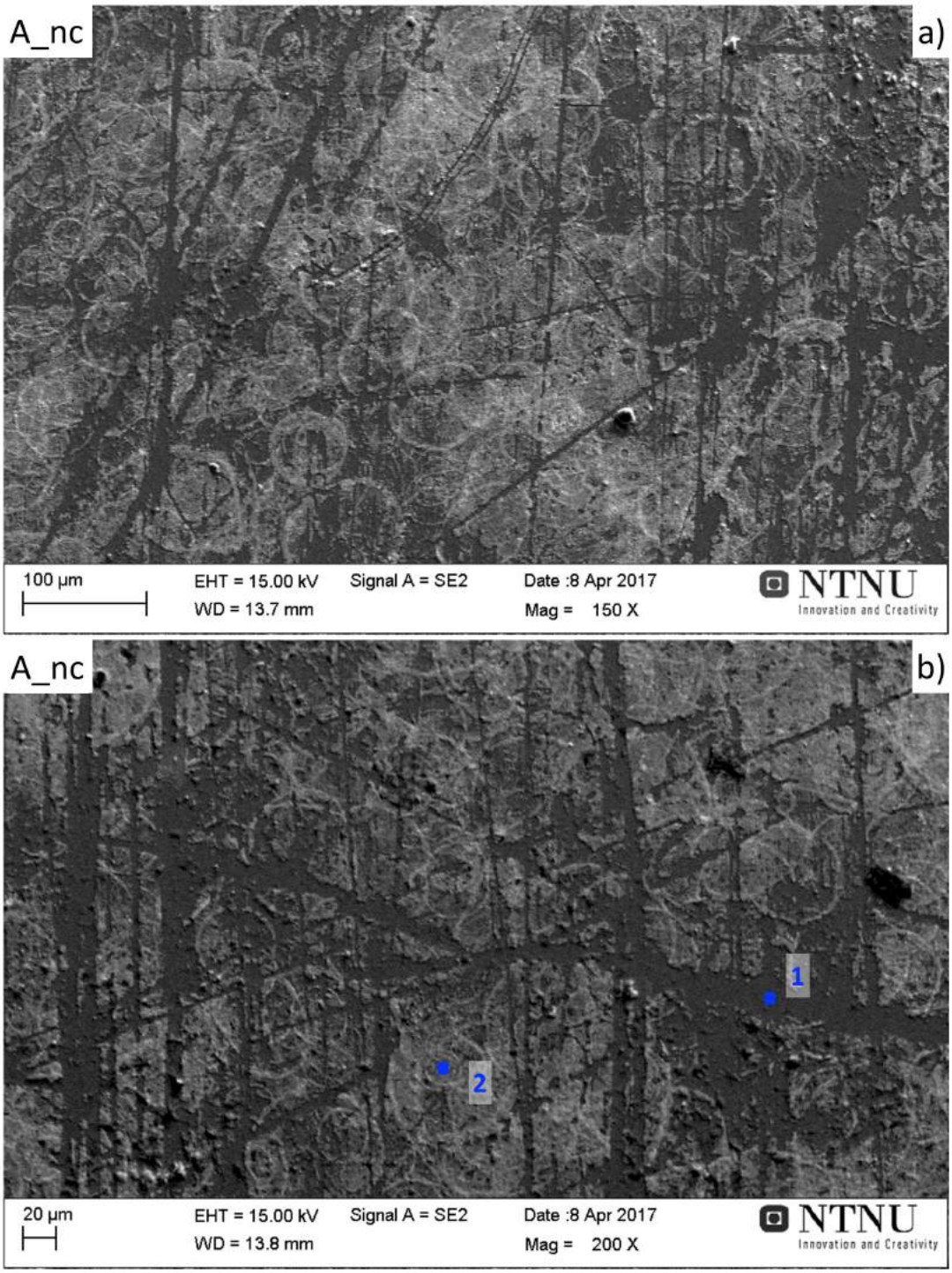

Figure 43: SEM images of the industrial coating on A_{nc} crucible pieces at magnifications 150× (a) and 200× (b). The white circular areas are representative of the spray coating pattern. Points 1 and 2 in blue are the locations investigated by EDS

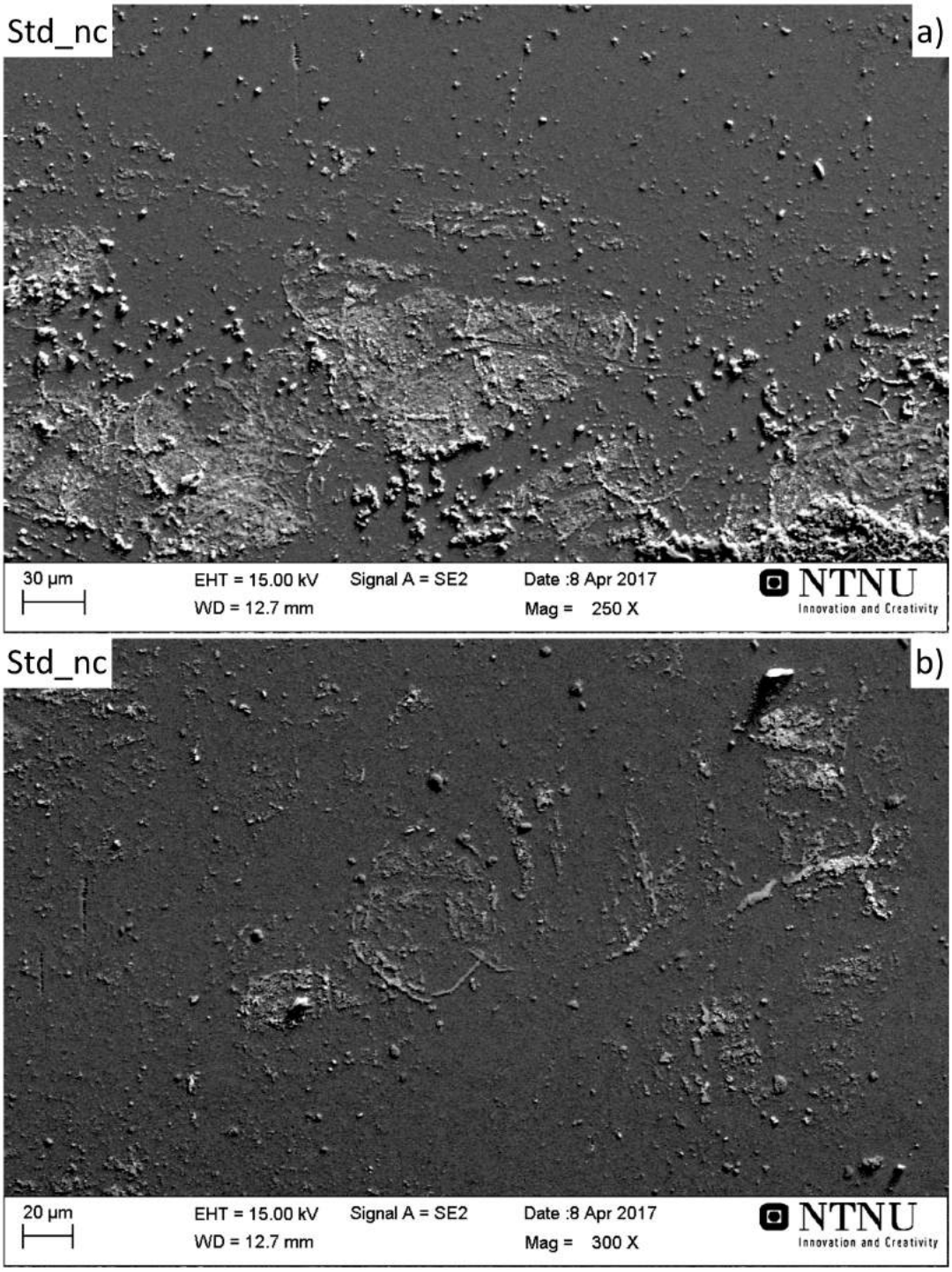

Figure 44: SEM images of the industrial coating on Std_{nc} crucible pieces at magnifications 250× (a) and 300× (b). The white areas are representative of the spray coating pattern

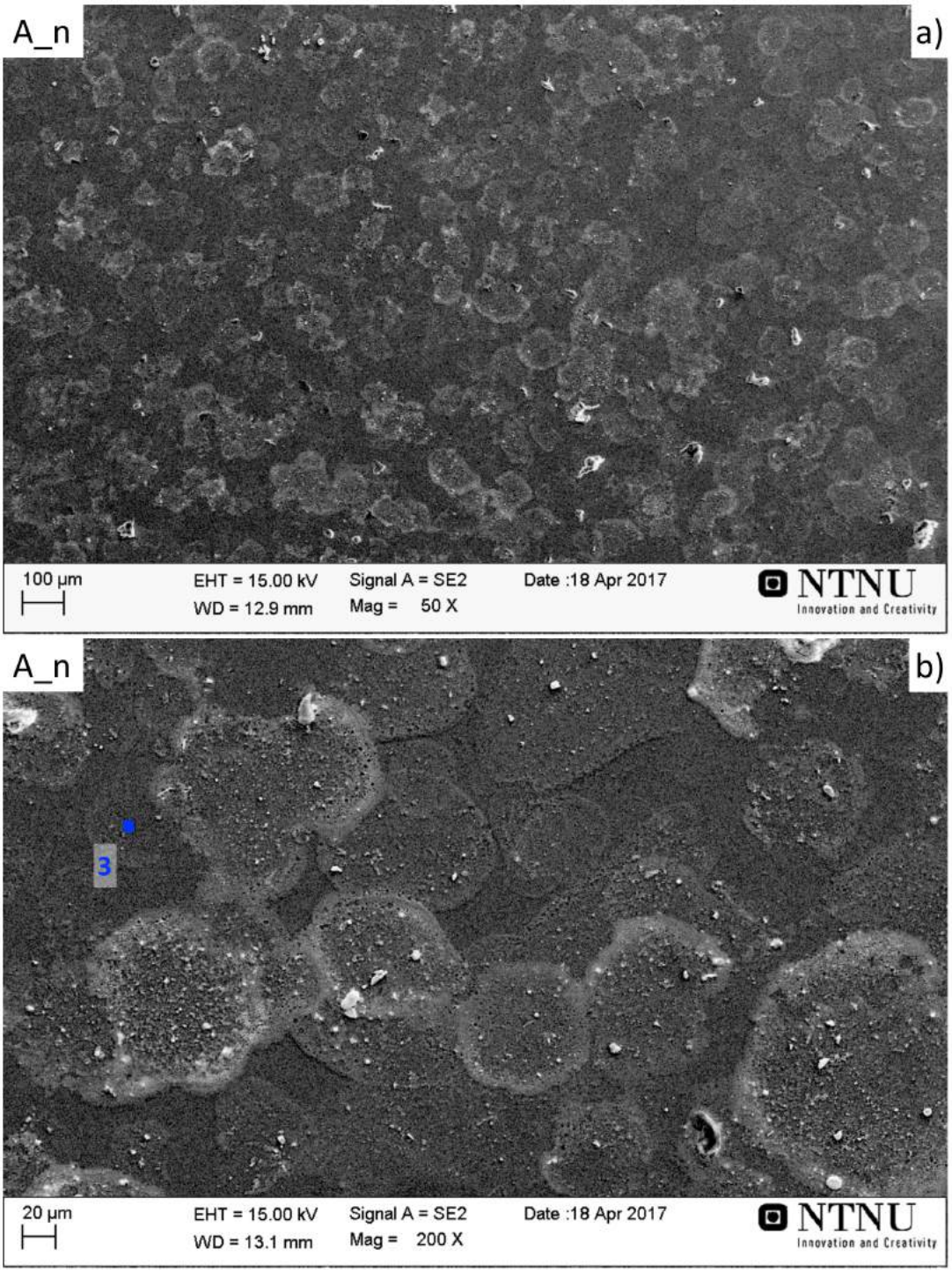

Figure 45: SEM images of the spray coating performed at NTNU on A_n crucible piece at magnifications 50× (a) and 200× (b). The white circular areas are representative of the spray coating pattern. Point 3 in blue is a location investigated by EDS

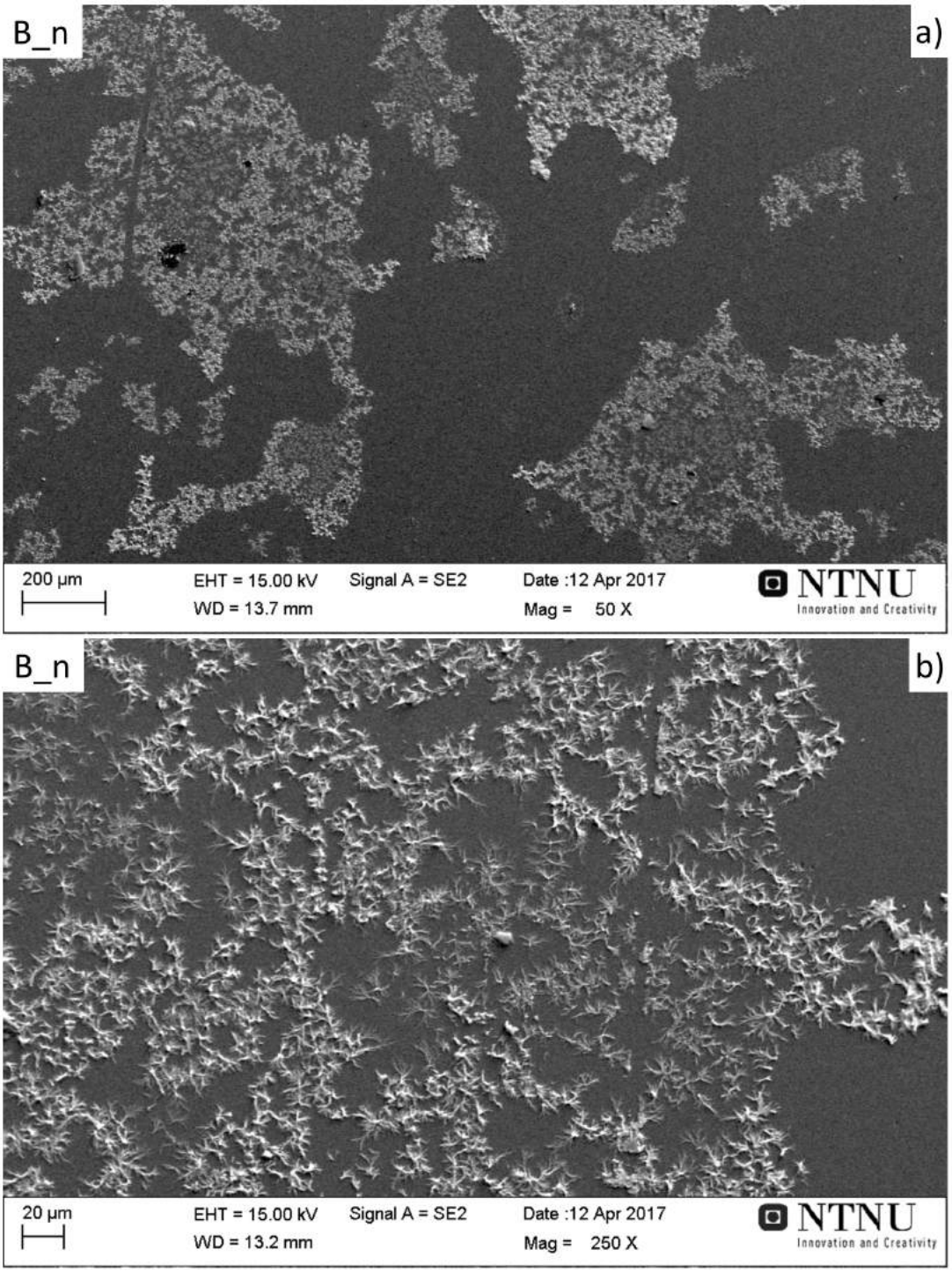

Figure 46: SEM images of the dip coating performed at NTNU on B_n crucible pieces at magnifications 50× (a) and 250× (b). The white elongated areas are representative of the dip coating pattern

In order to have a confirmation about the nature of the solid observed on the coated crucible pieces some EDS was performed on 5x5 μm white areas and 5x5 μm grey areas for each type of coating at magnification 700×, with a 15 keV beam and with a collection time of 60 s. The areas analysed are shown in blue on Figures 43b and 45b. The particles of higher volume that look darker than the rest of the sample surface on the SEM pictures are carbon based solids coming from the carbon sputtering procedure used to coat the samples in order to make their surface conductive enough for the SEM and EDS observations.

It can be seen on Figure 47 that on Point 1 analysed, corresponding to the grey surface on the SEM picture (Figure 43b), only Si and O are found with a bit of C from the carbon conducting coating. It is coherent with the suggestion that this area consists only in amorphous quartz with no coating. On Figures 48 and 49, for the coated parts of the surface (Points 2 and 3 from Figures 43b and 45b, respectively), the EDS identified Ba in addition to Si and O. This is again coherent since the coating is barium based. Those three EDS graphs are representative for the whole crucibles and types of coating observed.

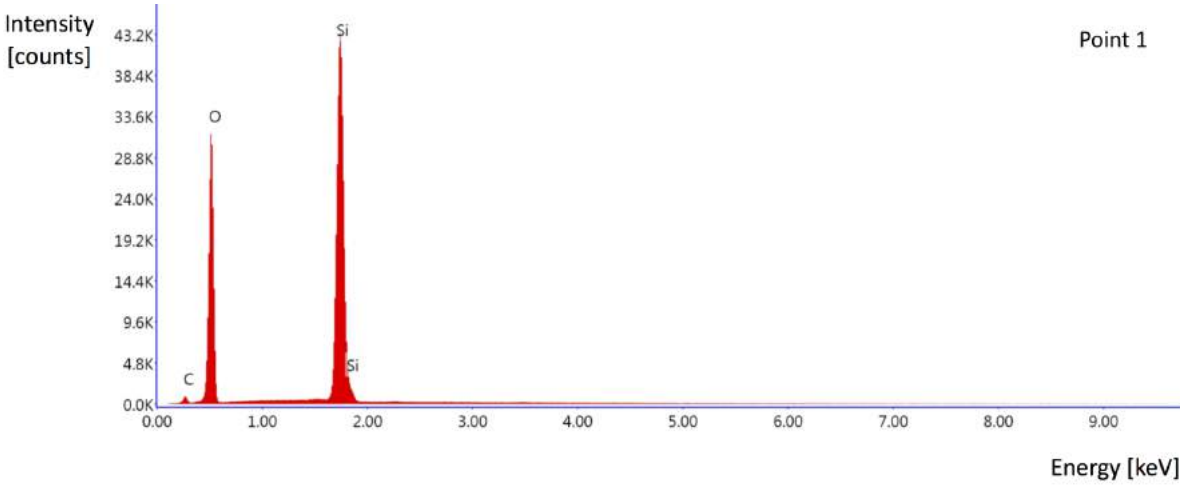

Figure 47: EDS analysis at 700× magnification on Point 1, a grey flat area of A_{nc} SEM picture, representative of the quartz surface for all the crucible types and coating types observed

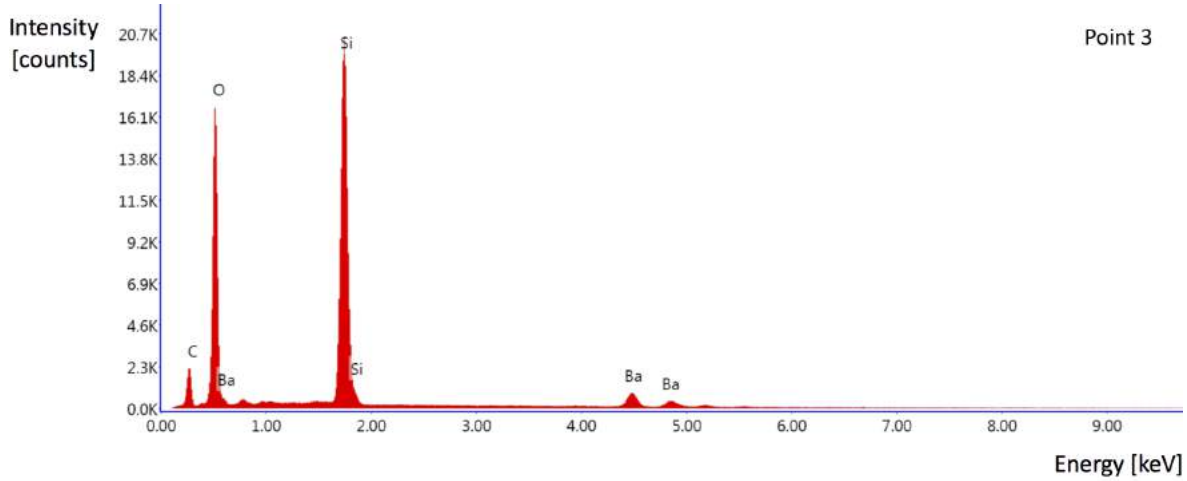

Figure 48: EDS analysis at 700× magnification on Point 2, a white area of A_{nc} SEM picture, representative of the barium containing coating for all the crucible types and coating types observed

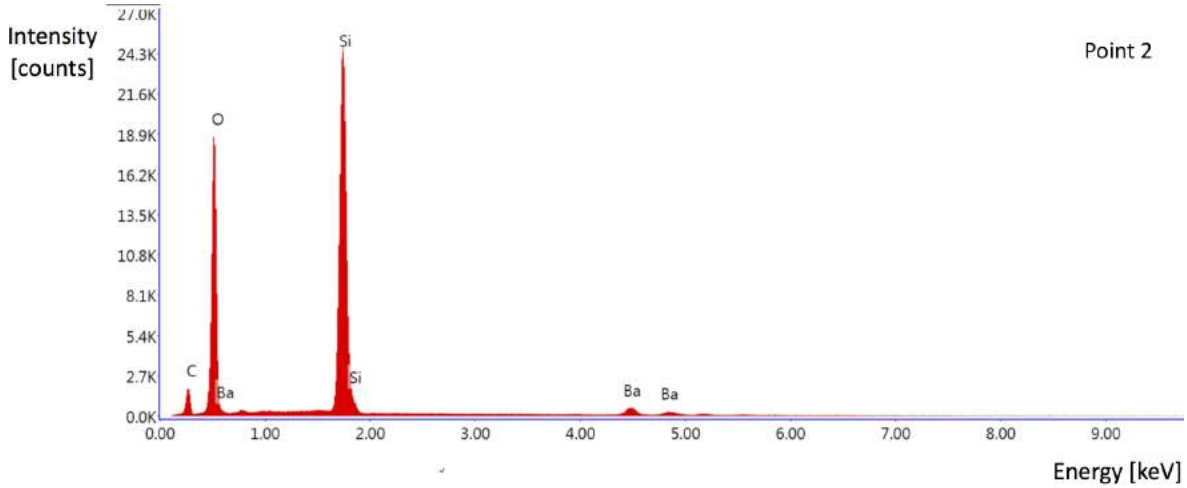

Figure 49: EDS analysis at 700× magnification on Point 3, the grey-like surface inside a ring pattern of the spray coated A_n crucible piece

The XRD measurements of the new coated crucible pieces have been conducted with a low crystallinity program set-up, in addition to the parameters presented in Table 9. The slides have been cut in a way that they have all approximately the same size, i.e. 1cmx1cmx0.2 cm, with variations of only 0.1 cm maximum in each direction.

Due to the lack of crucible material for B_{nc} and Std_{nc} in addition to a lack of time for sample preparation, only A_{nc} has been investigated for the representative analysis of the industrial coating. The XRD results for A_{nc} and the new crucible pieces coated at NTNU are shown on Figures 50, 51, 52 and 53 with $BaCO_3$ reference pattern in blue.

For A_{nc} (Figure 50) it can be seen that the sample is mainly recognised as amorphous quartz (large peak centered in 2θ=22) and small peaks representative of $BaCO_3$ have been identified and highlighted in red. In fact, the barium based coating is supposed to react on the quartz surface with the carbon dioxide in the air, forming $BaCO_3$ as explained in Section 2.3.3. The presence of $BaCO_3$ is then representative of the coating presence on the quartz sample.

For A_n and B_n spray coated (Figures 51 and 52), the large amorphous peak is still present but the main phase that is identified is the crystalline $BaCO_3$. For A_n dip coated (Figure 53), the results are similar to the observations made on A_{nc} with the large amorphous peak preponderant and small occurrences of $BaCO_3$.

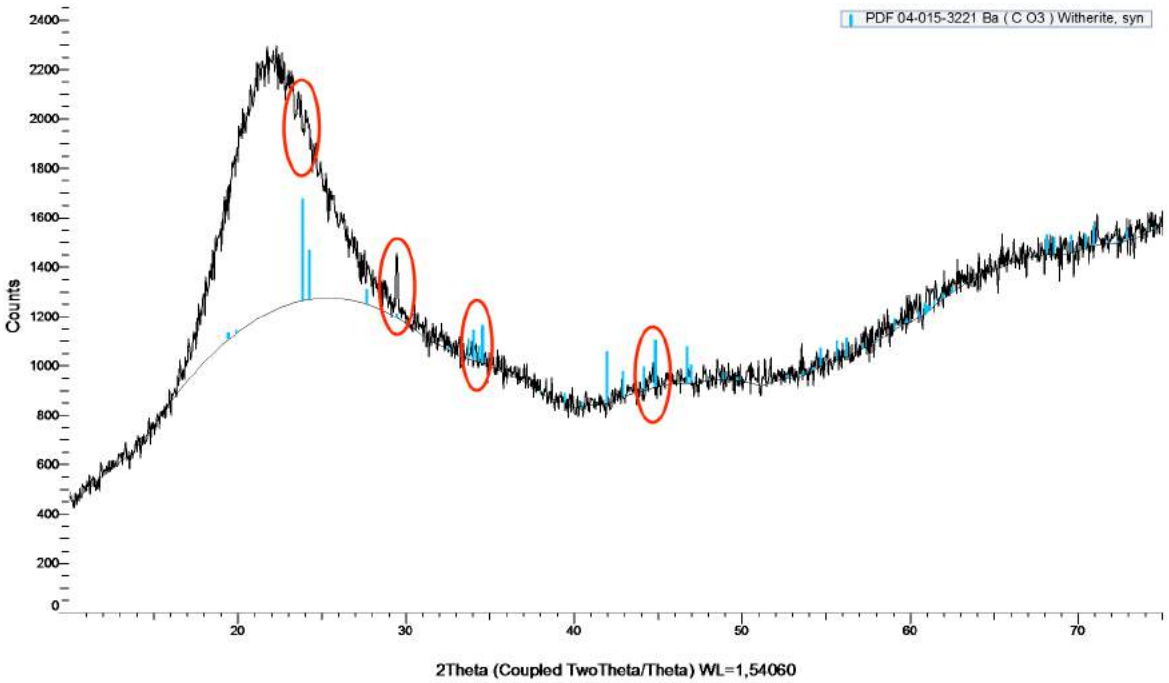

Figure 50: XRD pattern of A_{nc} with Barium carbonate reference pattern in blue: Large peak of amorphous quartz and some representative peaks of $BaCO_3$ highlighted in red

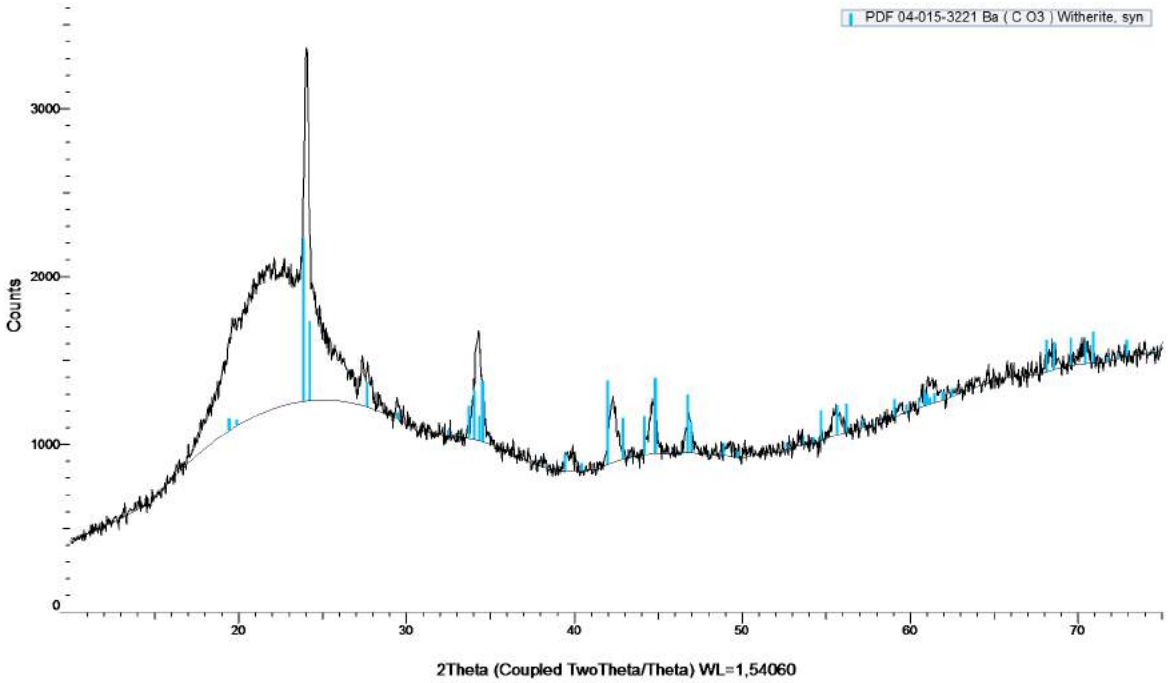

Figure 51: XRD pattern of A_n spray coated with Barium carbonate reference pattern in blue: Large peak of amorphous quartz and main representative peaks of $BaCO_3$ can be observed

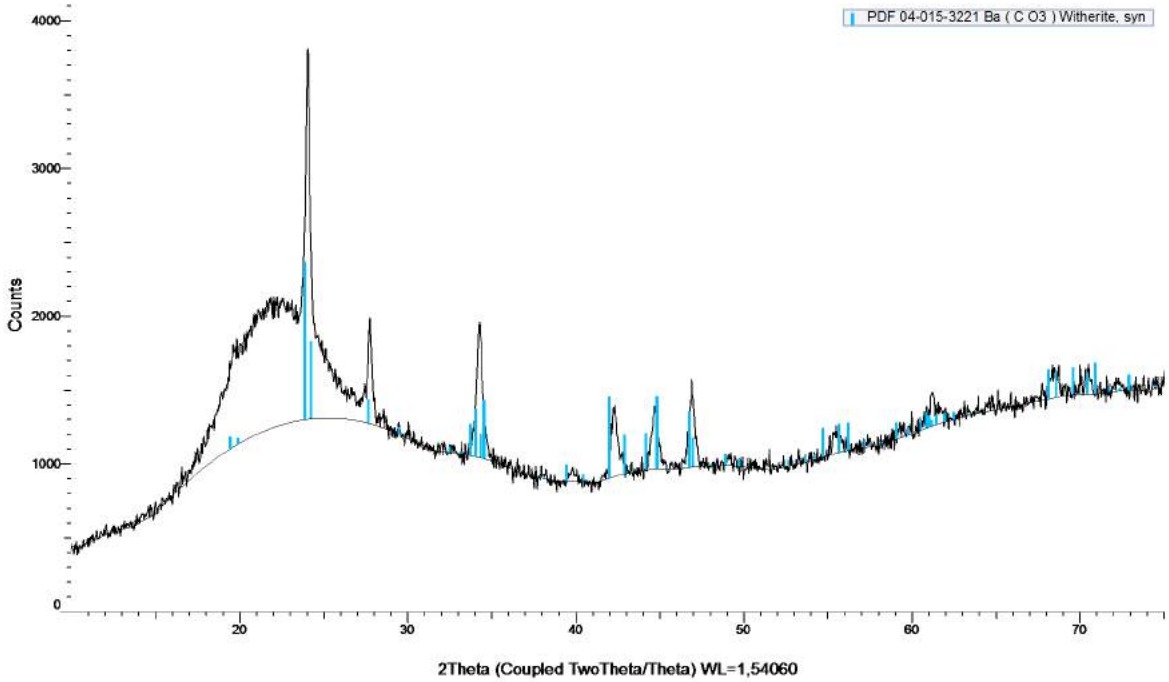

Figure 52: XRD pattern of B_n spray coated with Barium carbonate reference pattern in blue: Large peak of amorphous quartz and main representative peaks of $BaCO_3$ can be observed

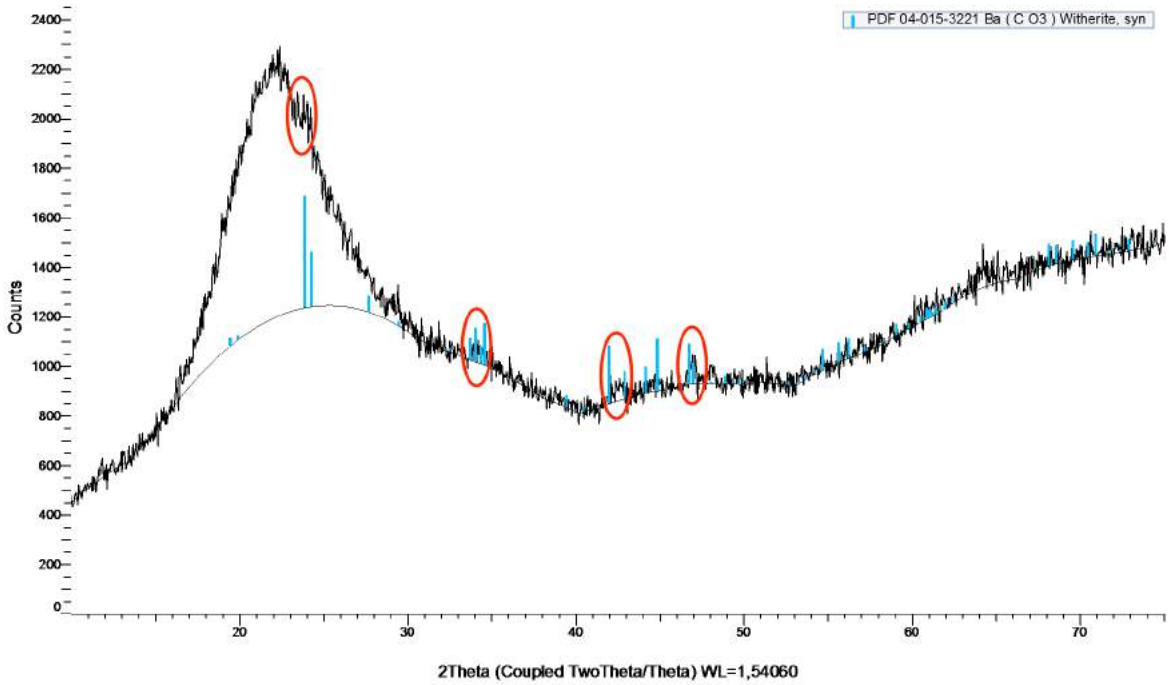

Figure 53: XRD pattern of A_n dip coated with Barium carbonate reference pattern in blue: Large peak of amorphous quartz and some representative peaks of $BaCO_3$ highlighted in red

4.1.2 Heat treatment 1: 90 min

Pictures of the resulting rod-containing crucibles after the 90 min heat treatment can be seen on Figure 54. It is observed that the small crucibles experience deformations and are subjected to cracks due to the pressure exerted on the wall by the expansion of the silicon feedstock when it solidifies. The cristobalite formation cannot be seen by eye on the rod surface except for the dip and spray coated pieces that, as it will be presented later, have developed a thicker cristobalite layer.

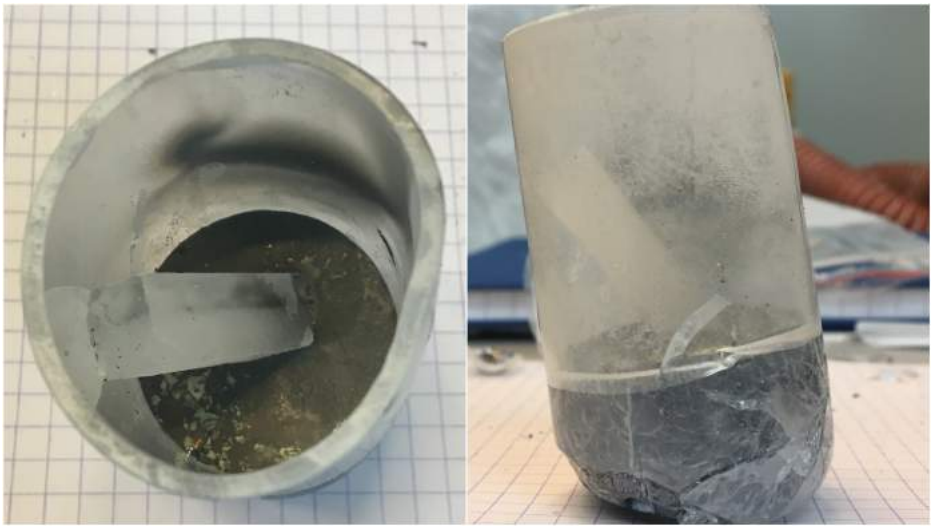

Figure 54: Resulting crucibles from HT1 of 90 min at high temperature

4.1.2.1 Cristobalite characterisation

Due to the presence of epoxy on the B_n, A_{nc} and Std_{nc}, the characterisation has been complicated or, in some cases, impossible. For B_n, no area without epoxy was observable at the light microscope. Figure 55 shows the most representative occurrences on A_n, B_{nc}, B_n (the epoxy cover) and Std_{nc} observed at the light microscope after 90min heat treatment. On Figure 56, the most representative cristobalite occurrences on A_{nc}, A_n spray coated, B_n spray coated and A_n dip coated are shown.

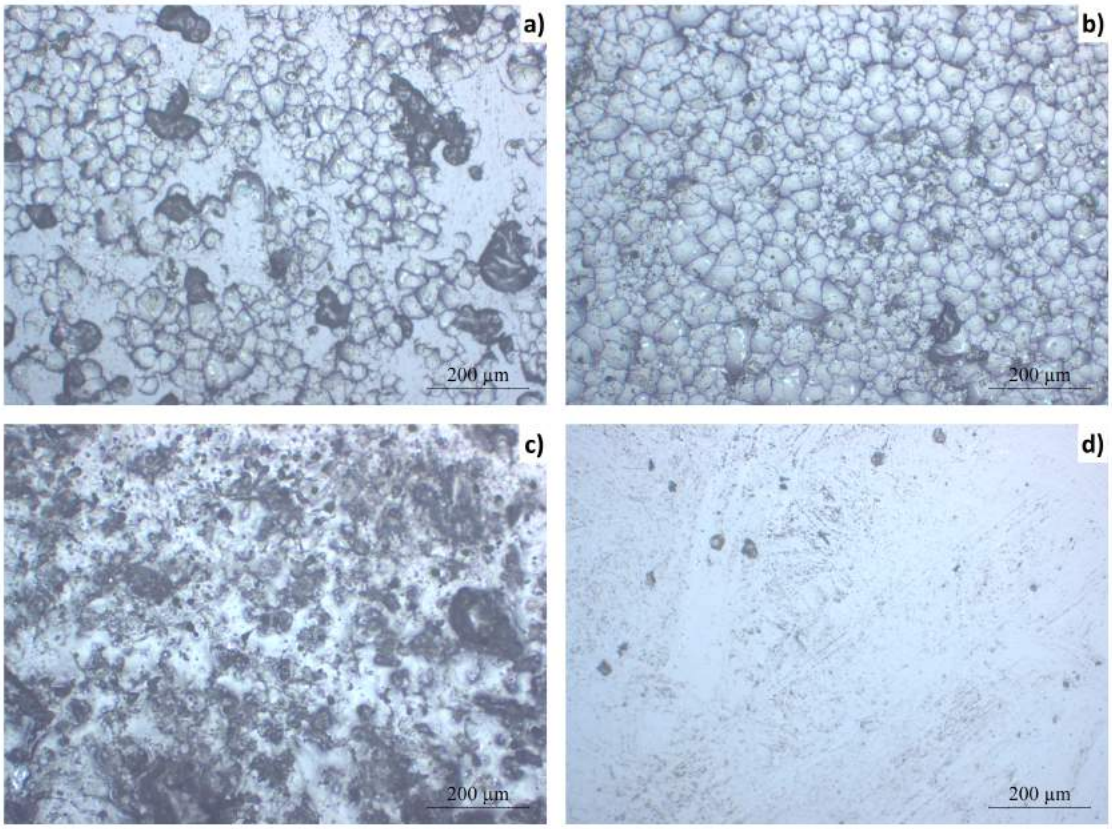

Figure 55: Light micrographs of the cristobalite occurrence after HT1 of 90 min: a) A_n, b) B_{nc}, c) B_n (epoxy cover), d) Std_{nc}

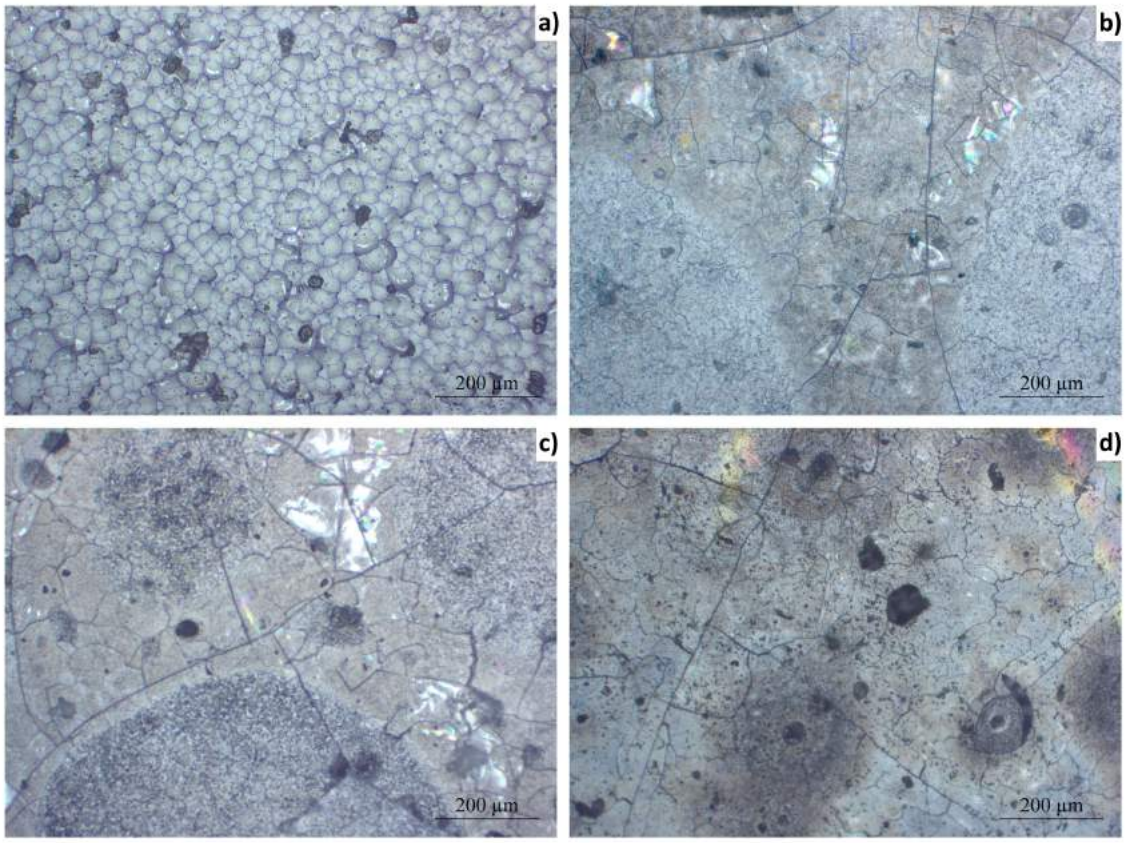

Figure 56: Light micrographs of the cristobalite occurrence after HT1 of 90 min: a) A_{nc}, b) A_n spray coated, c) B_n spray coated, d) A_n dip coated

As it can be seen from Figure 55d, for Std_{nc}, no occurrence of cristobalite has been found on the area that was not covered by epoxy while on A_n (Figure 55a), cristobalite is observed but no everywhere on the surface and for B_{nc} (Figure 55b), the cristobalite covers the entire surface of the sample.

On Figure 56a, it is observed that A_{nc} shows a similar morphology than B_{nc} with a presence of cristobalite on the whole surface while on the spray and dip coated pieces, the coating pattern seems to have influenced greatly the development of cristobalite. In fact, cristobalite seems to be present everywhere but inside the circular shape of the spray pattern, a denser cristobalite seems to have nucleated with mosaic tiles of smaller size than on the outside of the pattern where the brown appearance suggests a thiner layer with the tiles of larger dimensions. The same observations are made for the dip coated A_n crucible piece even if it is harder to see the elongated pattern at that magnification. Those observations are detailed on Figure 57 where the spray coating pattern is represented at lower magnification (5×) and a zoom inside the coating pattern and outside the coating pattern is made.

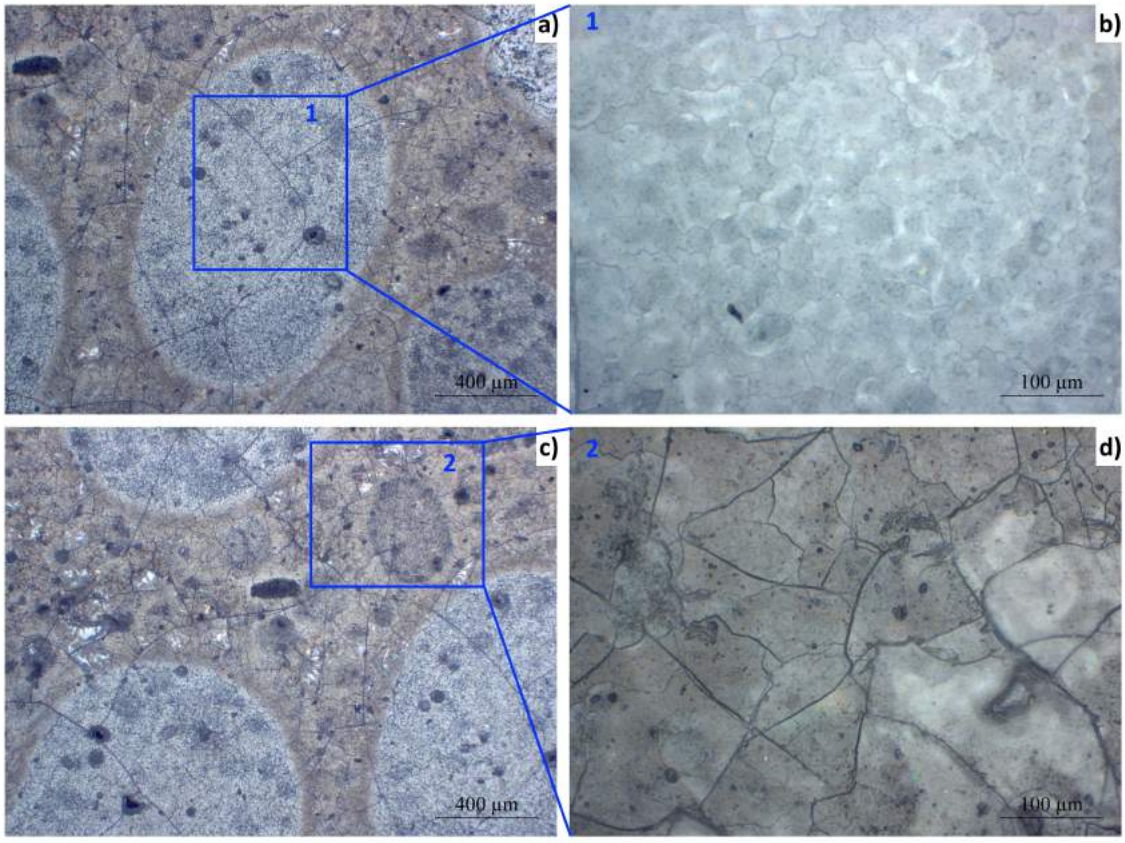

Figure 57: Light micrographs of the cristobalite occurrence after HT1 of 90 min: a) A_n spray coated, b) Zoom in Area 1 inside the spray coating pattern c) A_n spray coated, d) Zoom in Area 2 outside the spray coating pattern

On Figures 58, 59, 60, 61, 62, 63, 64 and 65, the XRD patterns are shown with the cristobalite reference pattern in red. It can be seen that for A_n, B_{nc} and A_{nc} (Figures 58, 59 and 62), the intensity ratios of the different peaks is similar to the reference pattern for "random" cristobalite. The preferred orientation is at an angle 2θ of 21.985 which corresponds to the orientation {101}.

The effect of the presence of the amorphous epoxy on B_n and Std_{nc} can be directly seen from the shape of the curves. For B_n, and Std_{nc} (Figures 60 and 61), a characteristic peak is observed at $2\theta = 28.439$ (orientation {111}) in addition to a low and large peak with a lot of background located at $2\theta = 21.985$. Those peaks have a really low number of counts (low crystallinity of the sample) so that no conclusion about a preferred orientation can be drawn.

Concerning the pieces coated at NTNU, it can be seen on Figures 63, 64 and 65 that the intensity ratios of the different peaks is not similar to the reference pattern for A_n dip and spray coated and B_n spray coated. They show a preferred orientation at 2θ of 36.080 which corresponds to the orientation {200}. In addition, the orientation $2\theta = 28.439$ (orientation {111}) seems proportionally more encountered on those samples than on the industrially coated samples.

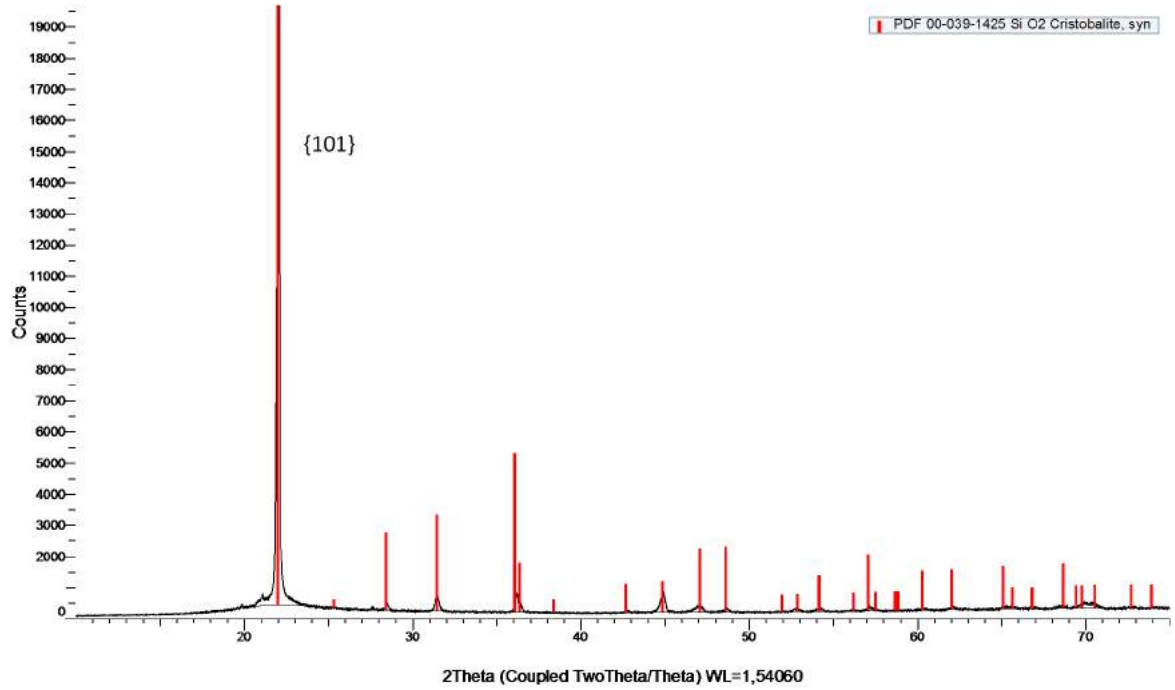

Figure 58: XRD pattern of A_n after HT1 of 90 min with cristobalite reference pattern in red

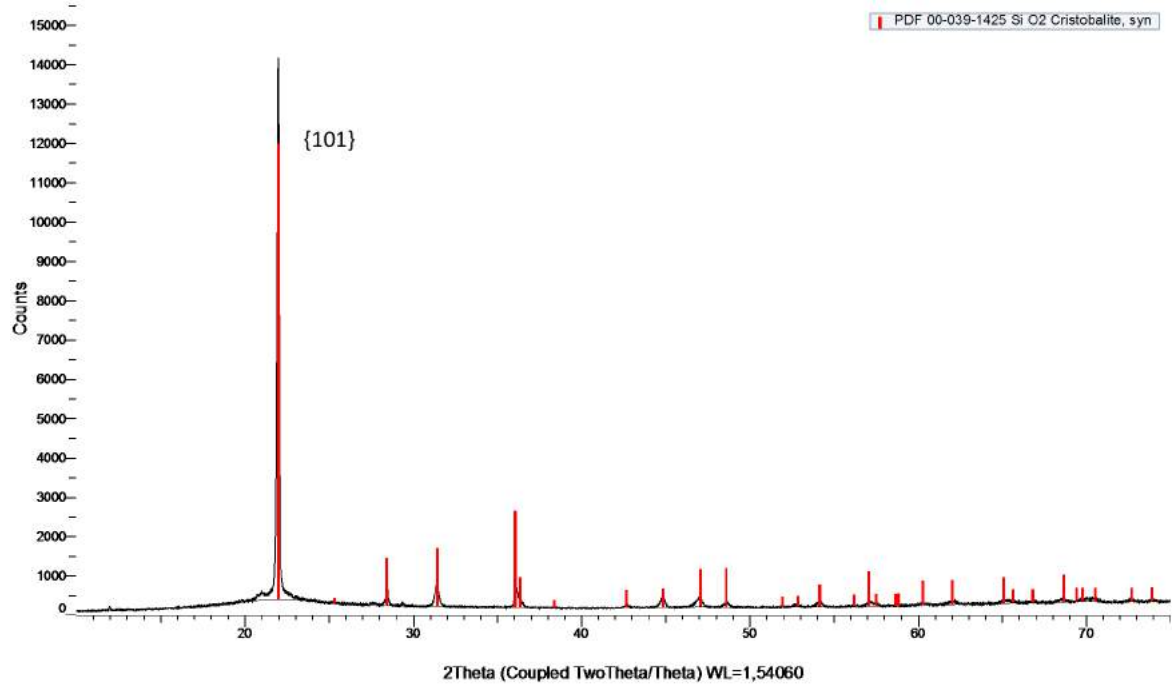

Figure 59: XRD pattern of B_{nc} after HT1 of 90 min with cristobalite reference pattern in red

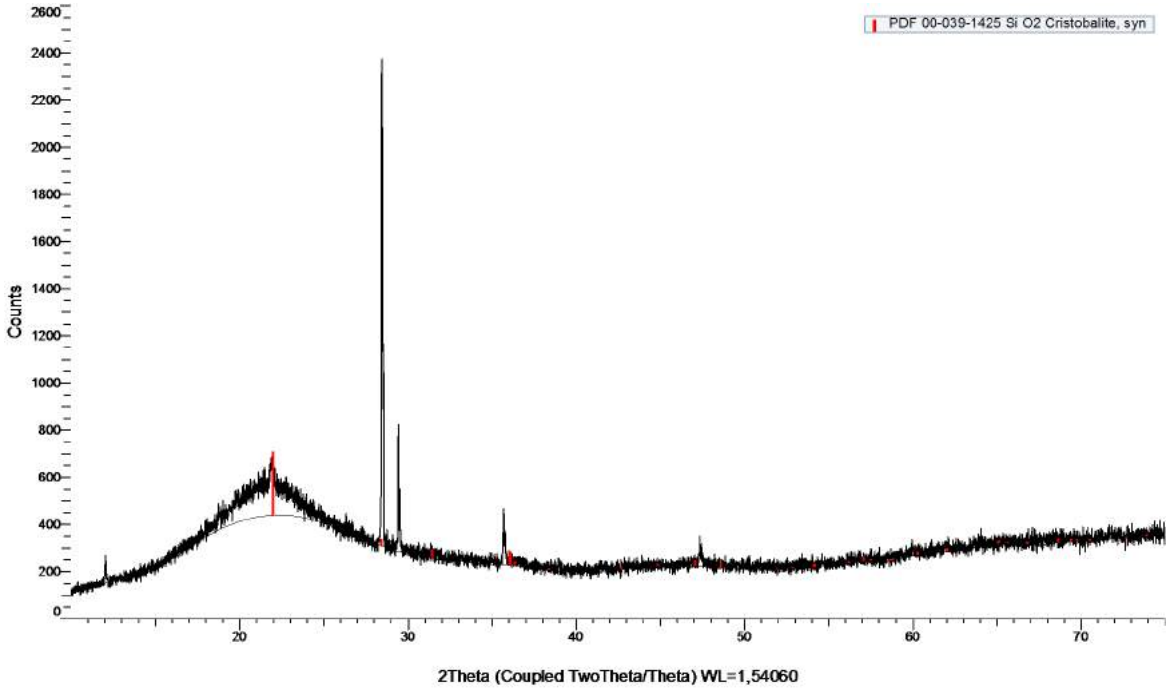

Figure 60: XRD pattern of B_n after HT1 of 90 min with cristobalite reference pattern in red

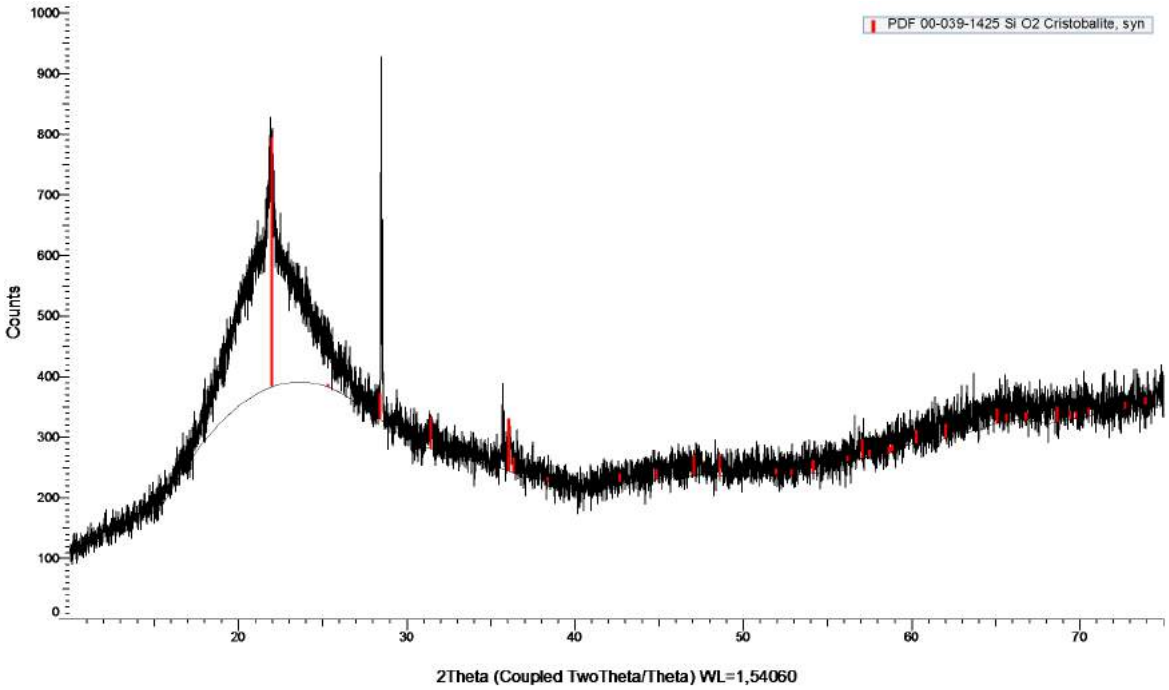

Figure 61: XRD pattern of Std_{nc} after HT1 of 90 min with cristobalite reference pattern in red

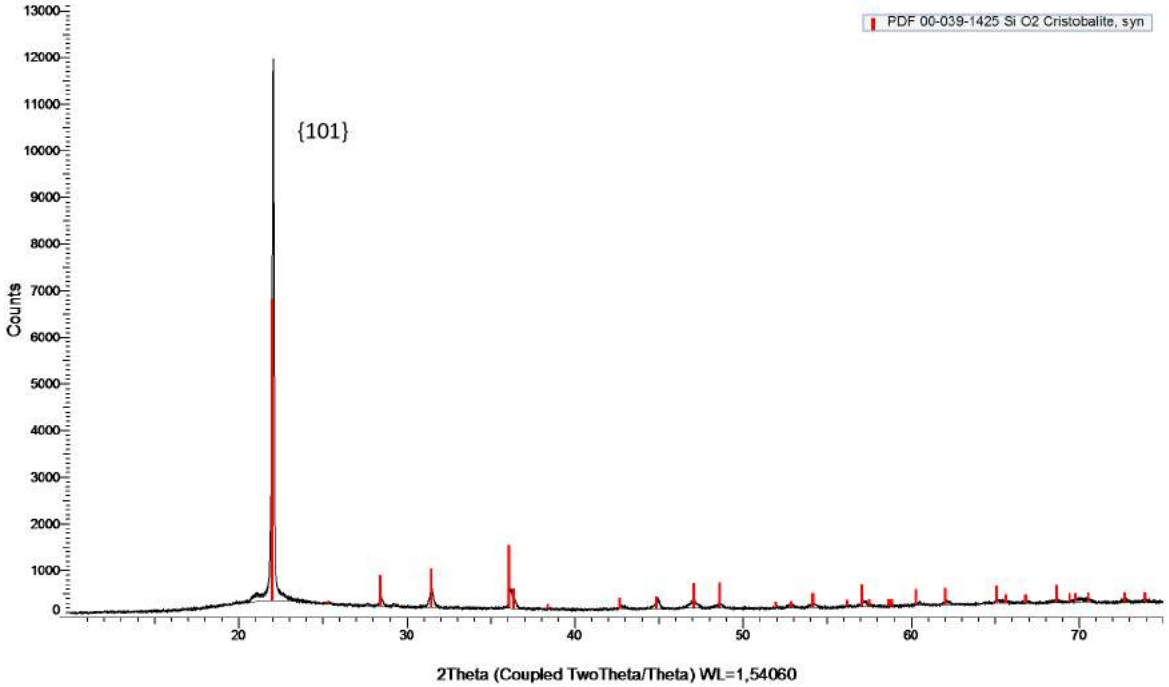

Figure 62: XRD pattern of A_{nc} after HT1 of 90 min with cristobalite reference pattern in red

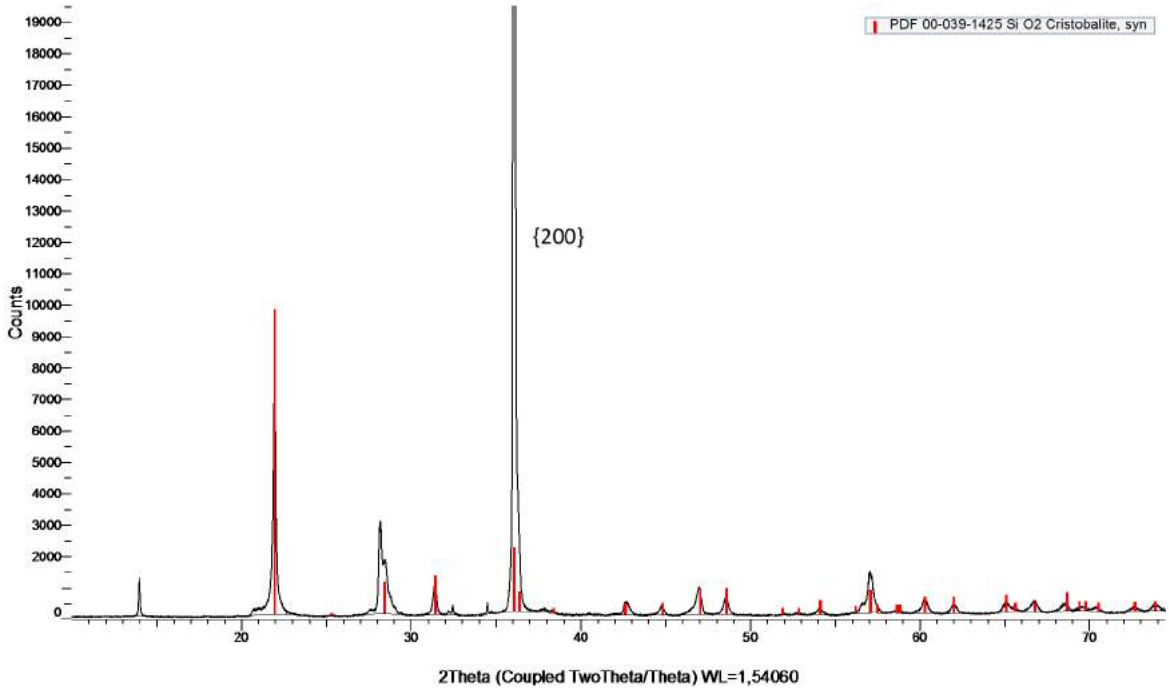

Figure 63: XRD pattern of A_n dip coated after HT1 of 90 min with cristobalite reference pattern in red

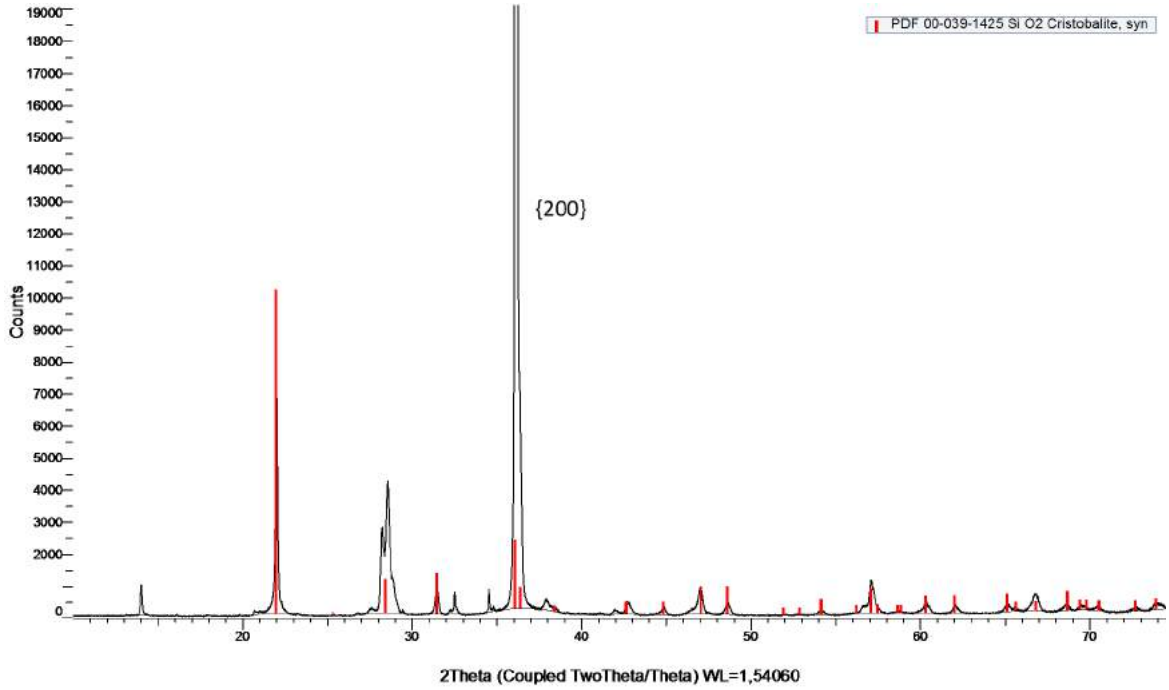

Figure 64: XRD pattern of A_n spray coated after HT1 of 90 min with cristobalite reference pattern in red

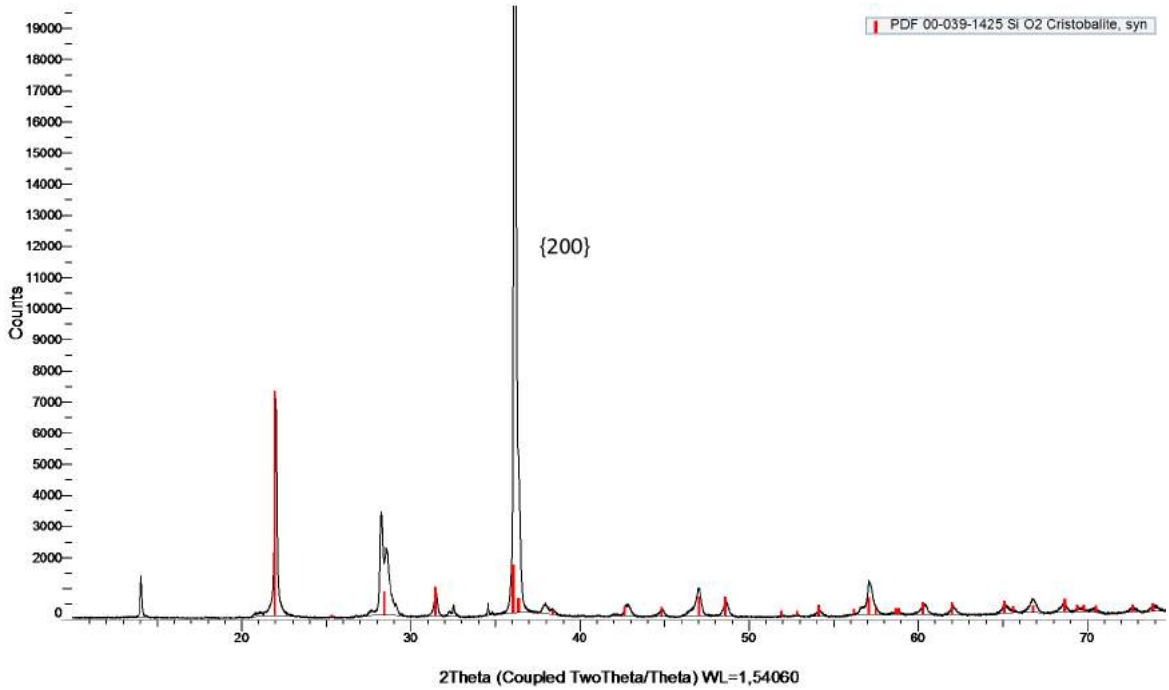

Figure 65: XRD pattern of B_n spray coated after HT1 of 90 min with cristobalite reference pattern in red

Figure 66 shows the intervals in which the thickness of the cristobalite layer observed on each crucible rod after HT1 of 90 min varies. In fact, most of the layers present large variations due to the dependence on the surface quality (e.g cracks, impurities) for the cristobalite nucleation and development. The most representative values for the different thicknesses are in blue on the graph. They correspond to the values that are homogeneous on a large part of the cross section of the sample.

For B_n, the layer thickness varies too much so that no representative value is highlighted but the layer thickness varies in the range 10 to 58 μm. In general, it can be seen that the coated crucibles have a slightly thicker cristobalite layer in terms of representative values of the thickness but the difference with the non coated pieces is not large at all for the industrially coated crucibles. On the other hand, the pieces coated at NTNU show a large difference in term of representative thickness value.

Some representative pictures of the layers can be found in Appendix A.2 where it can be seen that the layers sometimes consist only in few crystals and are not homogeneous except for the pieces coated at NTNU. It has been observed that the cristobalite is thicker at the corner of the rods pieces but since there are no corners on an entire crucible used in the CZ process, those measurements were not considered as relevant for the study.

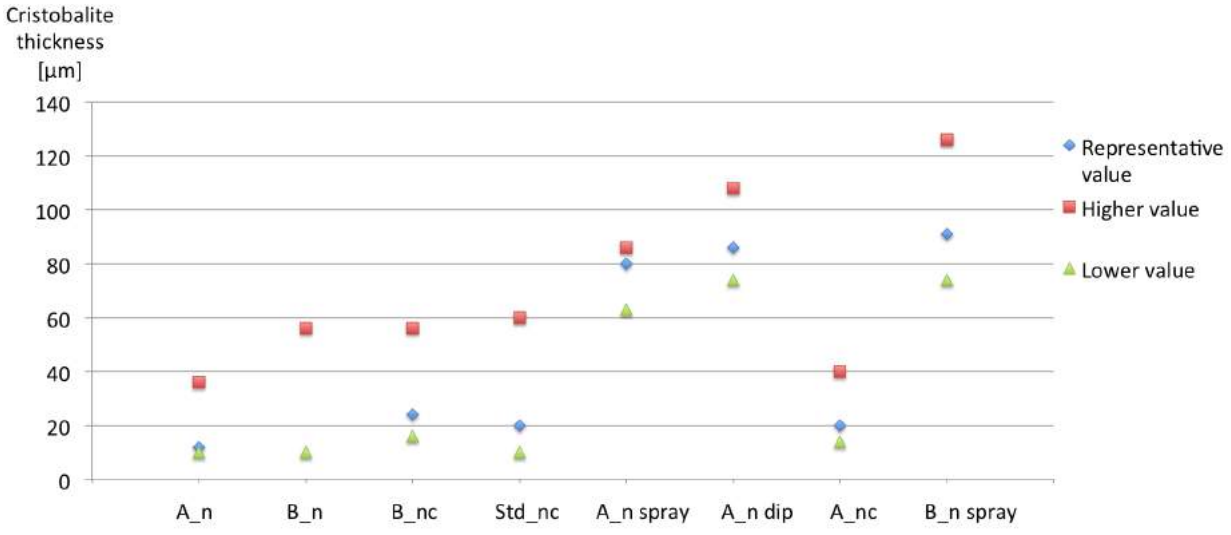

Figure 66: Intervals of values for the thickness of the cristobalite layer on the different types of crucibles after HT1 of 90 min

4.1.3 Heat treatment 1: 10 h

Pictures of the resulting rod-containing crucibles after the 10 h heat treatment can be seen on Figure 79. While for the 90 min experiment, the small crucibles were visibly subjected to deformations and cracks, a longer time exposure at high temperature seems to allow the development of a relatively homogeneously spread cristobalite layer on the crucible that improves the resistance of the crucible to the cracks and deformations. Cristobalite can be observed by eye on the rods but only on the corners of the piece except for the dip and spray coated pieces that are completely covered by a white cristobalite layer.

Figure 67: Resulting crucibles from HT1 of 10 h at high temperature

4.1.3.1 Cristobalite characterisation

Figure 68 shows the most representative cristobalite occurrences on A_n, B_{nc}, B_n and Std_{nc} observed at the light microscope after 10 h heat treatment while on Figure 69, the most representative cristobalite occurrences on A_{nc}, A_n spray coated, B_n spray coated and A_n dip coated are shown. As it can be seen, all of the samples show a cristobalite occurrence on their whole surface.

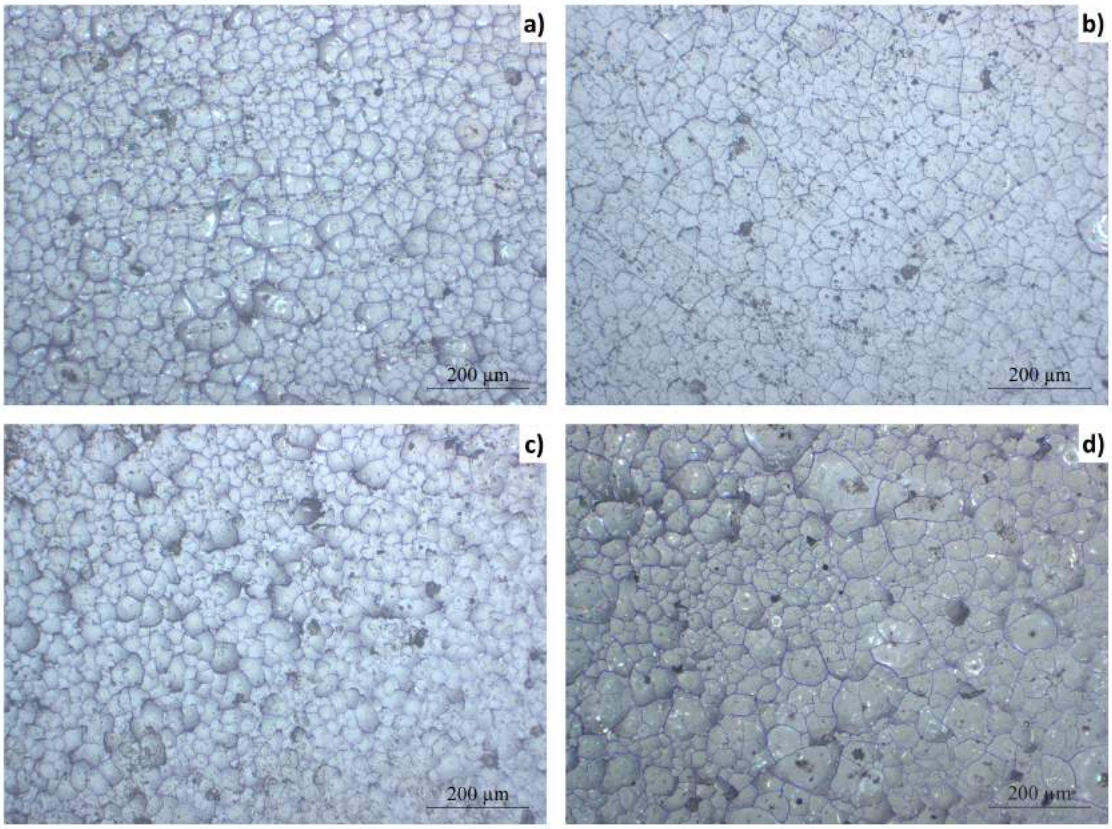

Figure 68: Light micrographs of cristobalite occurrence after HT1 of 10 h: a) A_n, b) B_{nc}, c) B_n, d) Std_{nc}

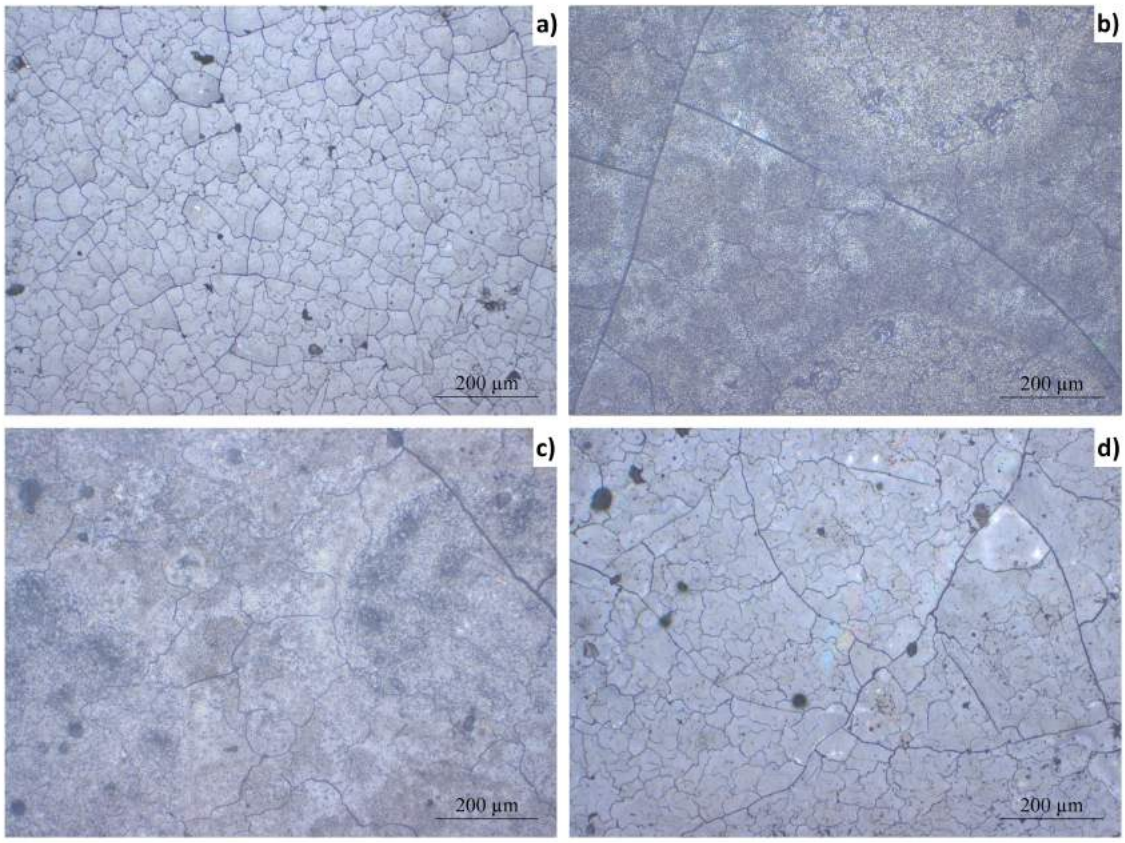

Figure 69: Light micrographs of cristobalite occurrence after HT1 of 10 h: a) A_{nc}, b) A_c spray coated, c) B_n spray coated, d) A_n dip coated

From Figure 68d, it can be seen that for Std_{nc}, the size of the tiles varies a lot and the maximum size is about two to three times the maximum tile size observed on A_n, B_{nc} and B_n. The layer that seems to have the most uniform morphology is the one observed on the industrially coated B_{nc} crucible (Figure 68b).

When looking at Figure 69, it can be highlighted that the layer on A_{nc} (Figure 69a) is similar to the one observed on B_{nc} (Figure 68b). On the other hand, the layers obtained from the crucible pieces coated at NTNU present different features. As already mentioned for HT1 of 90min, there is an influence from the coating pattern on the cristobalite development. It is still obvious for A_n spray coated and B_n spray coated (Figure 68b and 68c). However, for A_n dip coated (Figure 68d), the morphology is similar to the industrially coated pieces. What cannot be seen on Figure 68d but is represented on Figure 70 is that the morphology of A_n dip coated actually varies a lot.

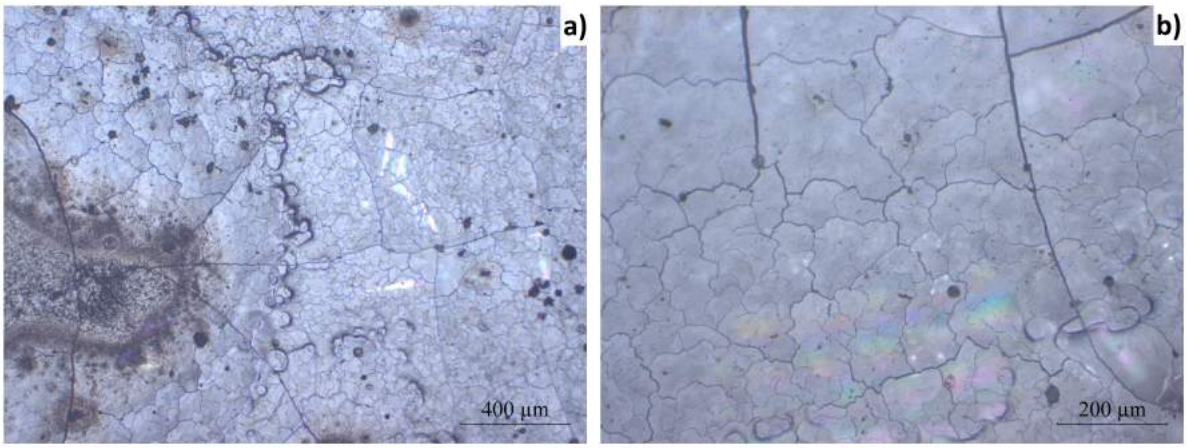

Figure 70: Light micrographs of the different cristobalite occurrences observed on A_n dip coated after HT1 of 10 h: a) At magnification 5× b) At magnification 10×

On Figures 71, 72, 73, 74, 75, 76 and 77 the XRD patterns are shown with the cristobalite reference pattern in red. Std_{nc} could not be characterised by XRD due to the lack of material available after heat treatment.

It can be seen that for A_n, B_{nc}, B_n and A_{nc} (Figures 71, 72, 73 and 74), the intensity ratios of the different peaks is similar to the reference pattern for "random" cristobalite. The preferred orientation is at $2\theta = 21.985$ which corresponds to the orientation {101} that seems independent of the presence of a coating. No other component pattern can be observed since every peak (even the smallest) seems to correspond to cristobalite.

On the other hand, for the pieces coated at NTNU, it can be seen on Figures 75, 76 and 77 that the intensity ratios of the different peaks is not similar to the reference pattern. For A_n dip coated (Figure 75), the preferred orientation is at 2θ of 36.080 (orientation $\{200\}$) but the orientation at $2\theta = 21.985$ ($\{101\}$) is also largely present.

Concerning A_n and B_n spray coated, the intensity ratios of the different peaks is also not similar to the reference pattern. They show a preferred orientation at 2θ of 36.080 which corresponds to the orientation $\{200\}$, same orientation observed for those coated crucibles after HT1 of 90 min. In addition, as after HT1 of 90 min, the orientation at $2\theta = 28.439$ (orientation $\{111\}$) also seems proportionally more encountered on those samples than on the industrially coated samples.

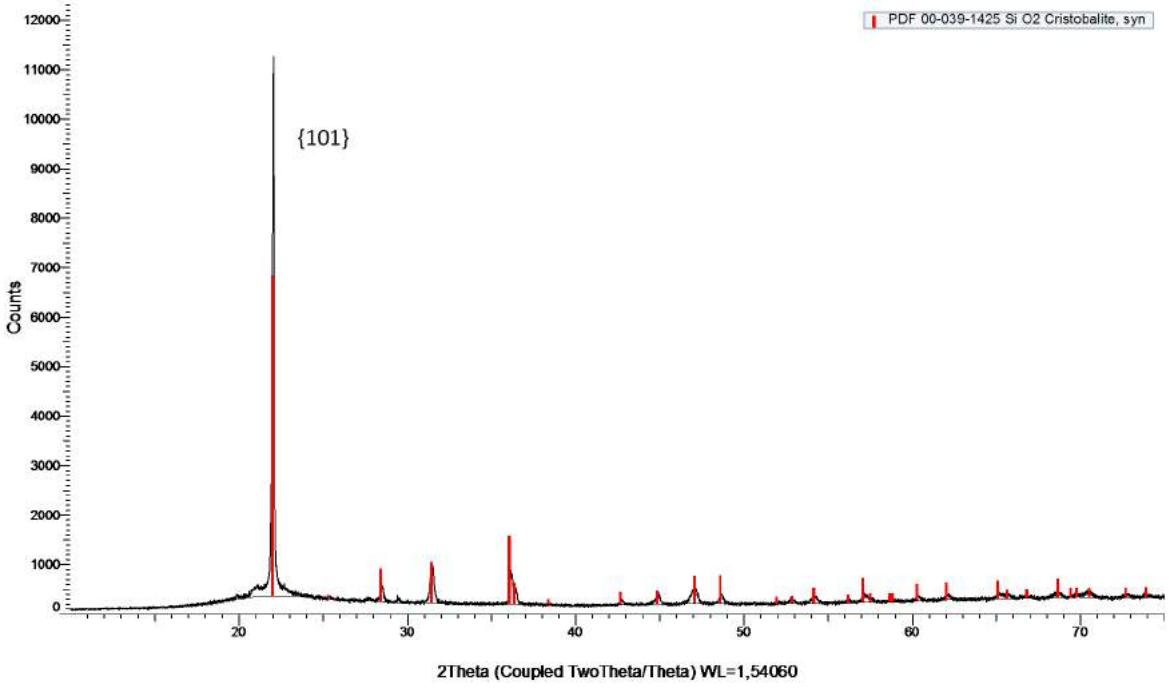

Figure 71: XRD pattern of A_n after HT1 of 10 h with cristobalite reference pattern in red

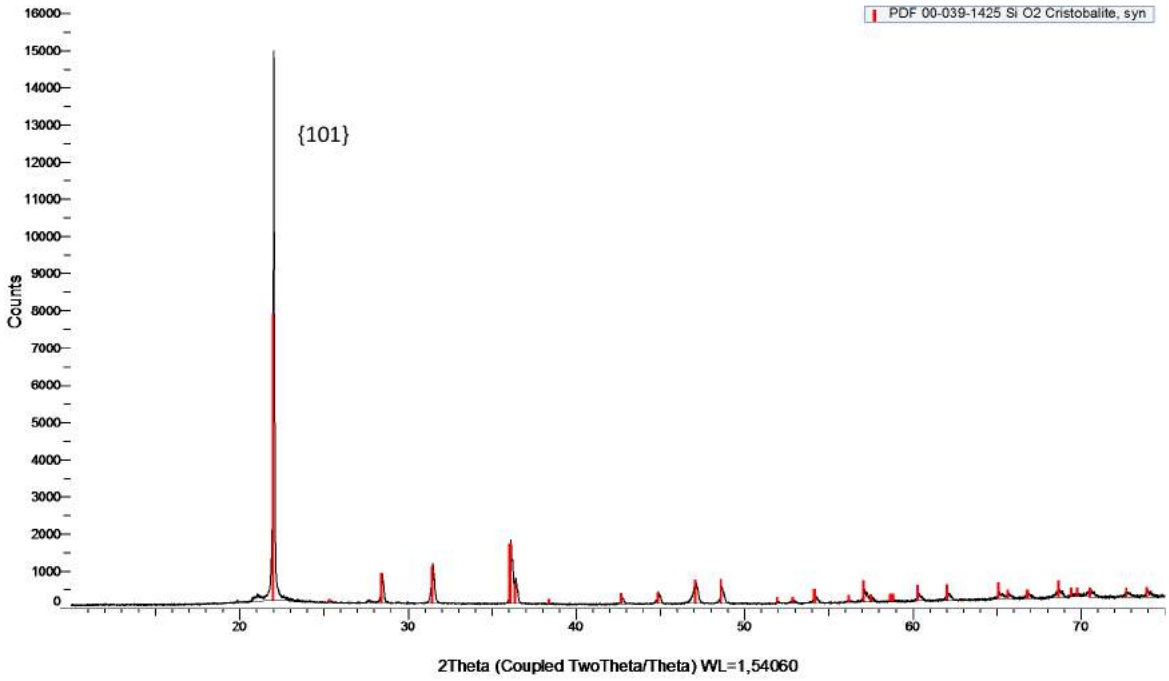

Figure 72: XRD pattern of B_{nc} after HT1 of 10 h with cristobalite reference pattern in red

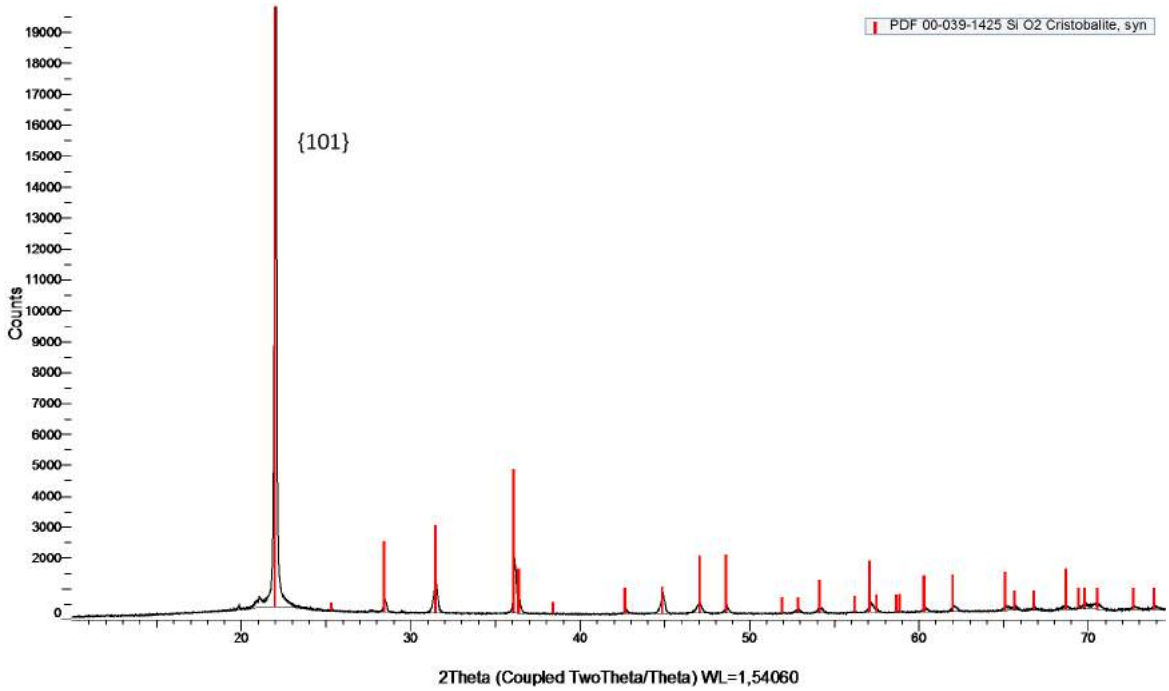

Figure 73: XRD pattern of B_n after HT1 of 10 h with cristobalite reference pattern in red

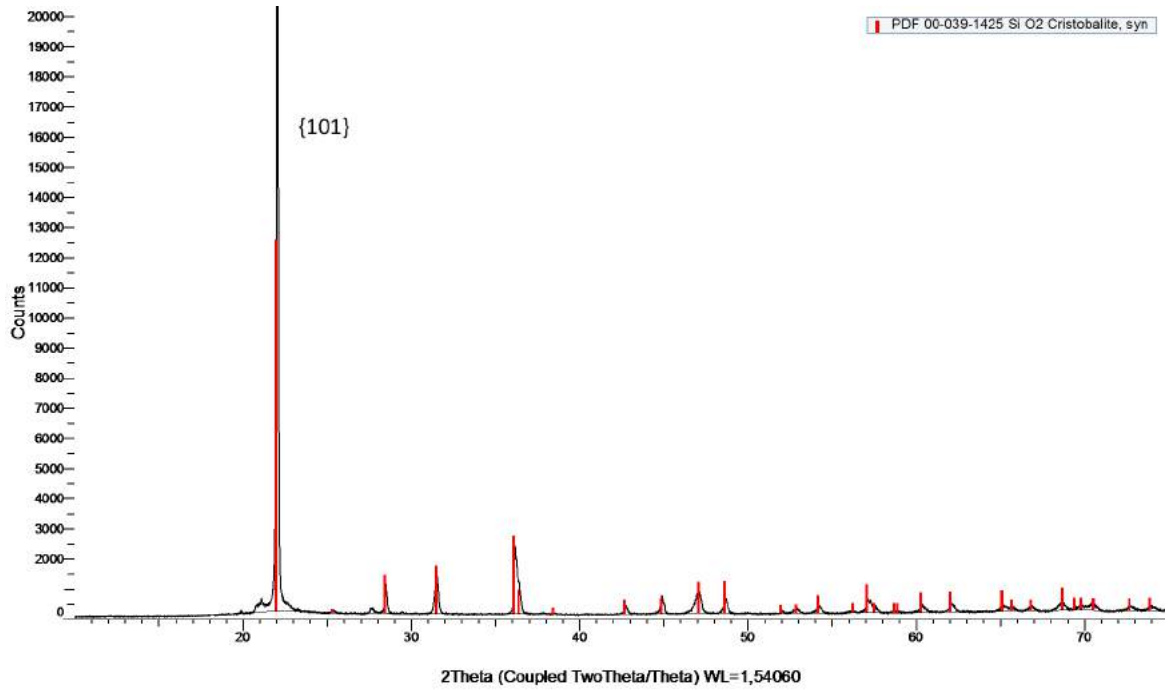

Figure 74: XRD pattern of A_{nc} after HT1 of 10 h with cristobalite reference pattern in red

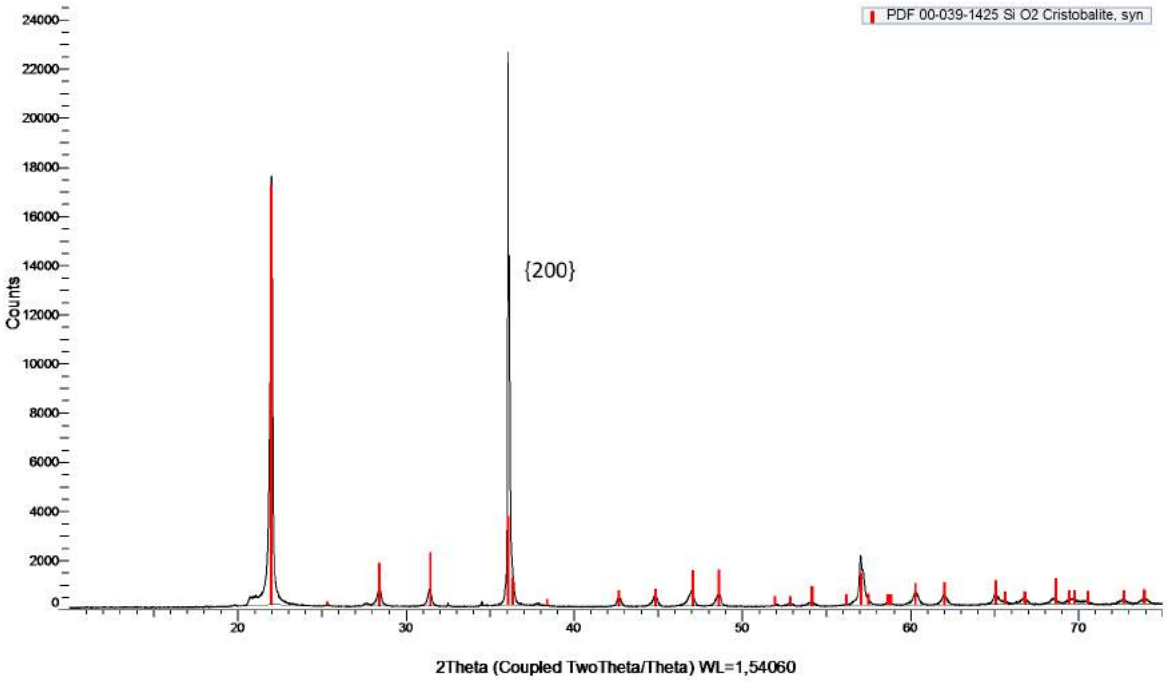

Figure 75: XRD pattern of A_n dip coated after HT1 of 10 h with cristobalite reference pattern in red

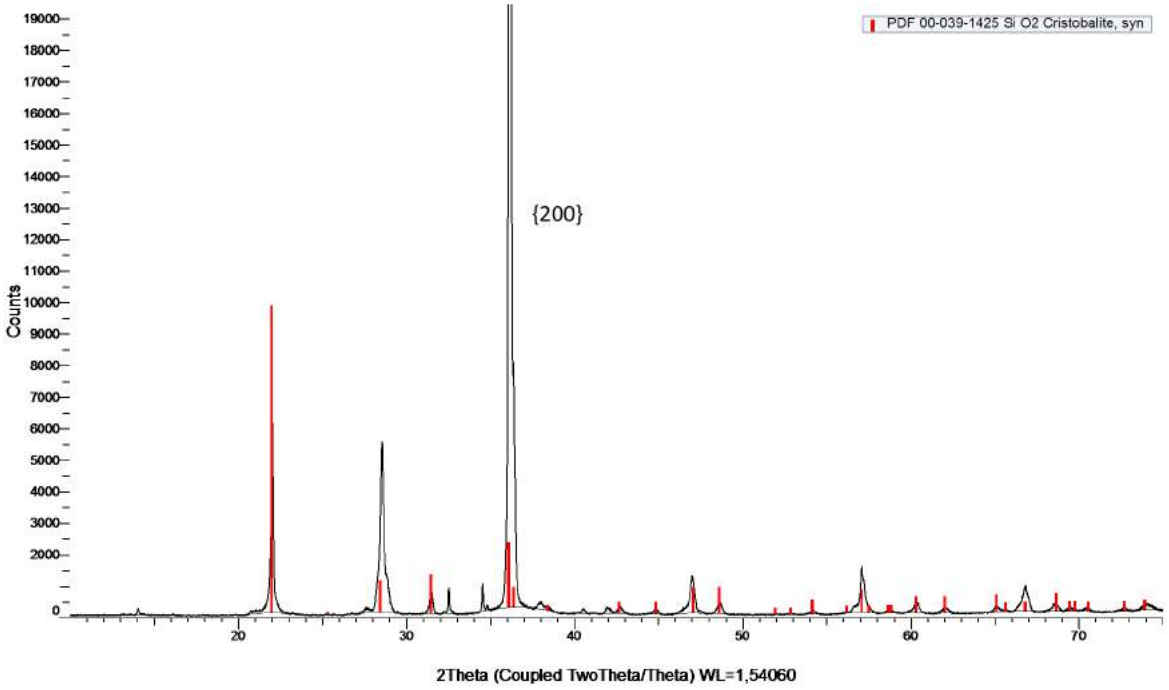

Figure 76: XRD pattern of A_n spray coated after HT1 of 10 h with cristobalite reference pattern in red

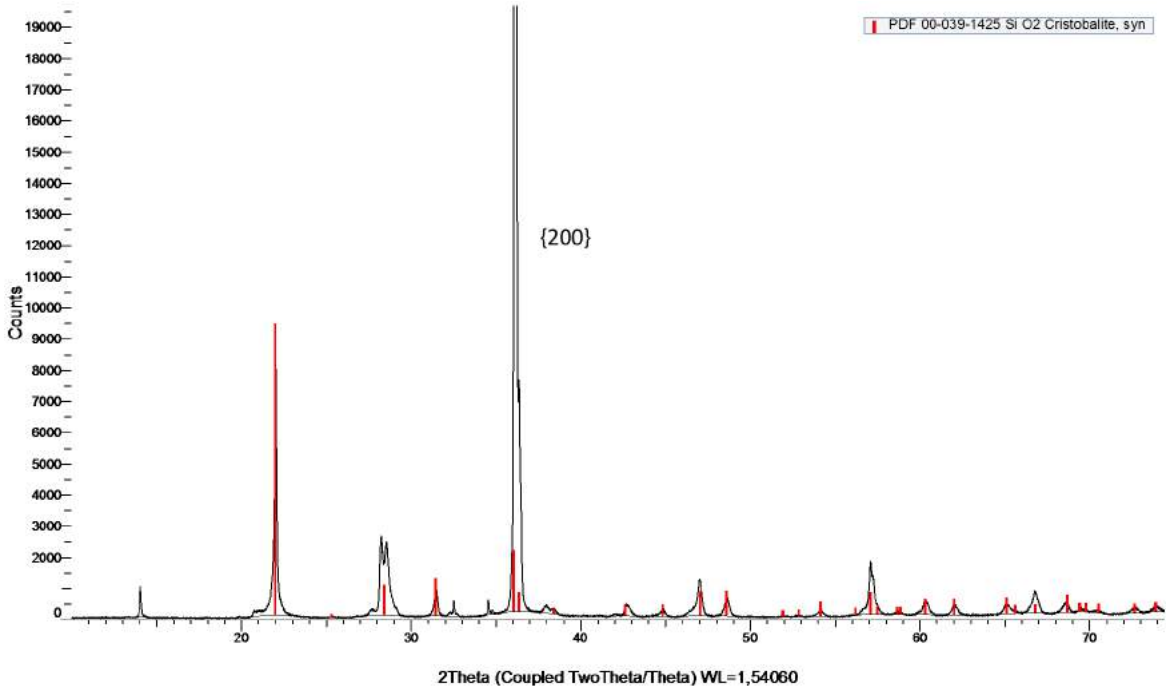

Figure 77: XRD pattern of B_n spray coated after HT1 of 10 h with cristobalite reference pattern in red

The graph on Figure 78 shows the intervals in which the thickness of the cristobalite layer observed on each crucible rod after HT1 of 10 h varies. As for HT1 of 90 min, some inherent inaccuracies are present but as it can be seen on the pictures in Appendix A.3, the thickness of the layers is more homogeneous than after HT1 of 90min in many cases. The most representative values for the different thicknesses are in blue on the graph. B_{nc} and A_{nc} have a higher value for the thickness than the non-coated crucibles. On the other hand, Std_{nc} has a low value that is similar to the one observed after HT1 of 90 min. Concerning the pieces coated at NTNU, they have again developed a thicker cristobalite layer than the industrially coated pieces.

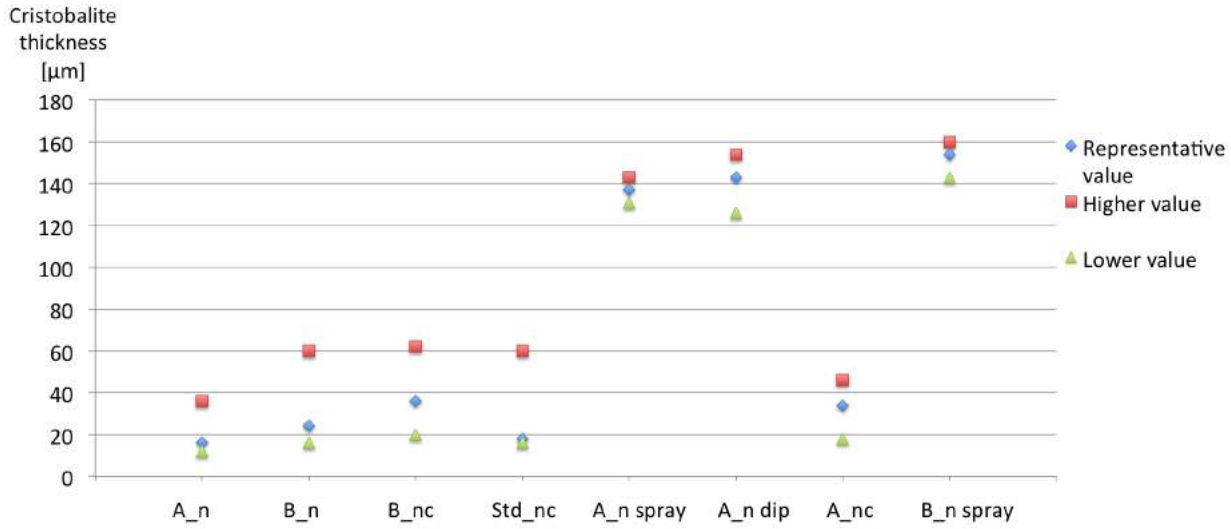

Figure 78: Intervals of values for the thickness of the cristobalite layer on the different types of crucibles after HT1 of 10 h

4.1.4 Heat treatment 1: 24 h

Pictures of the resulting rod-containing crucibles after the 24 h heat treatment can be seen on Figure 79. As for the 90 min experiment, the small crucibles have been subjected to cracks where the melt expanded upon cooling but the top part of the crucible does not seem deformed. However, there is way less cristobalite development on the crucible than after 10 h heat treatment. This might come from the quality and purity of those small quartz crucibles that was not reproduced between the batch used for the 10 h and the one used for the 24 h. In fact the quality of the quartz affects the cristobalite development as presented in Section 2.3. Concerning the rods, cristobalite can be observed by eye on all of them.

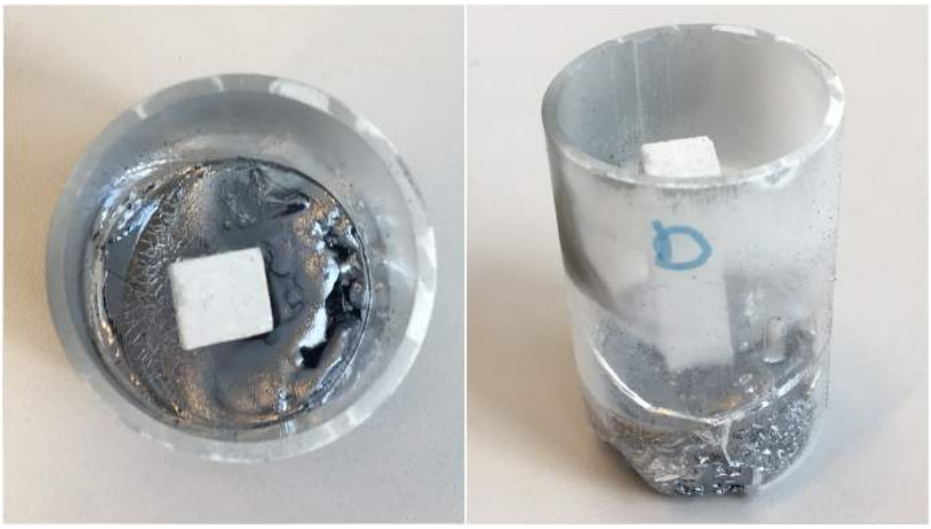

Figure 79: Resulting crucibles from HT1 of 24 h at high temperature

4.1.4.1 Cristobalite characterisation

The experiment was not performed on A_{nc}, A_n dip coated, A_n spray coated and B_n spray coated due to repetitive furnace failures that took a long time to be fixed so that no results concerning those crucible types and coating types are available for HT1 of 24 h.

Figure 80 shows the most representative cristobalite occurrences on A_n, B_{nc}, B_n and Std_{nc} observed at the light microscope after 24 h heat treatment. As it can be seen, all of the samples show a cristobalite occurrence on their whole surface. For A_n, the tiles are larger and vary more in size than on the other crucible pieces. It can be seen that, for all the samples, the layer looks dense and large cracks are present.

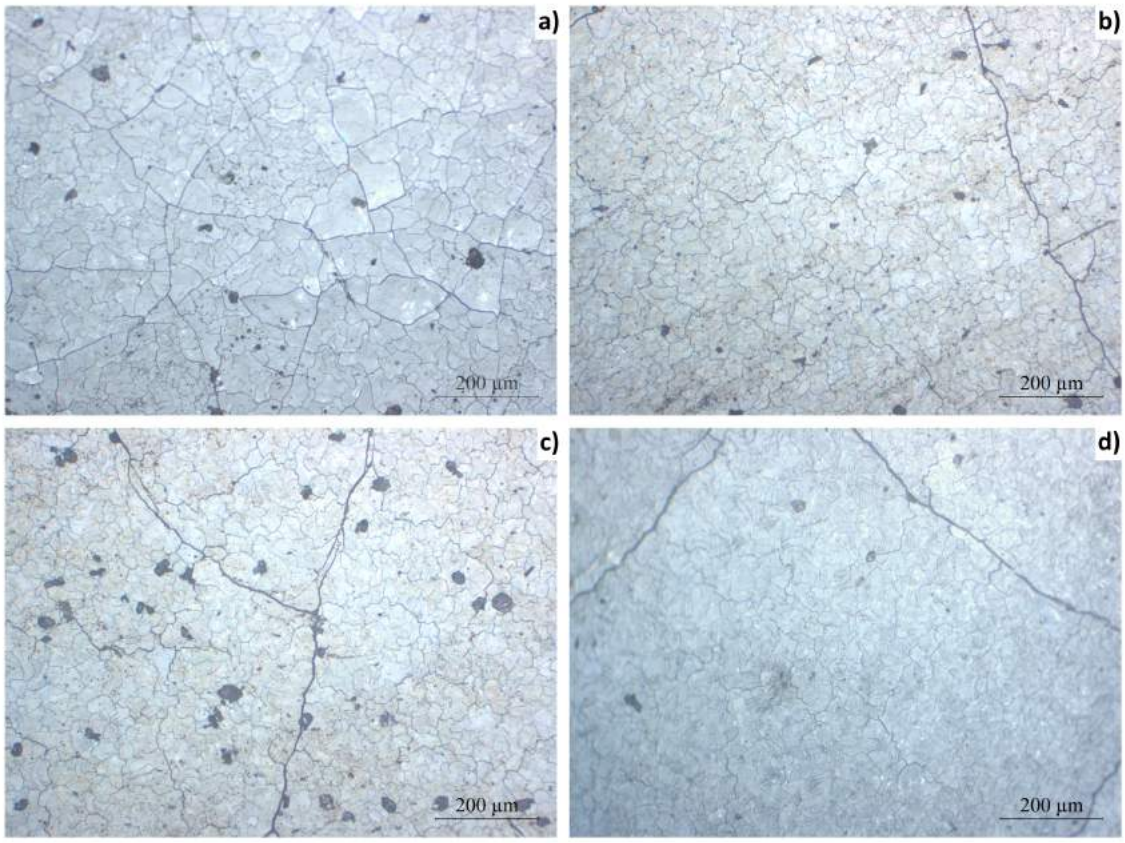

Figure 80: Light micrographs of cristobalite occurrence after HT1 of 24 h: a) A_n, b) B_{nc}, c) B_n, d) Std_{nc}

On Figures 81, 82 and 83, the XRD patterns are shown with the cristobalite reference pattern in red. B_{nc} could not be characterised by XRD due to the lack of material available after heat treatment. It can be seen that for A_n, B_n and Std_{nc}, the intensity ratios of the different peaks is similar to the reference pattern for "random" cristobalite. The preferred orientation is at an angle 2θ of 21.985 which corresponds to the orientation {101} that seems independent of the presence of a coating. No other component pattern has been identified.

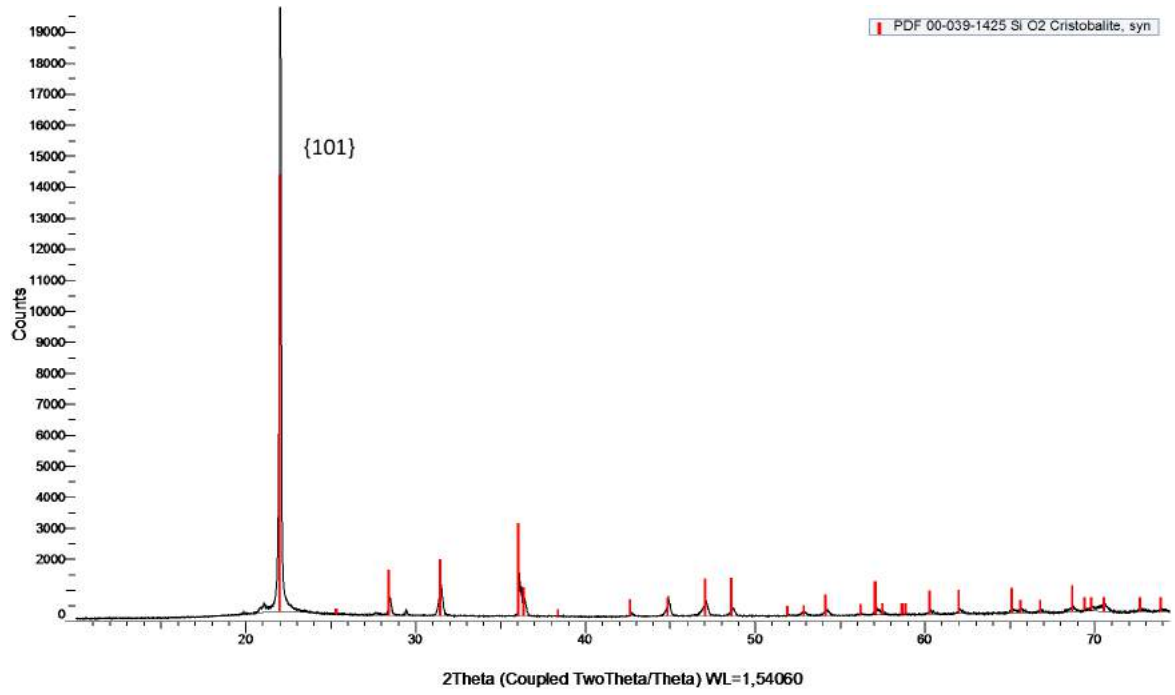

Figure 81: XRD pattern of A_n after HT1 of 24 h with cristobalite reference pattern in red

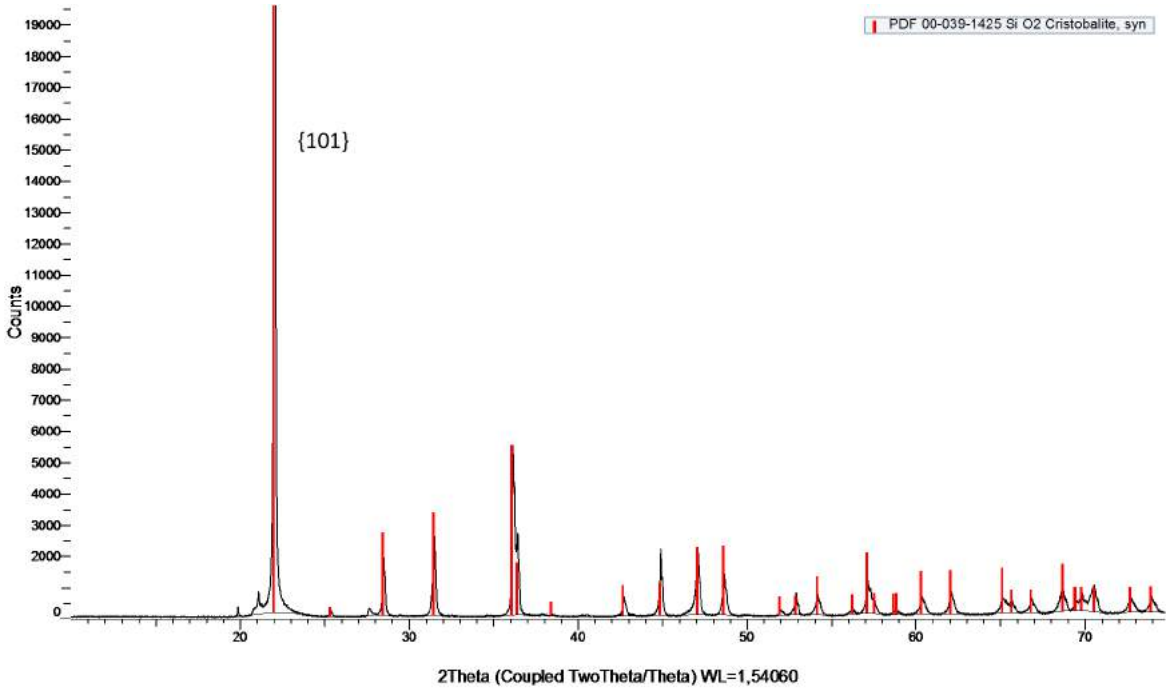

Figure 82: XRD pattern of B_{nc} after HT1 of 24 h with cristobalite reference pattern in red

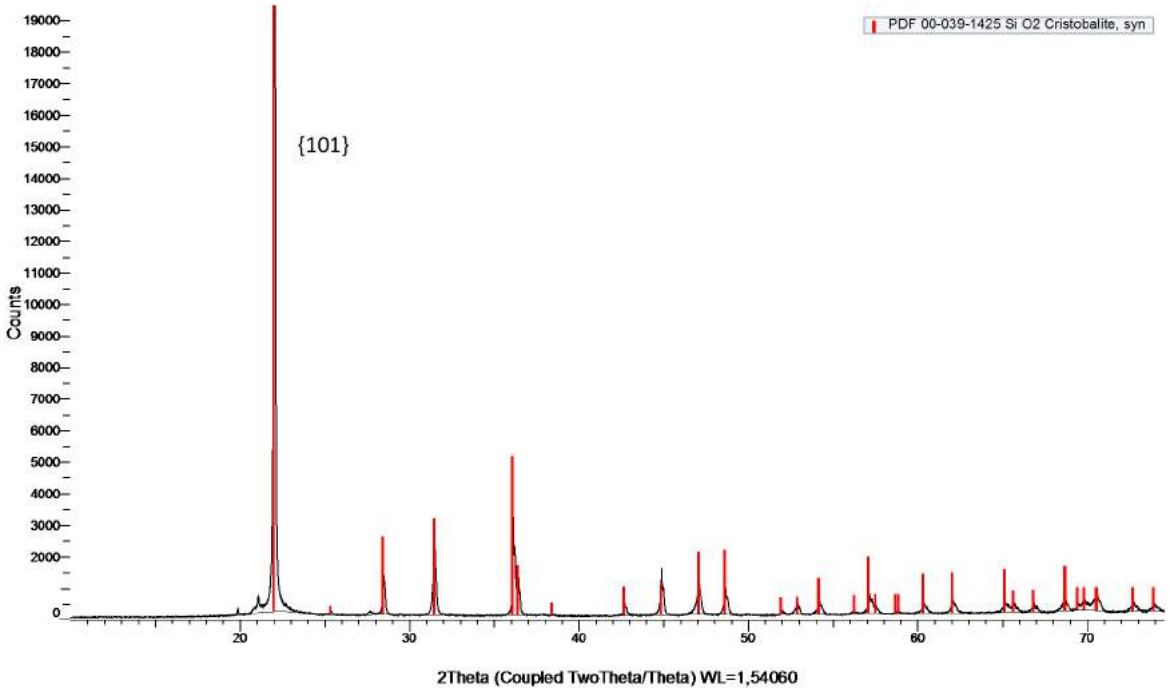

Figure 83: XRD pattern of Std_n after HT1 of 24 h with cristobalite reference pattern in red

The graph on Figure 84 shows the intervals in which the thickness of the cristobalite layer observed on each crucible rod after HT1 of 24 h varies. As for HT1 of 90 min and HT1 of 10 h, some inherent inaccuracies are present but as it can be seen on the pictures in Appendix A.4, the thickness of the layers is homogeneous, the variations mainly come from local points where the cristobalite certainly developed due to an intrinsic defect at the surface. The most representative values for the different thicknesses are in blue on the graph. B_{nc} has a higher value for the thickness than the non coated crucibles. In addition, the layer on B_{nc} is more homogeneous with only small differences between the lower, higher and representative values of the thickness measured. On the other hand, Std_{nc} presents a representative value for the thickness that is closer and even a bit lower than those observed for non coated crucibles (A_n and B_n).

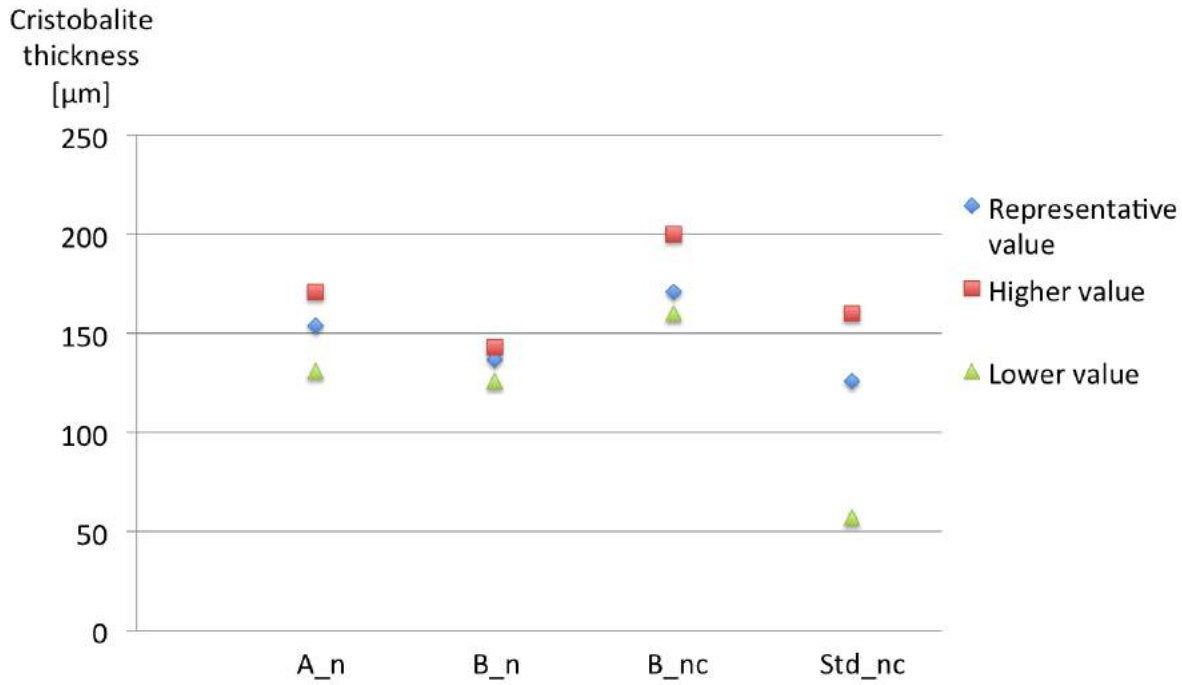

Figure 84: Intervals of values for the thickness of the cristobalite layer on the different types of crucibles after HT1 of 24 h

4.1.5 Heat treatment 2 (CZ): 10 h

Figure 85 shows the rods set-up for A_{nc} and Std_{nc} after HT2 in the Czochralski puller. It can be seen that the rods have a certain loss in thickness in the lengths that were dipped into the melt. This loss is approximately 1mm and is due to the dissolution of the quartz in contact with the very reactive silicon melt. The rod has been divided in 4 pieces of approximate dimensions 1.5x1x1 cm : pieces 2 (below the melt level) and 3 (right above the melt level) represent the material investigated while pieces 1 and 4 are used in the parallel study about the bubble content in quartz crucibles.

Figure 85: HT2 resulting rods after 10 h in the melt

4.1.5.1 Temperature simulation of the CZ furnace

The result from the temperature modelling in the CZ furnace performed by a SINTEF engineer with the logiciel CGSim is shown on Figure 86, where the entire furnace is represented with a small quartz rod in the center of the melt. A zoom on the quartz rod material dipped in the melt can be seen on Figure 87.

Table 11 summaries the surface temperature intervals (i.e. where the cristobalite forms) of the different pieces from the bottom of the piece to the top according to the simulation. The values are presented in degrees Kelvin and Celsius.

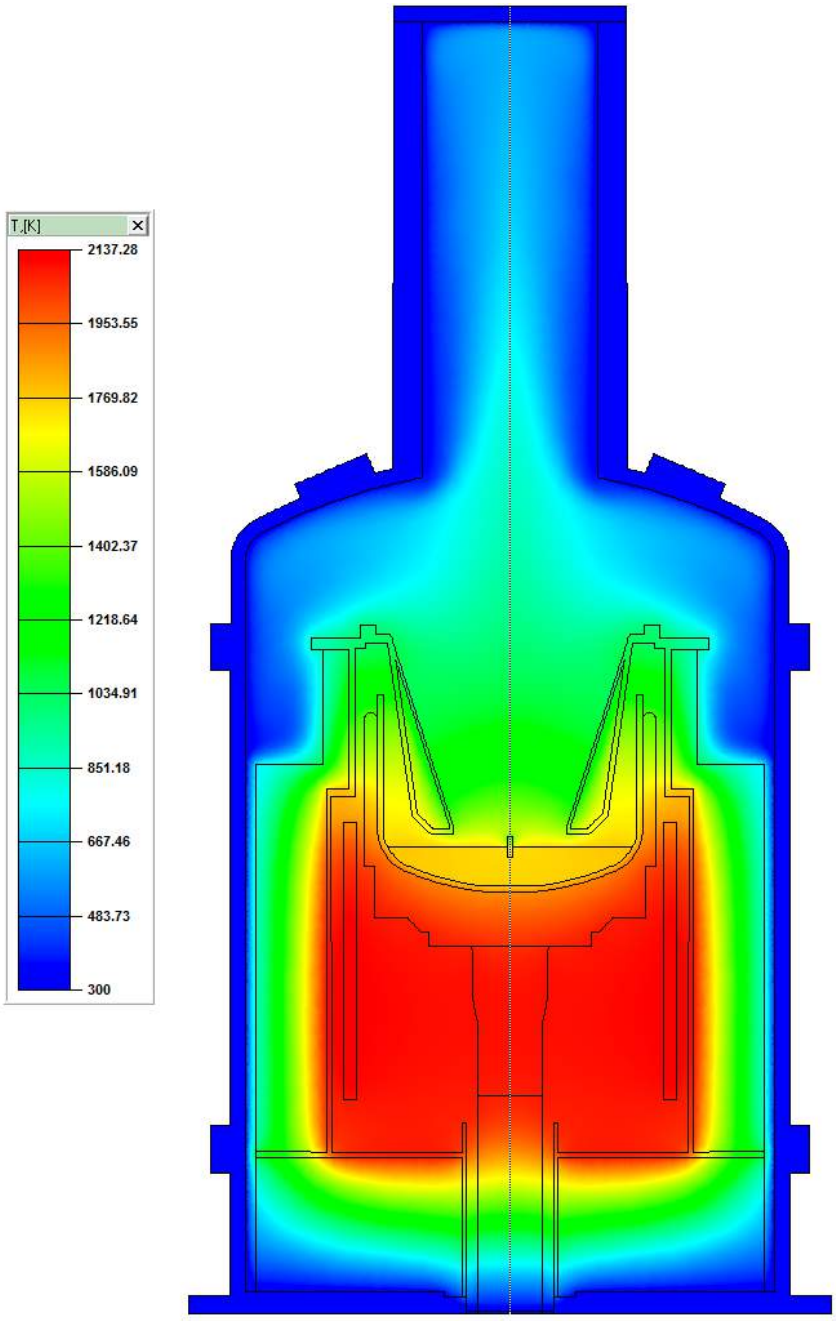

Figure 86: Temperature simulation of the CZ puller from the CGSim results [67]

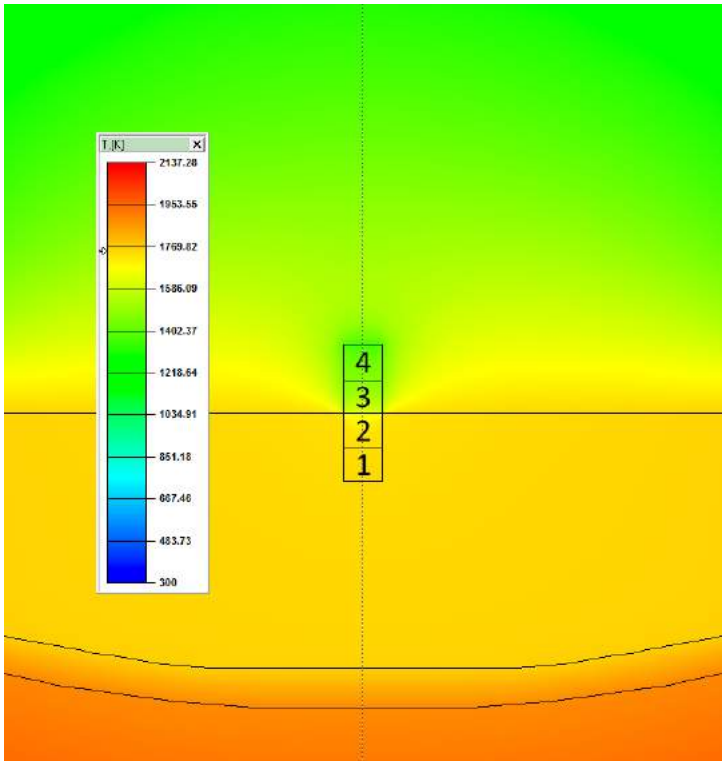

Figure 87: Quartz rod material temperatures during HT2 of 10h

Table 11: Approximate intervals of surface temperatures for the quartz rods during HT2 in function of the position on the rod

Position #	**1**	**2**	**3**	**4**
Surface temperature interval (bottom to top) [°K]	[1746 ; 1740]	[1740 - 1650]	[1650 ; 1465]	[1465 ; 1380]
Surface temperature interval (bottom to top) [°C]	[1473 ; 1467]	[1467 ; 1377]	[1377 ; 1192]	[1192 ; 1107]

This temperature simulation gives a good idea of the temperature difference between the two samples studied (Pieces 2 and 3). While "2", the part dipped in the melt during HT2, experiences temperatures of about 1400°C, "3", the part right above the melt level, is subjected to temperatures as low as 1200°C.

4.1.5.2 Cristobalite characterisation

The different occurrences of cristobalite for A_{nc} and Std_{nc} can be seen on Figures 88 and 89. Those light micrographs demonstrate the presence of cristobalite tiles on the top surface of the rod (Piece 3) for A_{nc} (Figure 88d) while for Std_{nc}, no growth has been observed (Figure 89d). For both A_{nc} and Std_{nc}, the morphology of the surface that was in contact with the melt (Piece 2) presents dissolved/corroded circular areas with some brownish cristobalite particles. In the case of Std_{nc}, it is the only occurrence observed with the rest of the surface that seemed to be filled with very small brownish particles and only two small cristobalite areas with tiles are observed. On the other hand, A_{nc} shows more "white" cristobalite on localised and large areas.

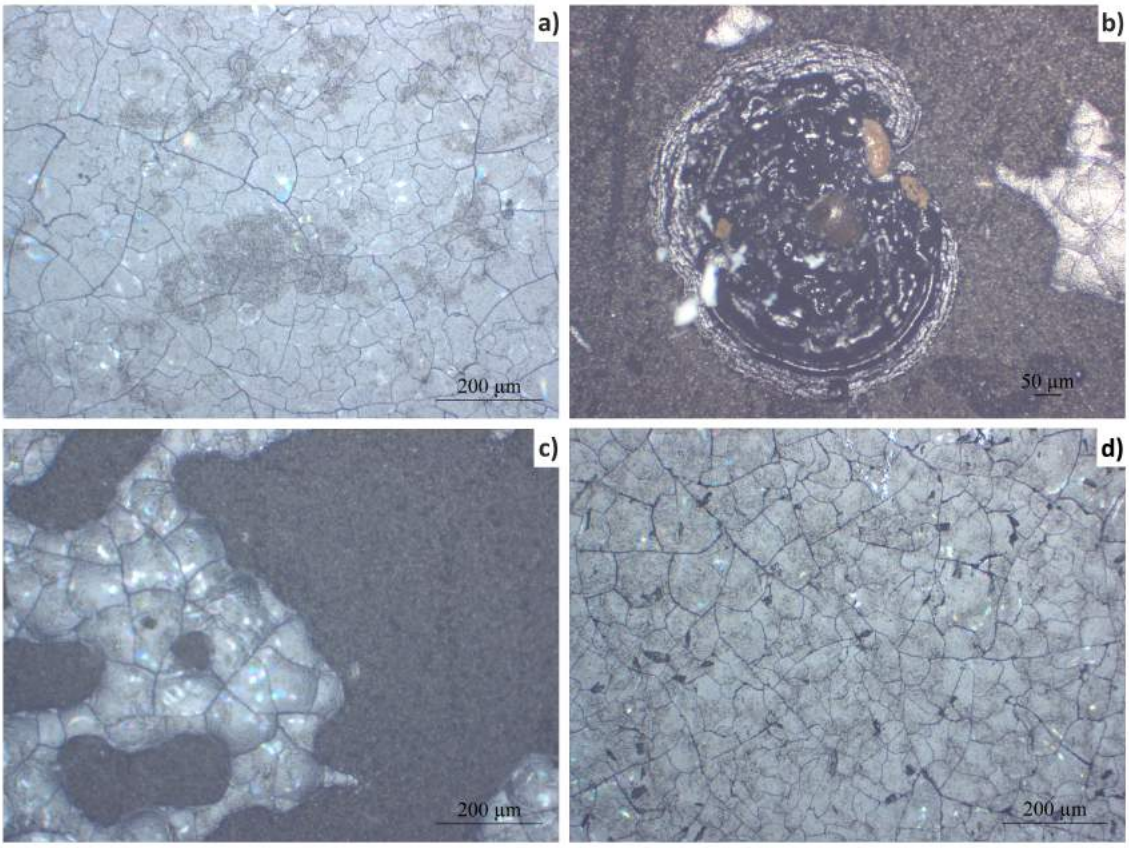

Figure 88: Light micrographs of the cristobalite occurrences on A_{nc} after HT2 of 10 h: a) Piece 2, b) Piece 2, c) Piece 2, d) Piece 3

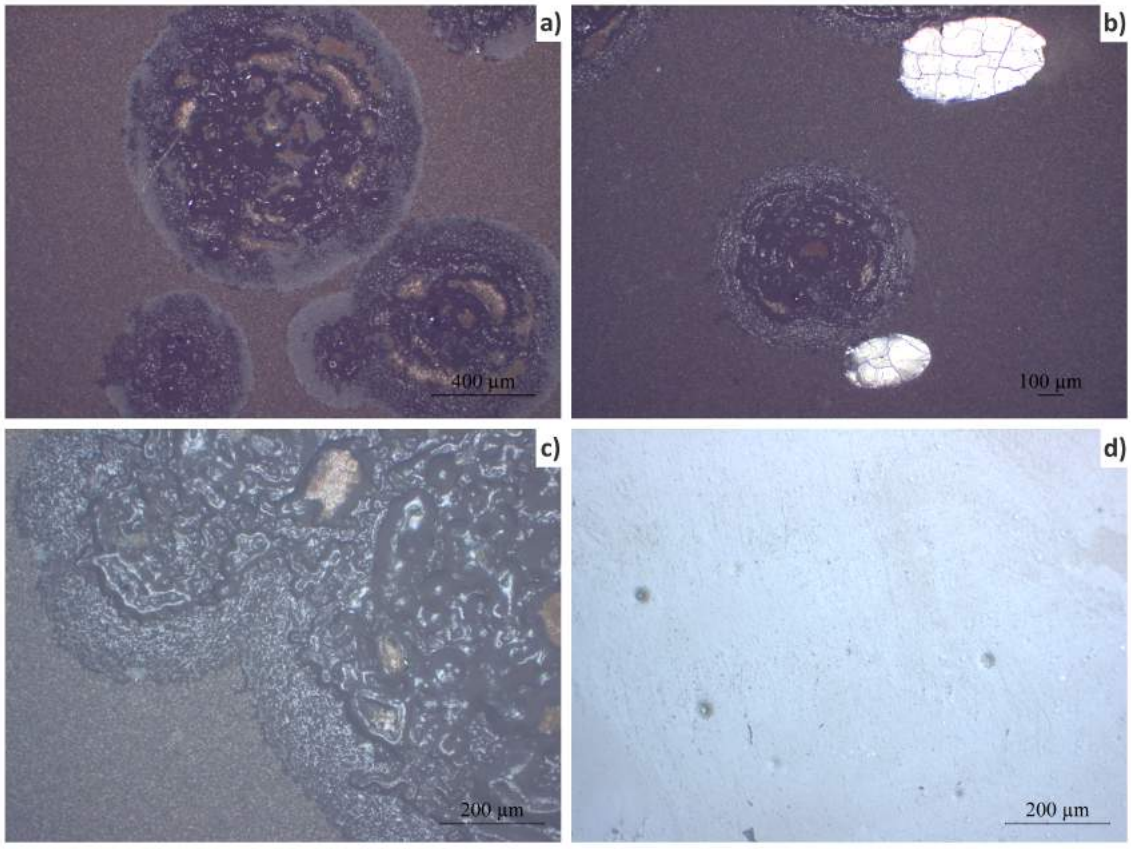

Figure 89: Light micrographs of the cristobalite occurrence on Std_{nc} after HT2 of 10 h: a) Piece 2, b) Piece 2, c) Piece 2, d) Piece 3

SEM pictures (see Figures 90, 91, 92, 93 and 94) of the samples help to see the dissolution patterns on the surface that was below the melt level (Piece 2) where the loss of thickness appeared in addition to the corrosion circles for Std_{nc} and some of the little areas of cristobalite tiles on A_{nc}. For the parts that were right above the melt level (Piece 3), the cristobalite formation observed on A_{nc} with the light microscope can also be seen while for Std_{nc}, some dissolution spots that were not seen with the light microscope can be observed.

On Figures 96, 95, 98 and 97, the representative XRD patterns are shown. It can be seen that for A_{nc}, for both the part above the melt (Figure 96) and the part that was in contact with the melt (Figure 95), the intensity ratios of the different peaks is different than for the reference pattern. There is a preferred orientation at an angle 2θ of 36.080 which corresponds to the orientation {200}.

For Std_{nc} (Figures 98 and 97), the patterns look like the one obtained when there was some epoxy on the samples. It must be characteristic of an amorphous component present on the surface of the crucible piece. No conclusion about a preferred orientation can be drawn for Std_{nc} after HT2 due to the low crystallinity of the sample.

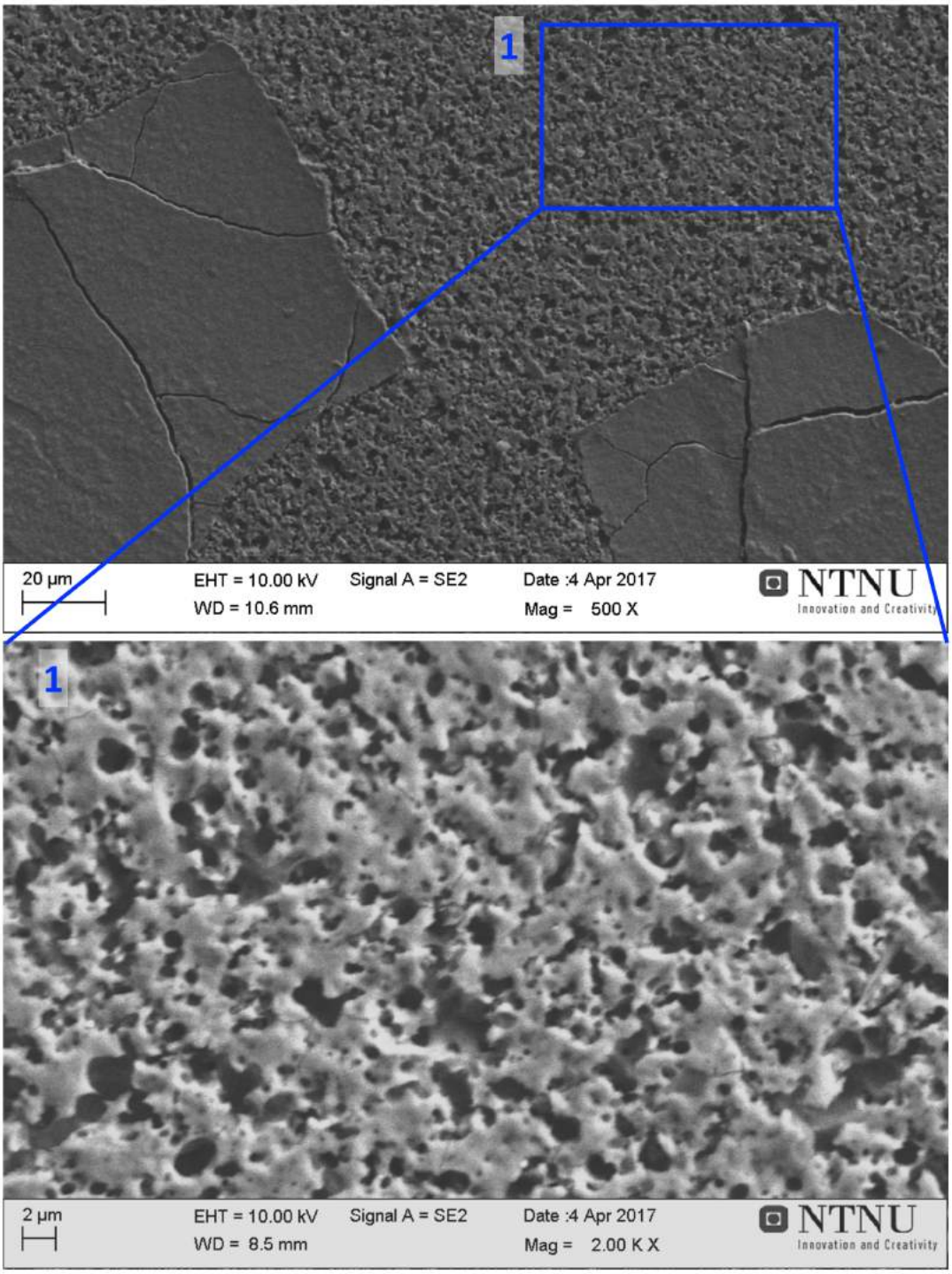

Figure 90: SEM pictures of the cristobalite occurrence on A_{nc} Piece 2 after HT2 of 10 h at magnifications 500× and 2000×

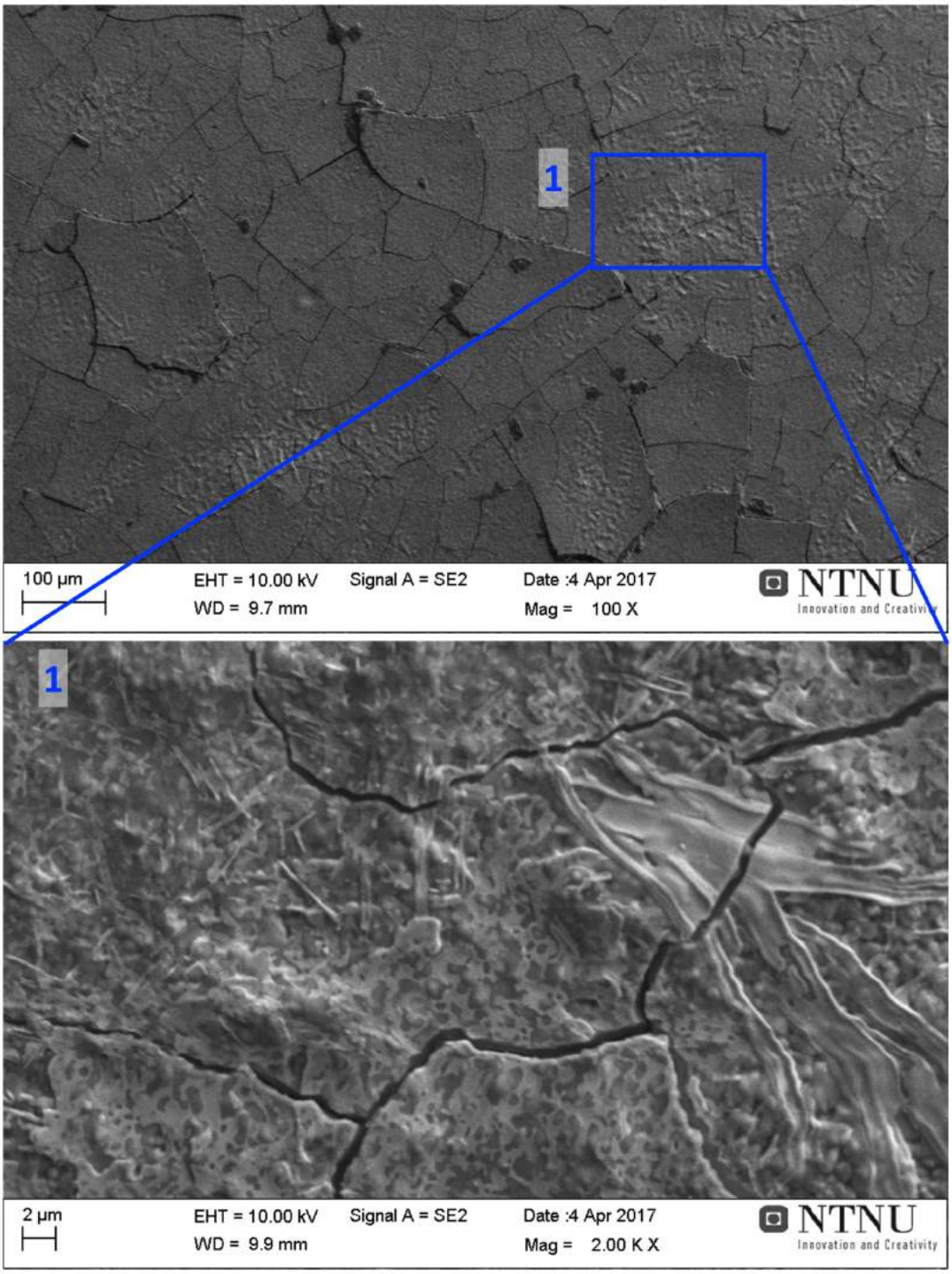

Figure 91: SEM pictures of the cristobalite occurrence on A_{nc} Piece 3 after HT2 of 10 h at magnifications 100× and 2000×

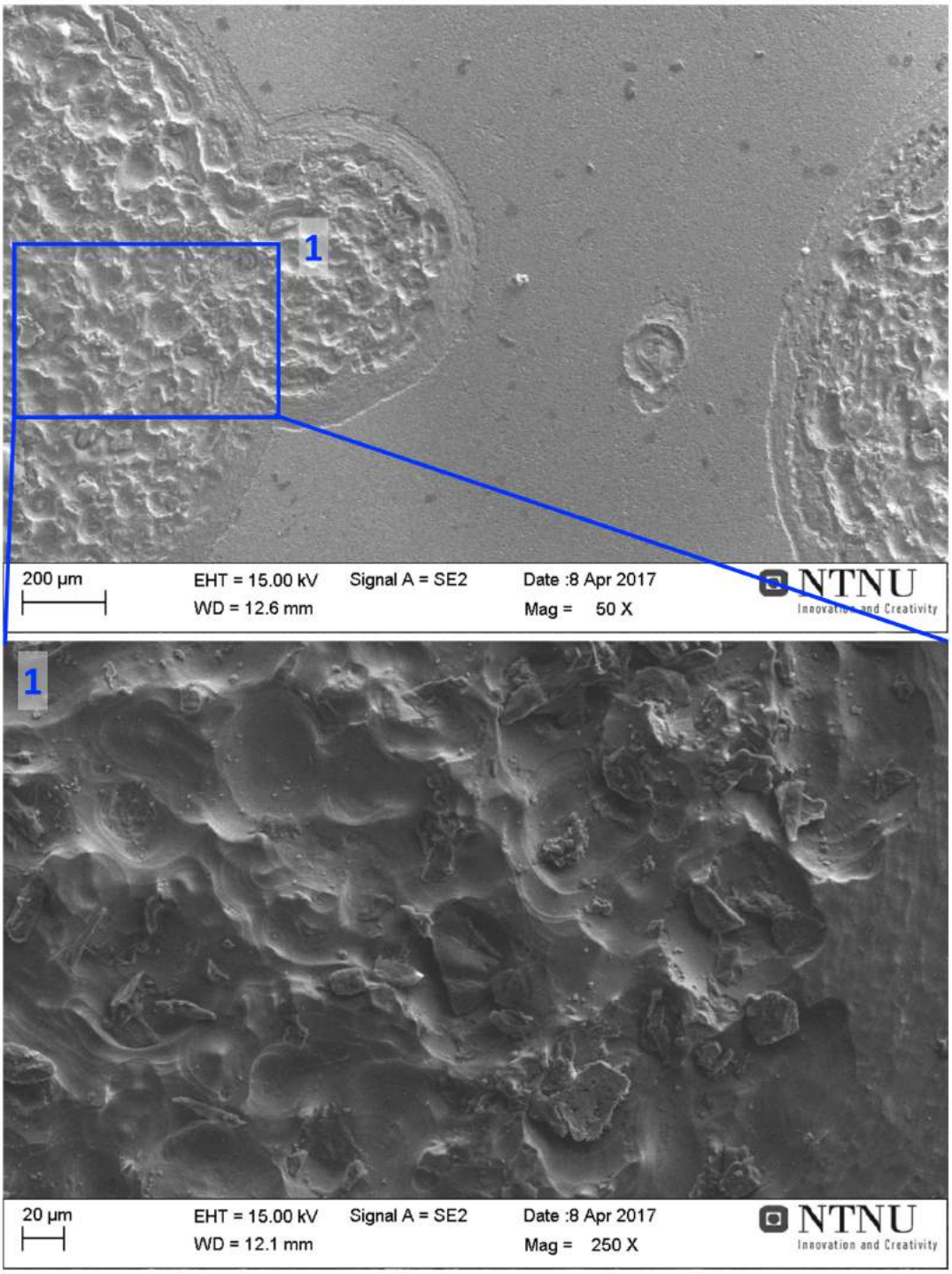

Figure 92: SEM pictures of the cristobalite occurrence on Std_{nc} Piece 2 after HT2 of 10 h at magnifications 50× and 250×

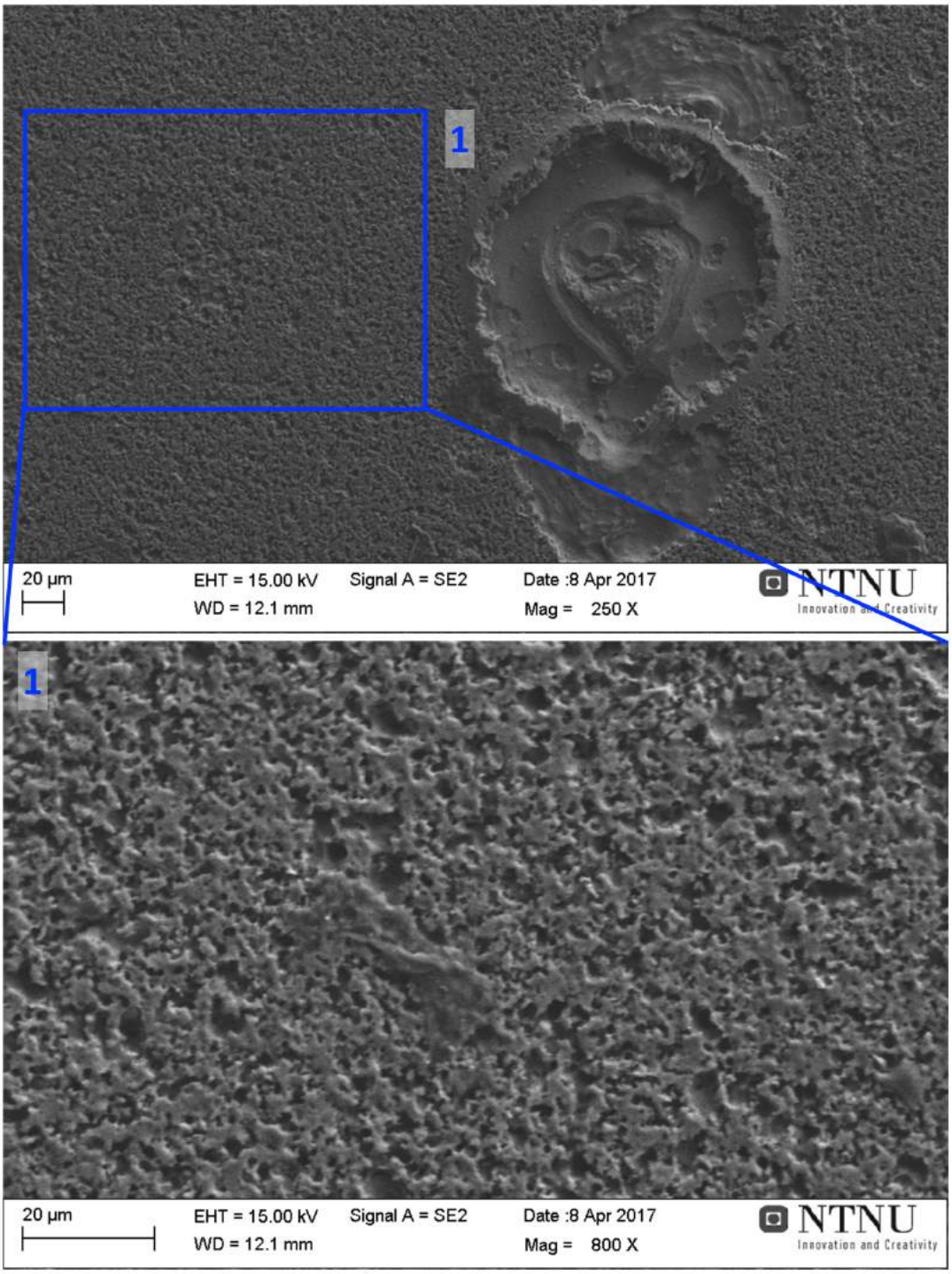

Figure 93: SEM pictures of the cristobalite occurrence on Std_{nc} Piece 2 after HT2 of 10 h at magnifications 250× and 800×

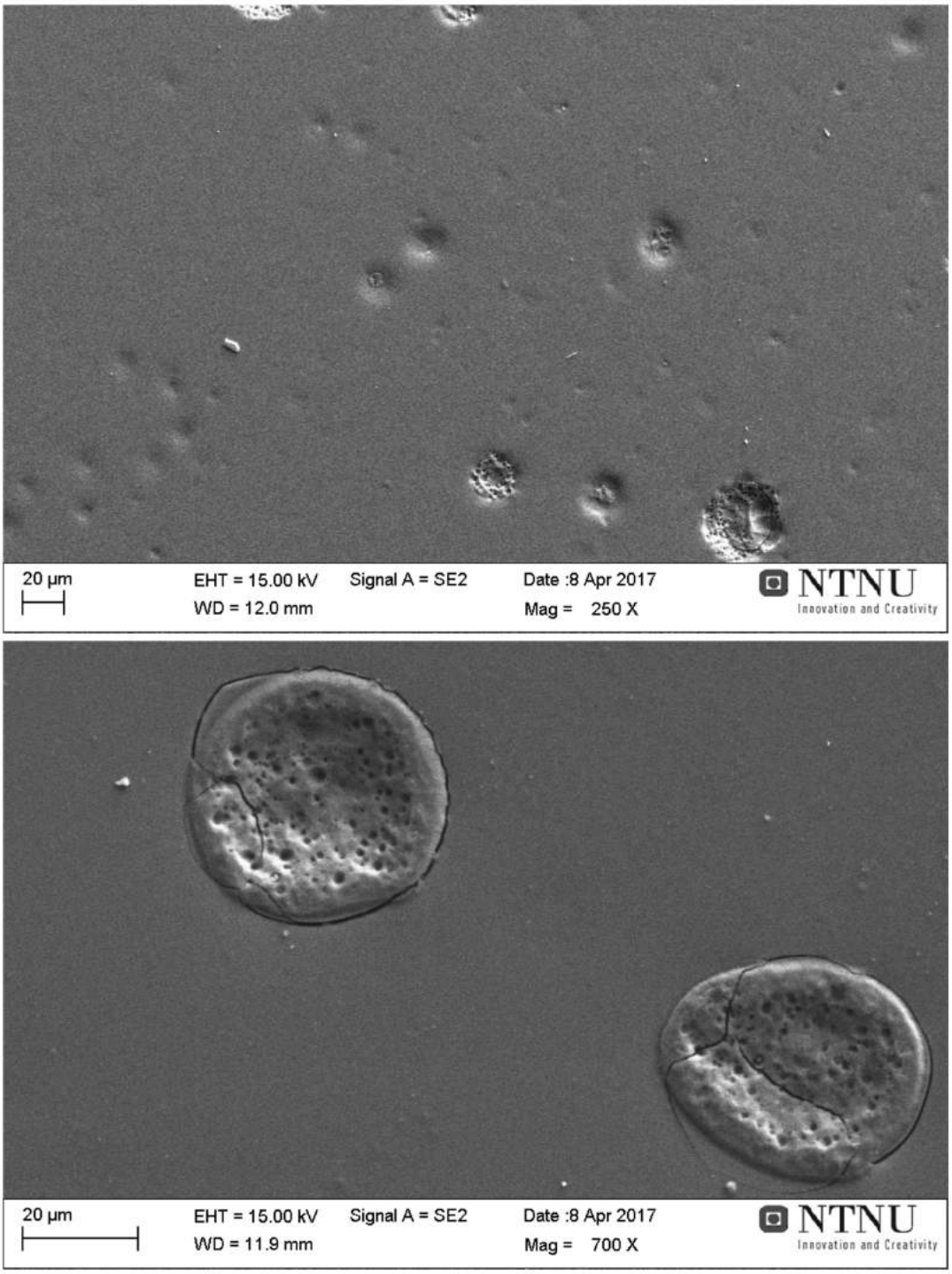

Figure 94: SEM pictures of the cristobalite occurrence on Std_{nc} Piece 3 after HT2 of 10 h at magnifications 250× and 700×

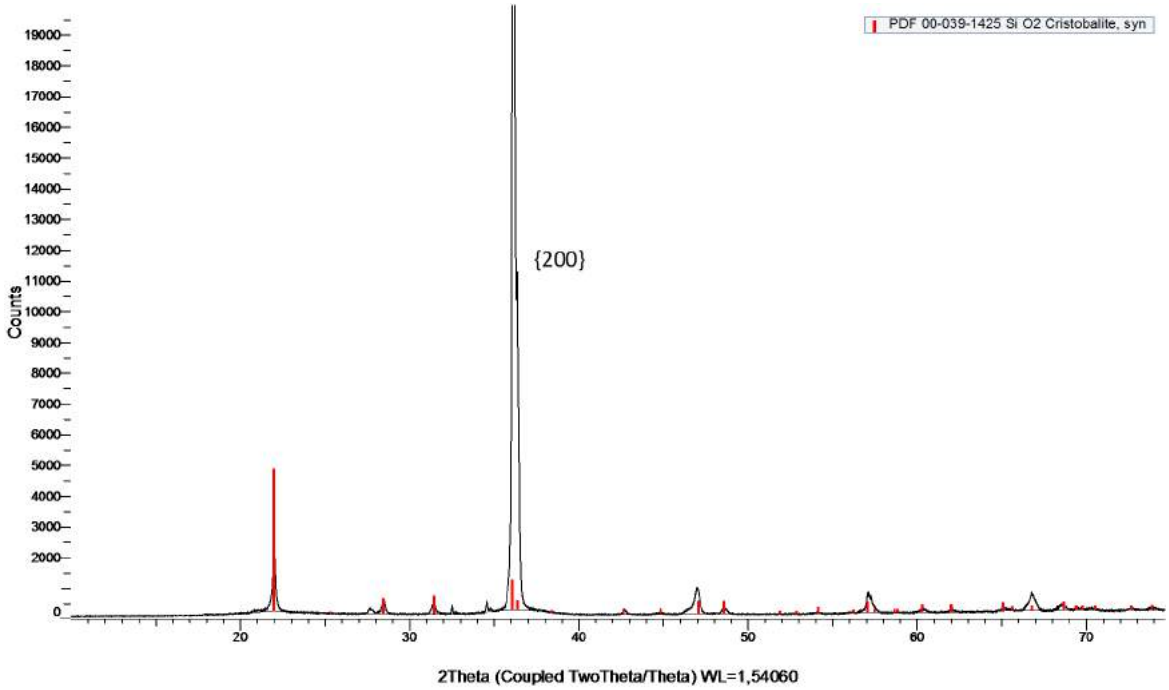

Figure 95: XRD pattern of A_{nc} Piece 2 after HT2 of 10 h with cristobalite reference pattern in red

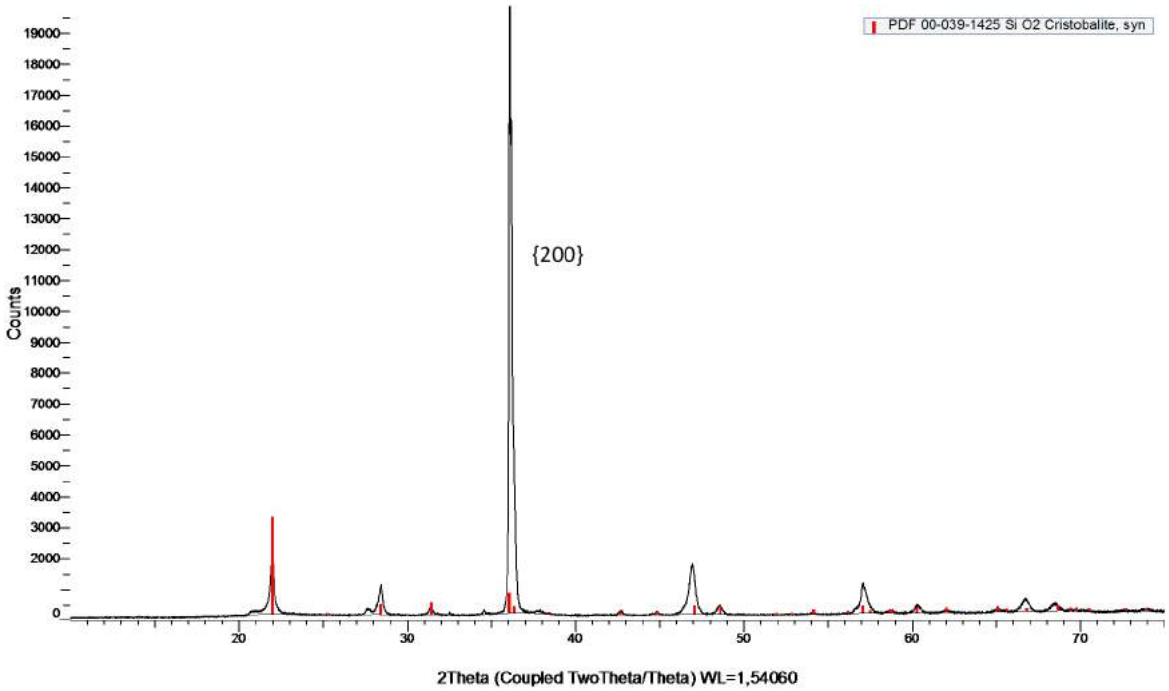

Figure 96: XRD pattern of A_{nc} Piece 3 after HT2 of 10 h with cristobalite reference pattern in red

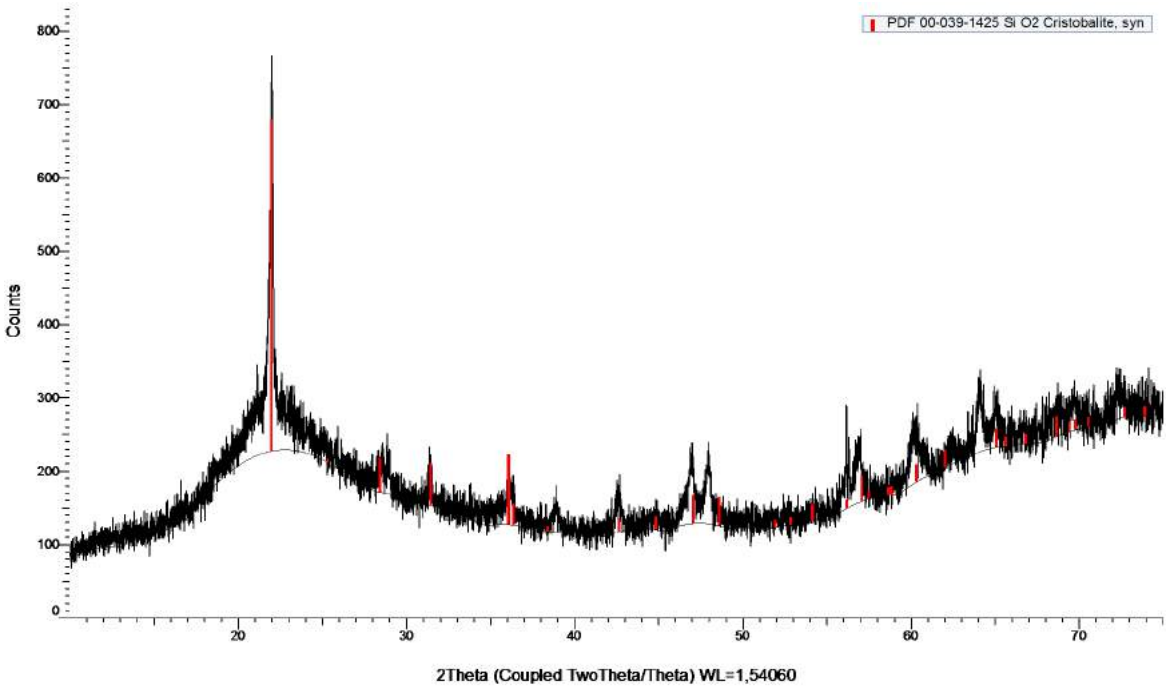

Figure 97: XRD pattern of Std_{nc} Piece 2 after HT2 of 10 h with cristobalite reference pattern in red

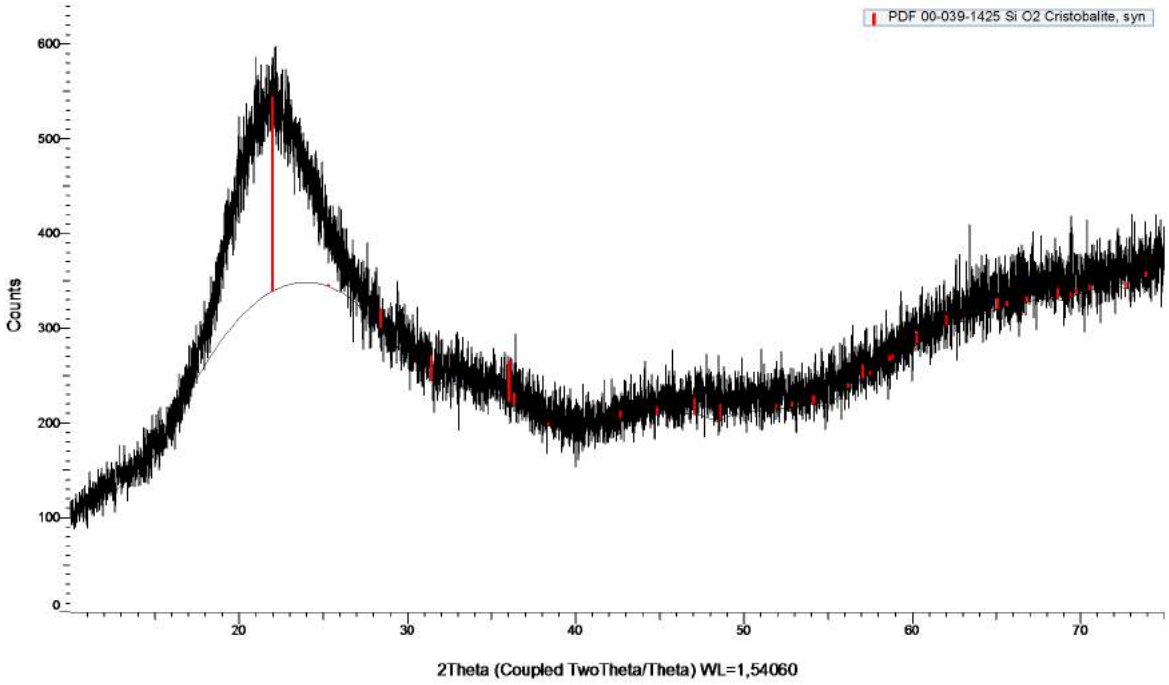

Figure 98: XRD pattern of Std_{nc} Piece 3 after HT2 of 10 h with cristobalite reference pattern in red

The graph on Figure 99 shows the intervals in which the thickness of the cristobalite layer observed on each crucible rod after HT2 of 10 h varies. Those values have also some inaccuracies and it can be seen from the pictures in Appendix A.5 that the layers are not homogeneous. In this case, it is not possible to highlight a representative value for the Std_{nc} part that was above the melt (Piece 3) due to a cristobalite occurrence on the surface only observed as tiny localised particles.

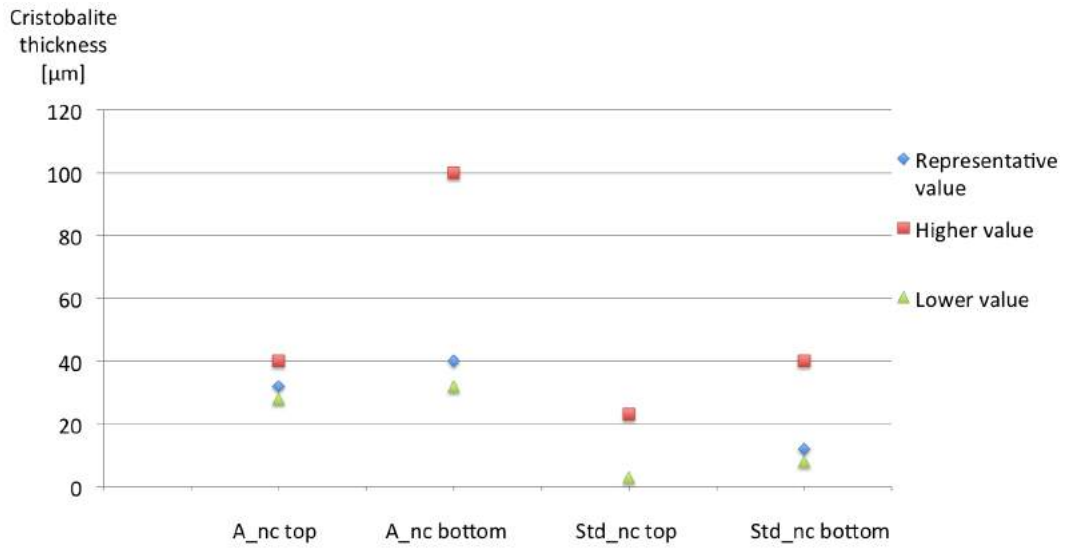

Figure 99: Intervals of values for the thickness of the cristobalite layer on A_{nc} and Std_{nc} after HT2 of 10 h

4.2 Used samples

4.2.1 Heat treatment 3: 100 h

Pictures from the different used crucibles as received from the industry can be seen on Figure 100. A_{uc}, B_{uc}, Std_{uc} and B_u are obtained after being used in the CZ process for the ingot pulling during approximately 100 h at high temperature. However, the pulling company has given the information that A_u was only kept at high temperature in the CZ process during approximately 40 h.

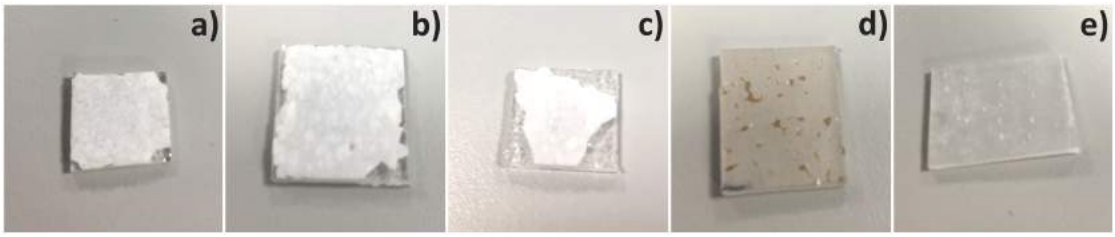

Figure 100: Pictures of the top surface of used crucibles slides (HT3): a) A_{uc} b) B_{uc} c) Std_{uc} d) A_u and e) B_u

While the coated pieces (Figure 100 a, b and c) have relatively similar morphologies with the white and brittle cristobalite layer, A_u shows the "brownish rings" occurrence with an almost transparent layer around and B_u also presents an almost transparent layer with a few white spots on it.

4.2.1.1 Cristobalite characterisation

The light micrographs shown on Figures 101, 102 and 103 demonstrate the presence of cristobalite occurrence on the top surface of the samples. It can be noticed that the coated samples on Figures 102 and 103 seem to have a denser cristobalite layer with less and smaller corrosion rings underneath. The morphology at this magnification (10×) does not differ between the different crucible types (A, B, Std) in comparison to the macroscopic differences observed on Figure 100.

SEM pictures (Figures 104, 105, 106 and 107) show a comparison between coated and non coated pieces of A and B crucibles at two different magnifications. It can be seen that the coated pieces have less and smaller (in depth and diameter) dissolution spots but present more large cracks due to the brittleness of the cristobalite layer formed. For the B_{uc} at 500× magnification on Figure 107b, a certain orientation of the cristobalite layer or the dissolution pattern seems to exist.

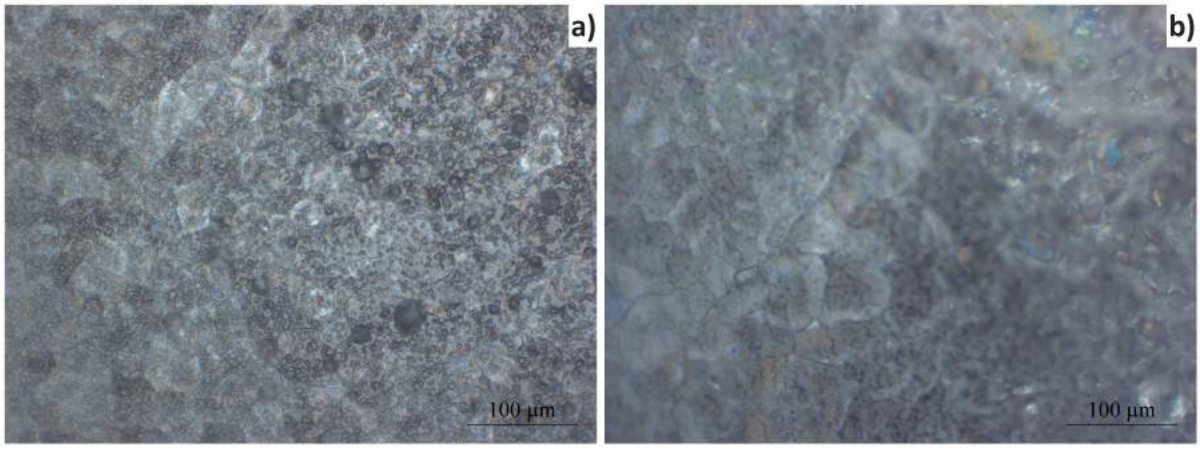

Figure 101: Light micrographs of cristobalite occurrence after HT3 of 100 h: a) A_u, b) B_u

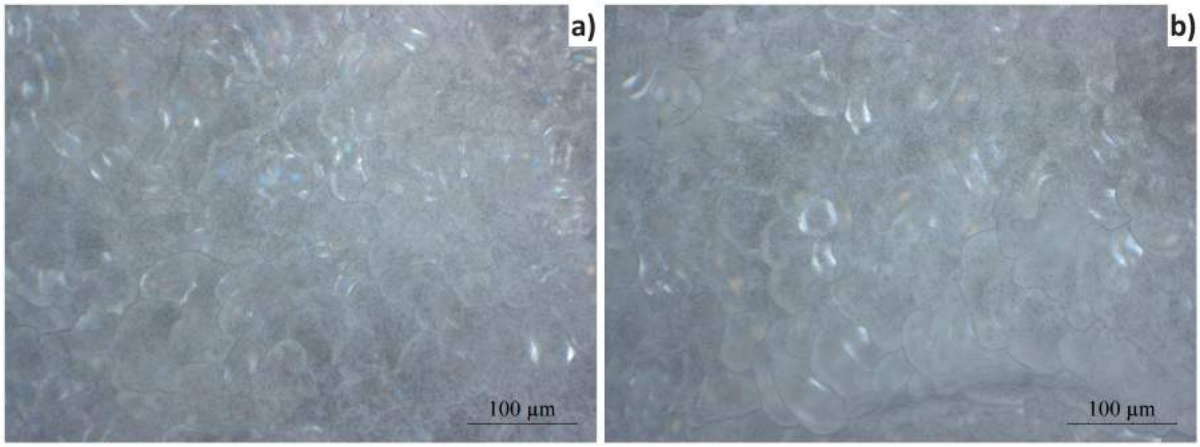

Figure 102: Light micrographs of cristobalite occurrence after HT3 of 100 h: a) Std_{uc}, b) A_{uc}

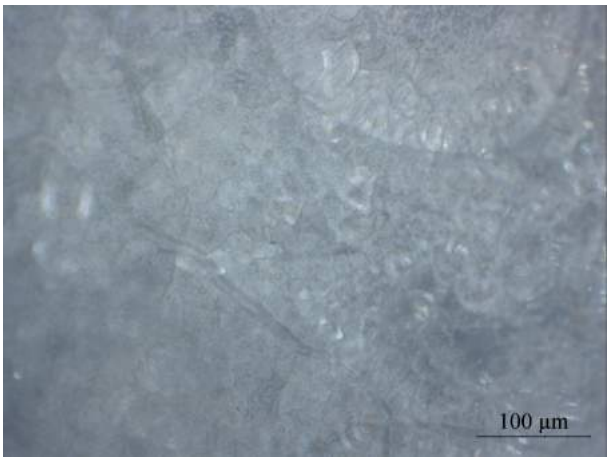

Figure 103: Light micrograph of cristobalite occurrence after HT3 of 100 h on B_{uc}

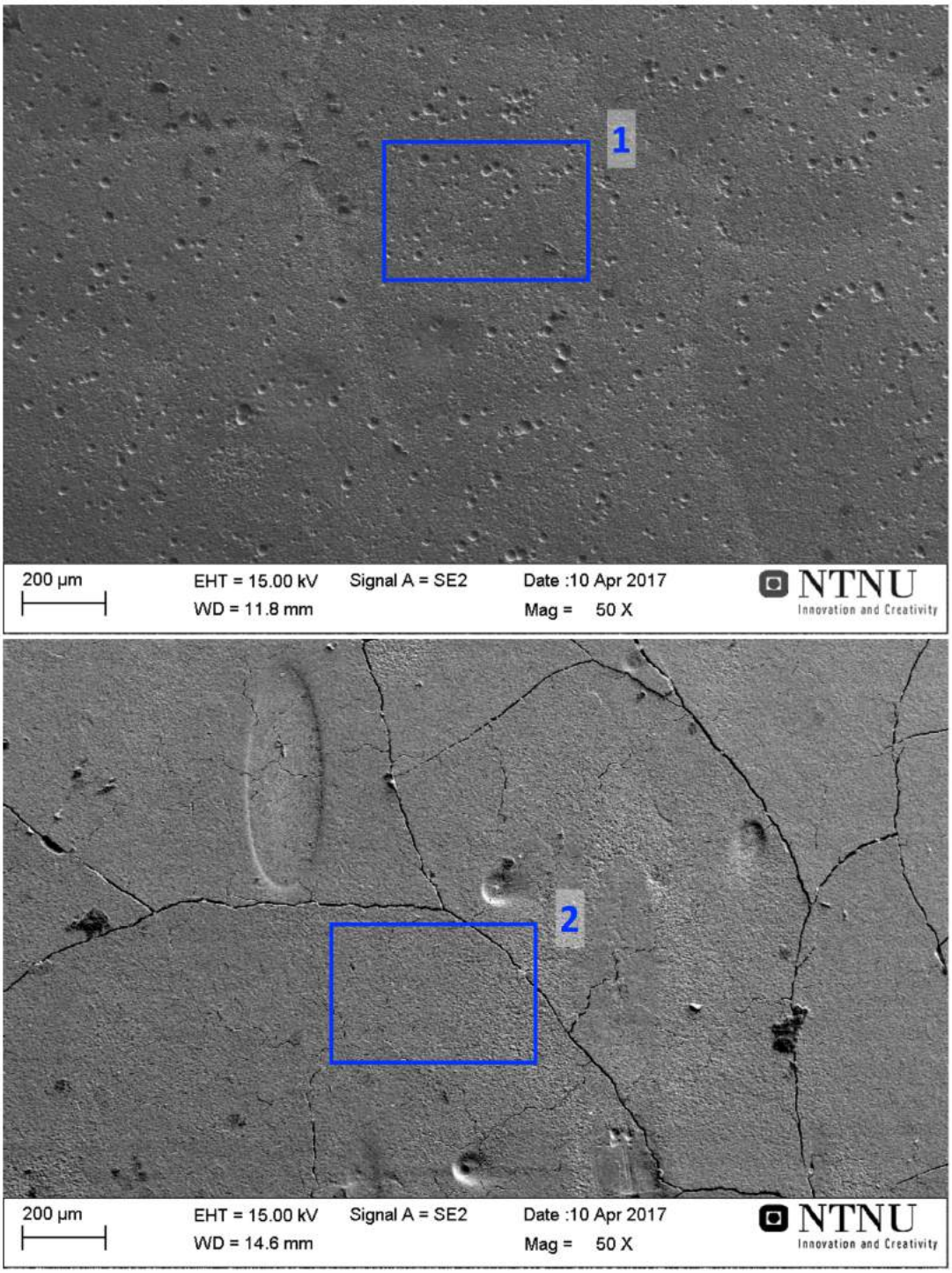

Figure 104: Overview SEM picture of the surface of A_u (top) and A_{uc} (bottom) crucibles after HT3, at magnification 50×. The blue areas 1 and 2 are represented at higher magnification on Figure 103.

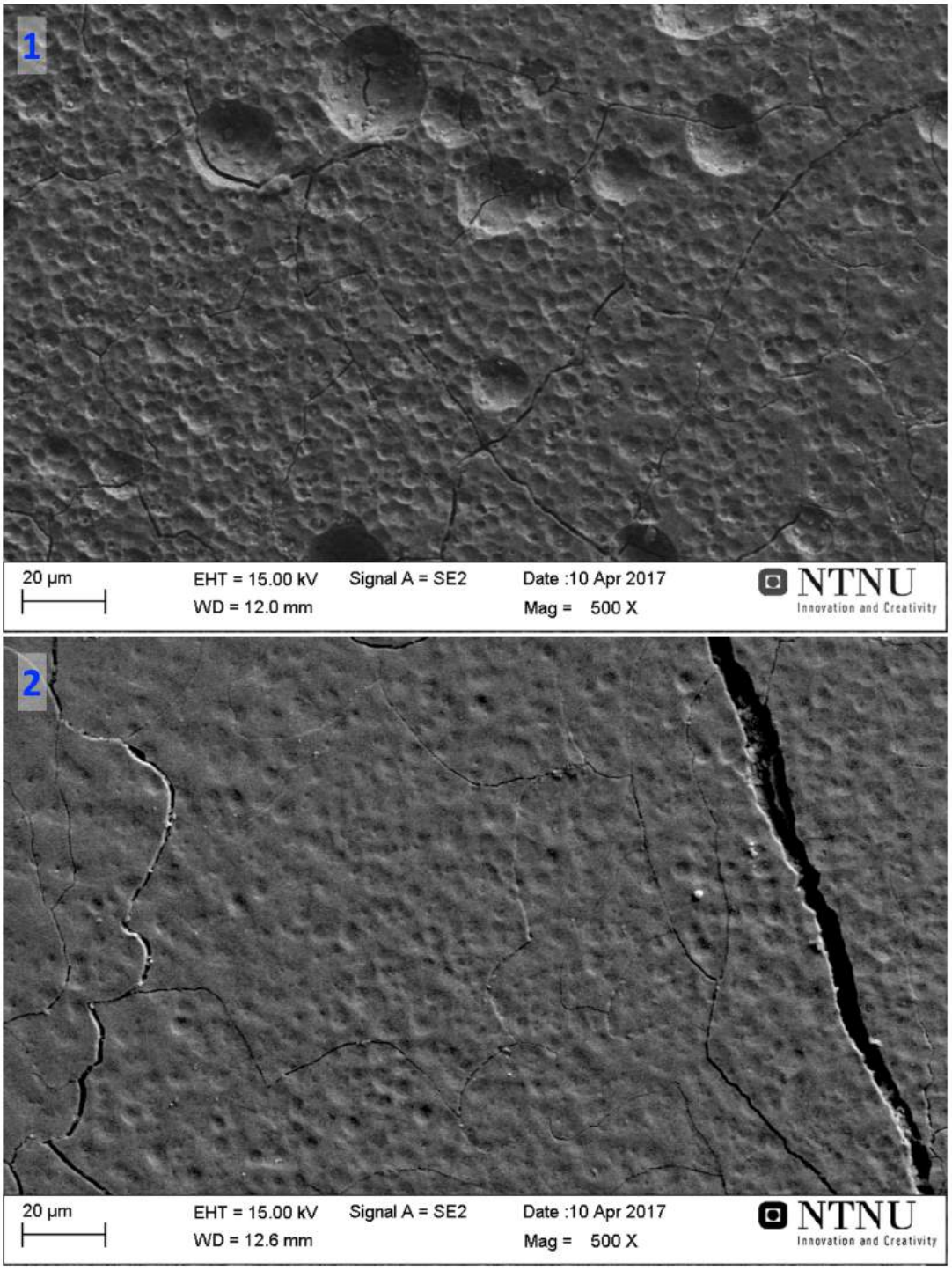

Figure 105: SEM picture of the surface of A_u area 1 (top) and A_{uc} area 2 (bottom) crucibles after HT3, at magnification 500×

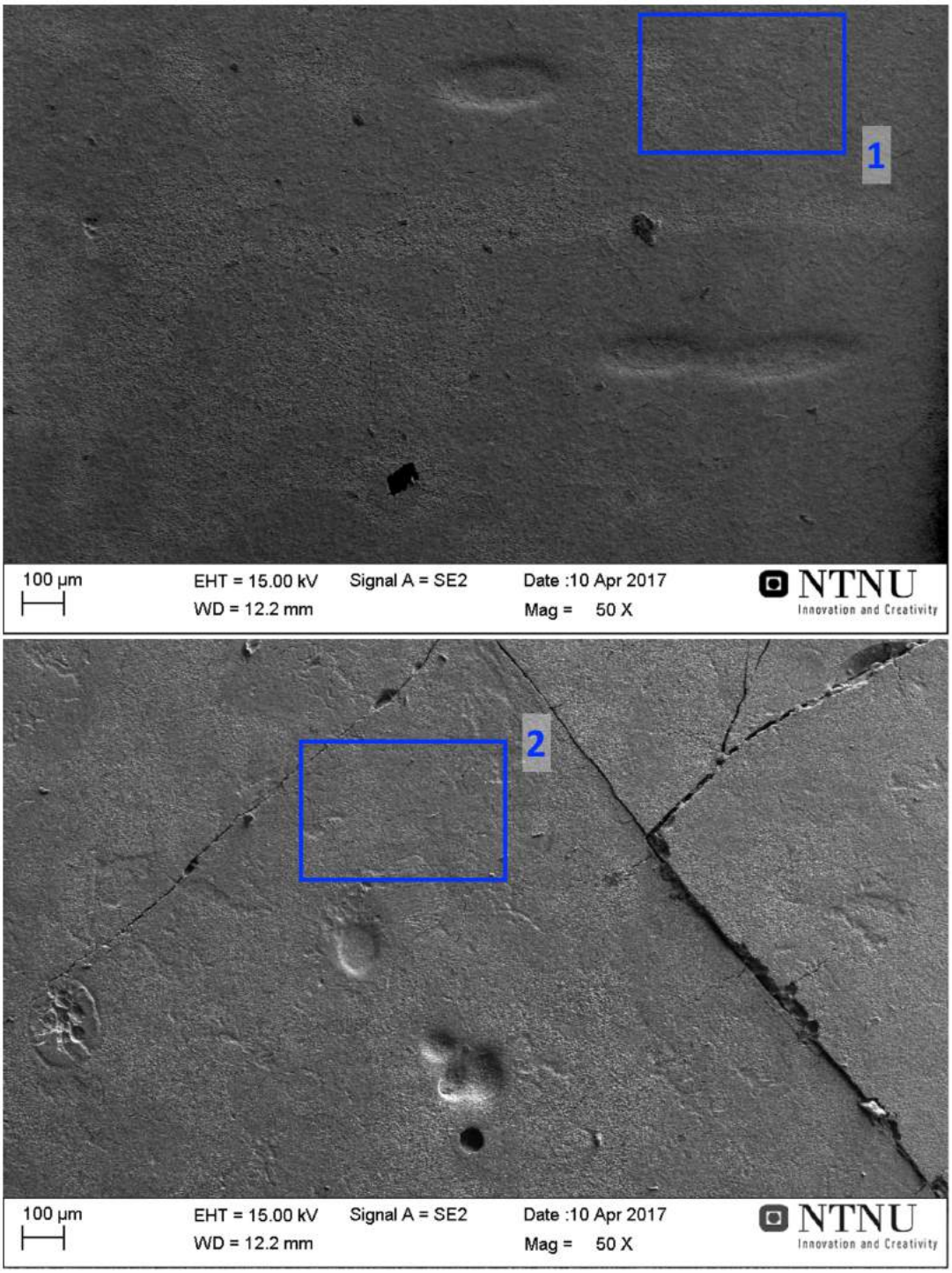

Figure 106: Overview SEM picture of the surface of B_u (top) and B_{uc} (bottom) crucibles after HT3, at magnification 50×. The blue areas 1 and 2 are represented at higher magnification on Figure 105.

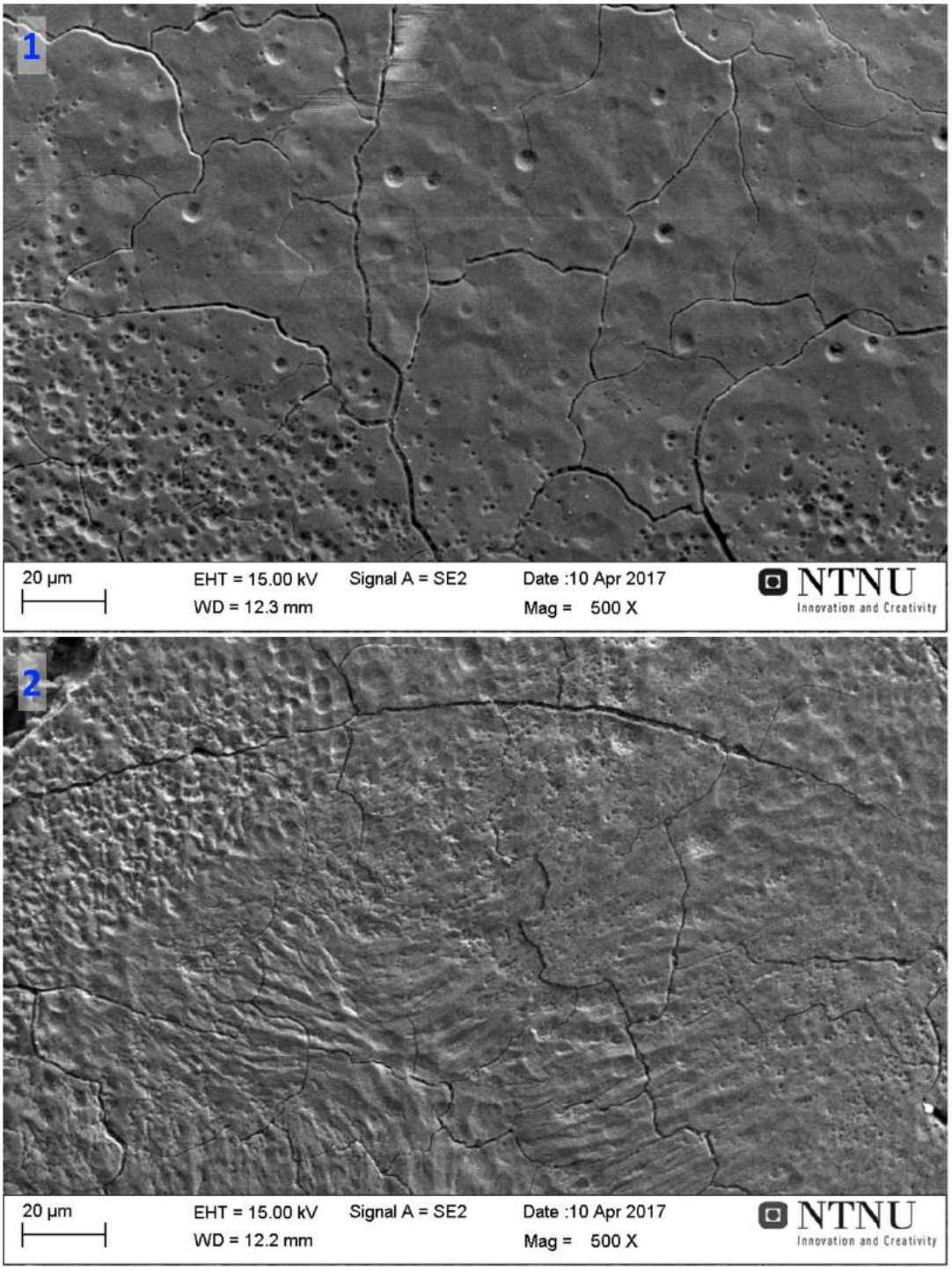

Figure 107: SEM picture of the surface of B_u area 1 (top) and B_{uc} area 2 (bottom) crucibles, magnification 500×

On Figures 108, 109, 110, 111 and 112, the XRD patterns are shown. It can be seen that for A_{uc}, B_u, B_{uc} and Std_{uc}, the intensity ratios of the different peaks is different from the reference pattern so there is a preferred orientation identified at an angle $2\theta = 36.080$ which corresponds to the orientation {200}. There is also some additional peaks more or less wide or high (especially for A_{uc}) at $2\theta = 32.5$-32.7 and 39.5-39.8. At first, they were assimilated to some barium silicate components ($BaSiO_3$ and $BaSi_2O_5$) but since they are also present on non coated crucibles pieces, this explanation has been rejected. No component matching correctly those peaks has been identified in term of possible elementary composition so that no conclusion can be made about their nature.

The only different XRD pattern is the one for A_u (Figure 108), where the preferred orientation is $2\theta = 21.986$ which corresponds to the orientation {101}.

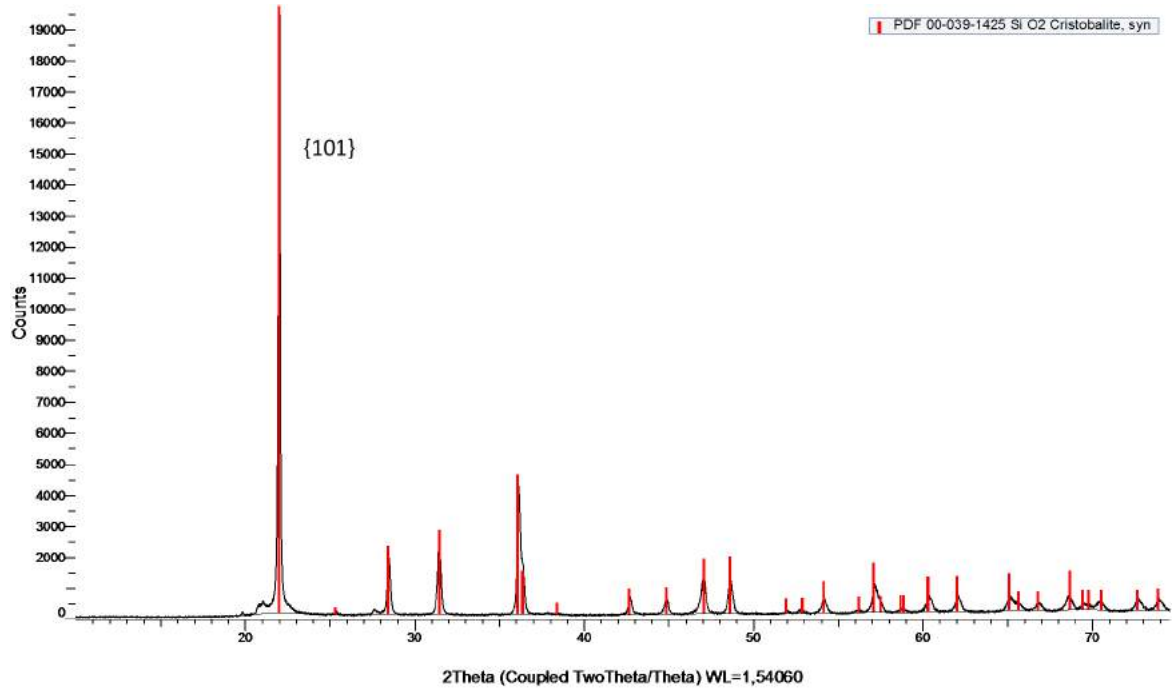

Figure 108: XRD pattern of A_u after HT3 of 100 h with cristobalite reference pattern in red

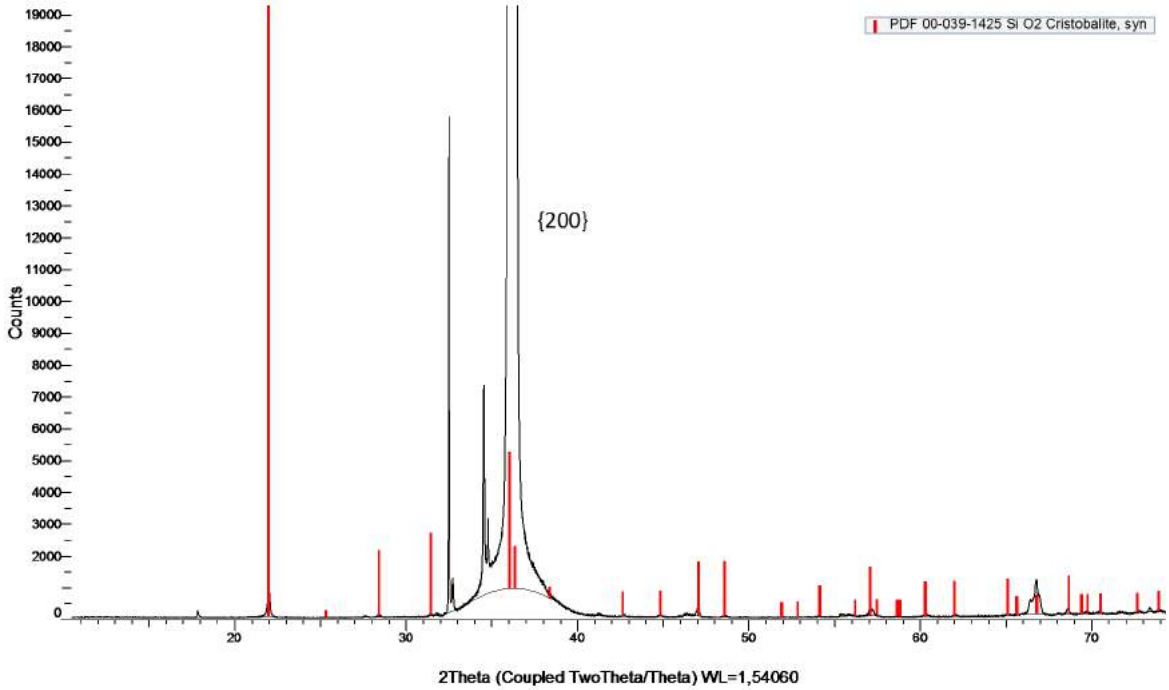

Figure 109: XRD pattern of A_{uc} after HT3 of 100 h with cristobalite reference pattern in red

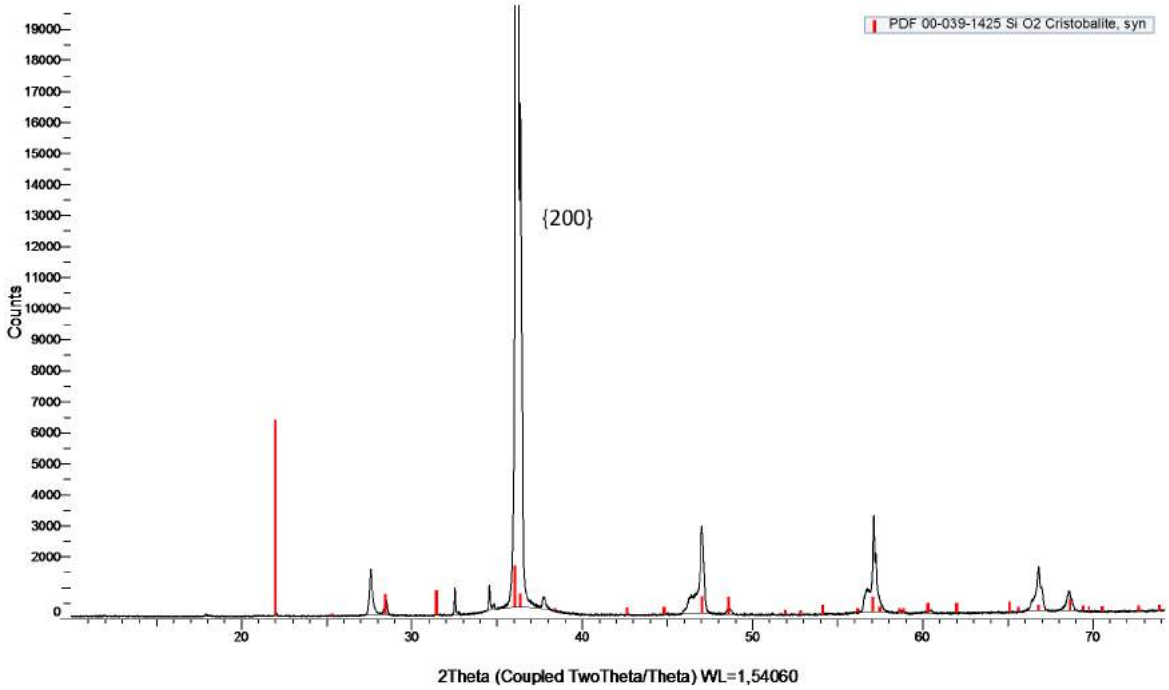

Figure 110: XRD pattern of B_u after HT3 of 100 h with cristobalite reference pattern in red

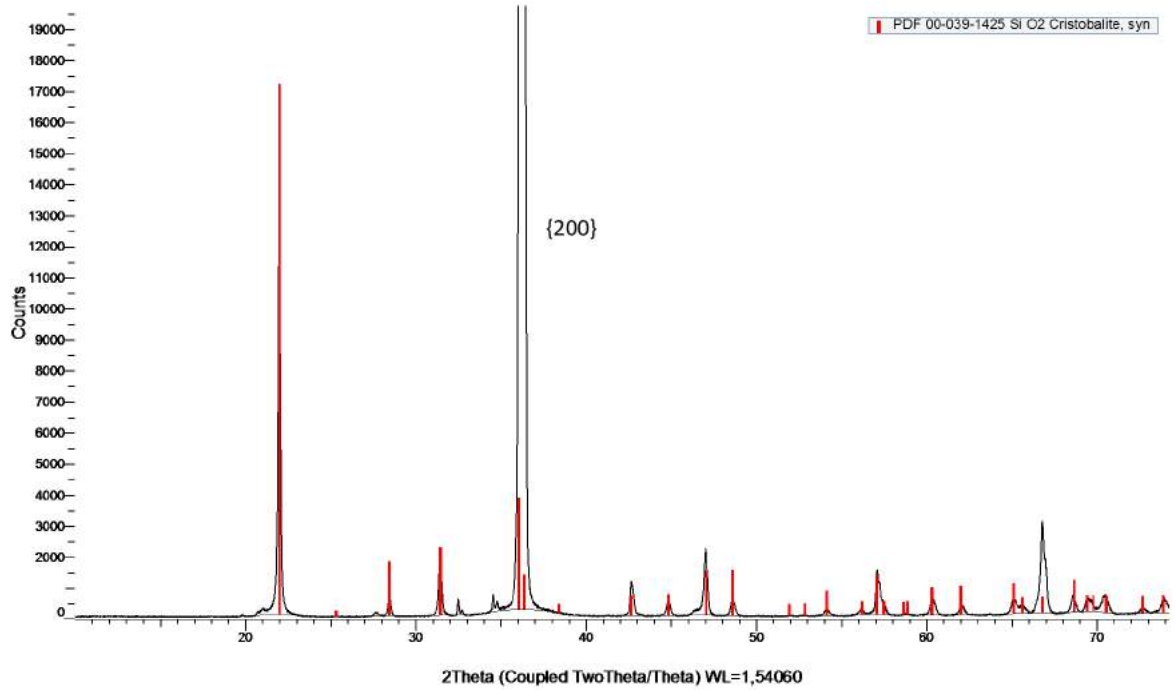

Figure 111: XRD pattern of B_{uc} after HT3 of 100 h with cristobalite reference pattern in red

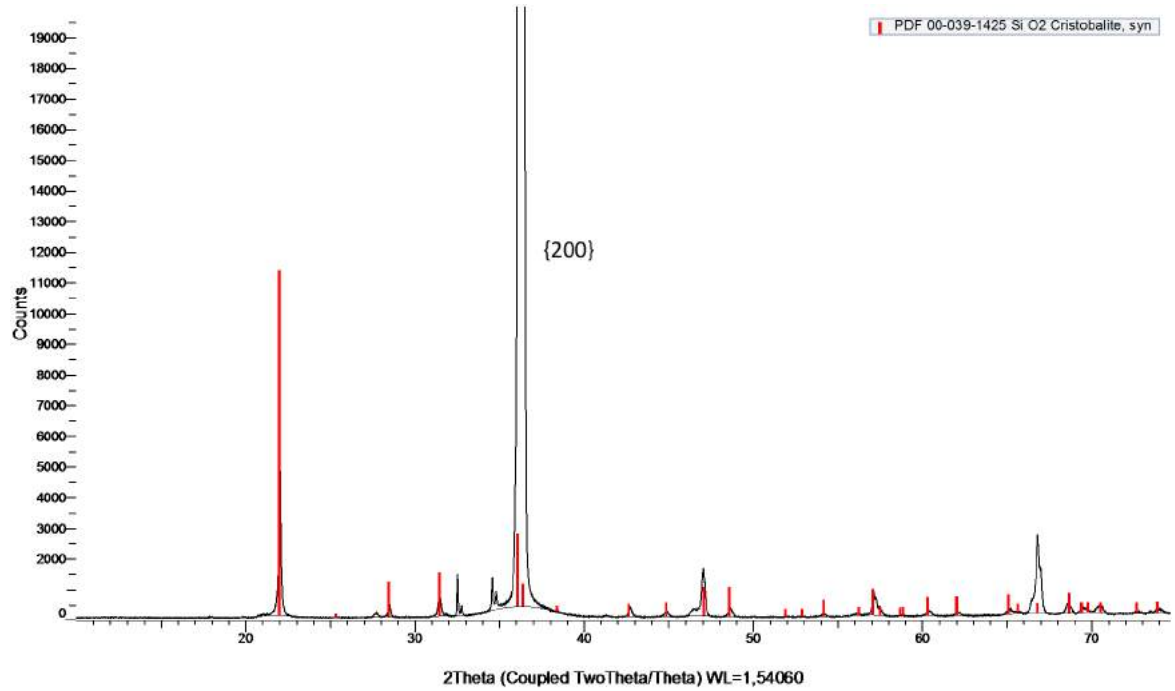

Figure 112: XRD pattern of Std_{uc} after HT3 of 100 h with cristobalite reference pattern in red

The graph on Figure 113 shows the intervals in which the thickness of the cristobalite layer observed on each crucible rod after HT3 of 100 h varies. Those intervals may seem large in terms of values but the layer thickness is actually very homogeneous (see pictures in Appendix A.6). A representative value for the different thicknesses is highlighted in blue on the graph. It can be seen that the coated pieces show way thicker cristobalite layers than the non coated pieces. For the coated pieces, in addition to the cracks observed on the top surface of the cristobalite layer, some cracks are also observed on the quartz under the cristobalite layer, as it can be seen on Figure 114.

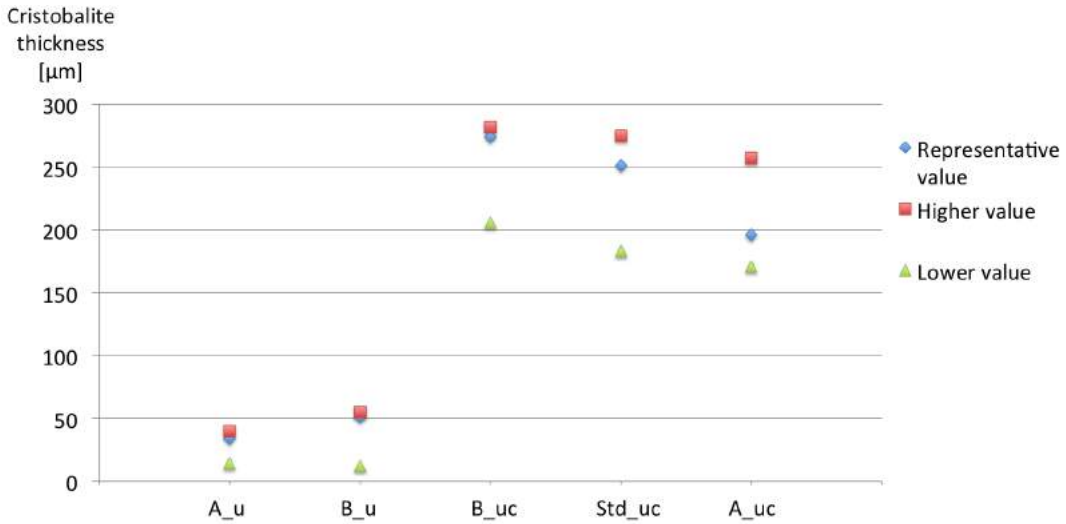

Figure 113: Intervals of values for the thickness of the cristobalite layer on the different types of crucibles after HT3 of 100 h

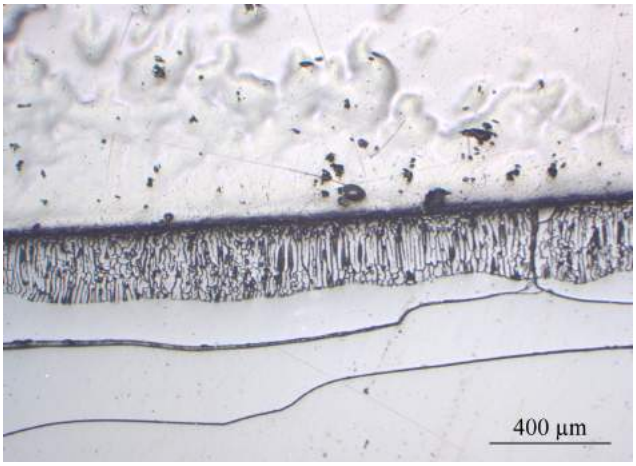

Figure 114: Example of cracks under the cristobalite layer observed on B_{uc} after HT3 of 100 h

5 Discussion

5.1 New samples

5.1.1 Coatings

On Figure 44, it was seen that the industrial coating was not covering homogeneously the crucible surface of Std_{nc}. This non homogeneity of the coating on the crucible pieces might have an impact on the development of the cristobalite that is supposed to be enhanced by the presence of the barium coating. Seeing that the coating observed on B_{nc} and A_{nc} was relatively well spread on the surface, it seems that either the Std_{nc} pieces come from a batch whose coating routine was not well conducted or that the intrinsic parameters of this crucible type (e.g. sand quality, size of the grains, bubble content) affect the adherence of the coating that was probably washed away during the sample preparation steps (i.e. cutting with large use of water, manual handling when preparing the sample for SEM).

From Figures 45 and 46, it was noticed that the spray coating routine performed at NTNU showed similar covering and shape than the industrial coating. However, the thickness of the coating seems higher with several layers sprayed and the barium solution used at NTNU might be more concentrated since no quantitative informations were available from the industrial coating process. Concerning the elongated shape of the dip coating patterns, it is certainly a consequence of the slow vertical removal of the crucible piece from the barium solution during the last step of the dip coating procedure. This coating also seemed thicker than the industrial coating even if it was less homogeneously spread. Those differences in coating thicknesses, spreading and maybe their barium concentration content, can have an influence on the cristobalite layer nucleated on the surface during the heat treatments.

The EDS results were consistent with the contents expected on coated and non-coated crucible pieces with Si and O presences on the amorphous quartz surface (Figure 47, where Point 1 corresponding to the grey surface on SEM pictures was analysed), C from the carbon conductive coating and Ba at the white solid coating occurrences. It seems that a slightly higher amount of C is observed on Figures 48 and 49 where Points 2 and 3 corresponding to the coating areas were analysed. It could come from the $BaCO_3$ presence resulting from the reaction of the $Ba(OH)_2$ coating with carbon dioxide from the air in addition to the C from the carbon conducting coating. However, this is quite uncertain since the C signal in EDS analysis tends to scatter and vary a lot from position to position on the carbon coated samples.

When looking at the XRD analysis of the new coated pieces (industrial coating and spray and dip coatings performed at NTNU), it was observed that $BaCO_3$ was present on the

amorphous quartz constituting the crucible piece. For A_{nc}, seeing the low number of peaks identified and their low number of counts, it is possible that either the coating was not present in high quantity on the surface (low spreading) or that the coating was quite thin. With the SEM results presented on Figure 41 for A_{nc}, and an additional verification that the coating was present on the slide observed at the XRD, it is the last explanation that was preferred i.e. that the industrial coating layer was really thin. For A_n and B_n spray coated, a larger amount of $BaCO_3$ was identified in comparison with A_{nc}. It suggested that the spray coated pieces at NTNU presented a thicker coating layer (seeing that their spreading observed with the SEM was close to the one observed on A_{nc}, so that this is not considered as the main influence). However, the intensity ratios of the different peaks are not always similar to the reference pattern. It indicated that $BaCO_3$ nucleated with preferred orientations. With crucible slides of same dimensions observed, the small differences of the peak heights observed between A_n and B_n spray coated suggested that the coating was a bit thicker on B_n so that the coating routine did not provide a good reproducibility and control of the coating thickness.

In the case of A_n dip coated, the low presence of $BaCO_3$ came most likely from the fact that the dip coating was washed away during the cutting of the slide. In fact, it was observed that the dip coating was easily removed from the quartz surface even if it looked quite thick when deposited.

Those results about the presence of the amorphous peak and the oriented crystalline $BaCO_3$ were consistent with the observations made in a study performed by SINTEF. [68] However, the fact that $BaCO_3$ could not be identified easily on industrially coated crucibles is surprising. If it is confirmed that it was due to the thinness of the coating, then a solution to be considered is the use of Grazing Incidence Diffraction (GID). In fact, a common XRD is not surface sensitive enough for the analysis of thin depositions on the surface and will intensify the signal of the substrate material (amorphous quartz). Using GID might help when it comes to identifying the thin layer of $BaCO_3$ but knowing that the coatings have most of the time a variable thickness, the analysis might not be quantitative. [69]

5.1.2 Heat treatment 1: 90 min

The cristobalite occurrence observed after 90 min on each crucible type coated or not was variable. For A_{nc} with industrial, dip and spray coatings and B_{nc} with industrial and spray coatings, the use of the devitrification agent offered many nucleation sites for cristobalite so that the layer was spread on the whole surface. On the other hand, for Std_{nc}, on which the coating seemed not homogeneously spread (see 5.1.1), no occurrence of cristobalite was observed after 90min and on the non coated A_n (B_n being covered by epoxy thus not conclusive), cristobalite was present but not on the whole surface analysed.

When comparing the spray and dip coated pieces with the industrially coated pieces,

while the covering of the cristobalite on the surface looked similar, the size of the mosaic tiles was different with a smaller tile size on the industrially coated pieces. This suggested that the industrial coating offered a higher number of nucleation sites for cristobalite. In addition, the tile size varied a lot for the spray and dip coated pieces so that it seemed that the development of cristobalite was less controlled than with the industrial coating.

Concerning the XRD results for HT1 of 90 min, for the non coated and industrially coated pieces, the cristobalite layer presented a main orientation of {101} (random cristobalite formation) that seemed independent of the presence of the coating. On the other hand, the dip and spray coated pieces had a preferred orientation of {200} in addition to a larger presence of {111} oriented crystals. It can be suggested that the coating performed at NTNU had an influence on the nucleation direction of the cristobalite during this heat treatment type but it is hard to know if it was the coating technique, the barium concentration or the thickness of the coating that influenced the crystal orientation.

With such a short heat treatment time and for most of the samples, the cristobalite did not develop so much after HT1 of 90 min so that the thickness measurements were subjected to inaccuracies. In fact, high magnifications were required to distinguish the cristobalite particles and the focus at those magnifications was not good so that the measurements were probably biased. In addition, since the measurements were made manually from the scale obtained on the LM pictures, they were subjected to inaccuracies i.e. up to 5 μm of uncertainty in the measurements. For low thickness layers, it represents a large relative variation. Nevertheless, some trends were highlighted : the cristobalite layer seemed slightly thicker on industrially coated crucible than on the non coated pieces. The pieces coated at NTNU developed a layer up to about 4 times the layer observed on pieces with industrial coating (in terms of the representative values shown in Figure 64). It can be due to a higher barium concentration on the surface or the thickness of the layer deposited that were not controlled with those coating routines.

5.1.3 Heat treatment 1: 10 h

The cristobalite occurrence after HT1 of 10 h on each crucible type coated or not is quite similar: A_n, A_{nc} with industrial, dip and spray coatings, B_n, B_{nc} with industrial and spray coatings and Std_{nc} all presented a cristobalite layer on the whole surface but with different tile sizes. While A_n, A_{nc}, B_n and B_{nc} had tiles of quite homogeneous size, the tiles on Std_{nc} varied more, with sizes up to 3 times the size observed on A_n, A_{nc}, B_n and B_{nc}. This might be a consequence of the non homogeneous presence of the coating on Std_{nc} that allowed the promotion of local cristobalite developments where the coating was present while the areas not covered by the coating grew cristobalite afterwards.

As for HT1 of 90 min, the spray coated pieces had a cristobalite development influenced by the coating pattern. However, for the dip coated pieces, after 10 h, the coating pattern did not seem to influence the final morphology of the cristobalite developed. In fact, some local occurrences (Figure 67d) looked very similar to the occurrences observed on A_n, A_{nc},

B_n, B_{nc} and Std_{nc} but the global morphology was highly variable in terms of tile sizes. It might suggest that the cristobalite formation was not well controlled by dip coating (probably due to the easy removal of this coating type) with a devitrification agent while spray coating (industrial and at NTNU) offered a more coherent morphology of the layer nucleated.

Concerning the XRD results, for the non coated and industrially coated pieces, the cristobalite layer presented a main orientation of {101} (random cristobalite formation) that seemed independent of the presence of the coating. It is the same preferred orientation that was observed for those pieces after HT1 of 90 min. On the other hand, the dip and spray coated pieces showed a main preferred orientation of {200}. However, for the dip coated piece, the orientation {101} was also largely present. This last orientation is similar to the one observed on the non coated and industrially coated pieces. By looking back at the local cristobalite observed on A_n dip coated after HT1 of 10 h (Figure 67d) and comparing it to the morphology of the non coated and industrially coated pieces after HT1 of 10 h (Figures 66 and 67a) some similarities were noticed in terms of the tiles shape and size. The local occurrence observed for the dip coated piece on Figure 67b might correspond to an area where the dip coating was removed and where the cristobalite nucleated the same way than on the other non coated and industrially coated crucible pieces. This might explain why the orientation {101} was observed on A_n dip coated but seeing that its morphology varies a lot, it was not surprising to have another preferred orientation, i.e. {200}, that was also observed on A_n dip coated after HT1 of 90 min. Again, the coating seemed to have an influence on the nucleation direction of the cristobalite but maybe, before reaching a certain layer thickness, the cristobalite develops randomly (i.e. orientation {101}).

After HT1 of 10 h, the coated pieces seemed to have a thicker cristobalite layer than the non coated pieces. The only exception was Std_{nc} that presented a similar value for the thickness than after HT1 of 90 min. This value was in the same range as for the non coated pieces after HT1 of 10 h. It is difficult to conclude anything only based on those measurements but from the LM top surface pictures presented on Figures 66 and 67 and the layer pictures in Appendix A.3, it was seen that while the thickness of the cristobalite stayed constant between 90 min and 10 h of HT1 for Std_{nc}, the layer became more homogeneous and spread on the whole surface. It seemed that the nucleation of cristobalite on Std_{nc} occurred later than on other crucible. This might be dependent on this crucible intrinsic quality close to the inner surface.

As for HT1 of 90 min, the pieces coated at NTNU showed a layer up to 4 times thicker than the one observed on the pieces with the industrial coating. As mentioned earlier, this can be a consequence of the coating thickness, pattern (from the method of coating) or the concentration of barium on the surface.

5.1.4 Heat treatment 1: 24 h

This heat treatment was only performed on A_n, B_{nc}, B_n and Std_{nc}. The cristobalite morphology, after HT1 of 24 h, presented a layer denser and more homogeneous than for HT1 of 90 min and 10 h. Large cracks were present for each crucible type. Those cracks obviously appeared during the cooling when the cristobalite contracted due to the beta-alpha phase transition.

The XRD results showed the same preferred crystal orientation of {101} (random cristobalite formation) for all the crucible types heat treated. This orientation seemed independent of the presence of a coating and was the one observed for those same crucible types after HT1 of 90 min and 10 h.

When looking at the cristobalite layers thickness, several trends were highlighted : the layers observed were very homogeneous (more than after 90 min and 10 h) and thicker than 120 μm for coated and non coated crucibles. B_{nc} showed a thicker layer than the one observed on B_n. Std_{nc} had the lowest value, even lower than for non coated crucibles. As mentioned earlier, this might be a consequence of a slower development of cristobalite on Std_{nc} due to intrinsic properties of that crucible type.

5.1.5 Heat treatment 2 (CZ): 10 h

5.1.5.1 Temperature simulation of the CZ furnace

The temperature simulation performed by a SINTEF employee with the logiciel CGSim provided useful informations about the temperature experienced by the rods during HT2 of 10 h. It was observed that the pieces investigated experienced different temperature ranges during the heat treatment. In fact, the simulation suggested that the part dipped in the melt was subjected to a temperature of about 1400°C while the part just above the melt level was subjected to temperatures as low as 1200°C. Knowing that cristobalite can start nucleating on HPQ crucibles at around 1000°C and that the development is promoted by higher temperatures, differences between the cristobalite occurrences on Pieces 2 and 3 (below and above the melt level, respectively) were expected.

However, this simulation included many inaccuracies. In fact, the model took into account only one rod while a set of 6 rods was dipped into the melt and the full dimension of each rod was not taken into account i.e. only the 4 pieces investigated in this study and the parallel study about the bubble content were considered. In addition, the thermal conductivity of silicon and quartz were kept constant in the model when they would normally vary with temperature. It can be suggested that due to the low thermal conductivity of quartz, even lower temperatures could be experienced by the rods when put close to each others as they were in the set-up.

5.1.5.2 Cristobalite characterisation

Variable occurrences of cristobalite were observed on the two crucible types investigated in HT2 of 10 h. The Piece 2 of A_{nc} (below the melt level) presented localised dissolved circular areas coherent with the contact with the highly reactive melt in addition to localised and large areas of white cristobalite. Between the white cristobalite areas, the quartz surface showed a dissolution pattern also consistent with the contact with the melt. Concerning Piece 3 of A_{nc} (above the melt level), a homogeneous while cristobalite layer was observed. On the other hand, on Piece 3 of Std_{nc}, no occurrence of cristobalite was observed. This might be a consequence of the low temperature on that part of the rod that did not give sufficient energy to Std_{nc} to activate the cristobalite formation. For Piece 2 of Std_{nc}, only the localised dissolved circular areas and the dissolution pattern between them were observed. This non presence of white cristobalite below the melt level despite the higher temperature exposure might come from the slower nucleation mechanism of Std_{nc}, already mentioned during the discussion about the three HT1.

Concerning the XRD analysis, Pieces 2 and 3 of A_{nc} showed a preferred orientation of $\{200\}$. No conclusion concerning a preferred orientation for Std_{nc} (Pieces 2 and 3) was drawn due to the low crystallinity of the samples. A possible explanation for that low crystallinity is that the surface was still mainly composed of amorphous quartz that was not subjected to the phase transition to cristobalite during HT2. However, the presence at $2\theta = 21.985$ of a broad peak for the part that was above the melt level and a conventional peak with low height in addition to several other small characteristic peaks for the part that was in contact with the melt suggested that cristobalite nucleated locally on the surface.

The results of the thickness measurements showed that for A_{nc}, the representative values were close for Pieces 2 and 3 but with less homogeneity of the layer for Piece 2. Those variations came most likely from the different occurrences (dissolution spots, localised cristobalite, etc.) observed on the surface of that sample. The thickness values were close to the one observed on A_{nc} after HT1 of 10 h, which suggested that independently of the heat treatment type, the holding time at high temperature had a relatively same effect on the cristobalite formation. On the other hand, for Std_{nc}, a very non homogeneous layer of cristobalite was observed, more in the form of localised particles of small sizes. The thickness values were even lower than on Std_{nc} after HT1 of 90 min. This was coherent with the observations of the cristobalite morphology (quasi-inexistant) and it suggests again that the nucleation of cristobalite on Std_{nc} was initiated at a slower rate.

5.2 Used samples

5.2.1 Heat treatment 3: 100 h

The morphology of the used crucible pieces observed by light microscopy showed similarities between coated and non coated pieces with a cristobalite coverage of the whole surface and tiles of approximately equal and constant size. However, it was noticed that for the non coated pieces, the white cristobalite layer was less dense with more and larger corrosion rings underneath. This would suggest that the white cristobalite layer nucleated more rapidly on the surface of coated crucibles pieces and then protected it from further corrosion in contact with the melt while for the non-coated crucible pieces on Figure 101, the quartz surface reacted more with the melt before a homogeneous cristobalite layer had formed.

From the SEM observations, it was observed that the coated crucible pieces formed a denser cristobalite layer more subjected to cracks. The layer formed also seemed more resistant to the contact with the melt and the dissolution induced since it showed less dissolution spots on the surface, with smaller size and depth. This was more particularly noticed for the A crucible where the surface morphology of the coated and non coated crucible pieces was very different, as already seen on Figure 100a and d in the macroscopic view. Since A_u was only subjected to a HT3 of 40 h, this might have prevented a large growth of cristobalite, leading to a surface less resistant to dissolution.

Concerning the XRD results, it was seen that for A_{uc}, B_u, B_{uc} and Std_{uc}, a preferred orientation of {200} existed while for A_u, it was the random cristobalite orientation {101} that prevailed. This exception might come from the cristobalite morphology. In fact, as seen on Figures 100 and 101a), A_u has the "brownish" cristobalite occurrence which differs quite strongly from the other occurrences (shape, colour, corrosion pattern) which could indicate a different growth mode leading to a different orientation. In addition, since A_u was subjected to only 40 h at high temperature, this orientation might correspond to an "early" random growth of cristobalite (as observed after HT1 of 90 min, 10 h and 24 h) since no coating was present to influence the nucleation.

The cristobalite layer thicknesses observed after HT3 confirmed that the coating induced a larger development of cristobalite. In fact, on coated pieces, layer thicknesses up to 8 times the ones observed on non coated pieces were measured. In addition, after HT3, the layer were very homogeneous, even for the non coated pieces. While cracks were observed on the top surface of the cristobalite layer certainly due to the change of density during the beta-alpha transition of cristobalite upon cooling where the cristobalite contracted, for the coated pieces, cracks on the quartz surface under the cristobalite layer were also noticed. They could come from stresses exerted by the cristobalite layer on the quartz also due to the contraction upon cooling. Those cracks under the cristobalite layer were most likely the reason for the easy removal of the white brittle cristobalite layer on A_{uc}, B_{uc} and Std_{uc}.

5.3 General comparison

5.3.1 Heat treatments

One has to keep in mind that the different heat treatments (HT1, HT2 and HT3) results studied cannot be compared easily due to the many parameters involved that vary and the uncertainties linked to each of those processes.

HT1 brought many inaccuracies in comparison to the industrial process (better represented by HT3). First of all, a VGF furnace was used while the used samples provided by the industry were obtained from a CZ process. This induced differences in the melt behaviour and movements that should impact the reaction at the melt/crucible piece interface. The solidification process was different, in addition to the temperature profile. The heat distribution in the furnace was not well known but seeing the small scale of the chamber, it was supposed relatively homogeneous around the small crucibles used. Another limitation was the fact that only the top parts of the rods were studied while the volumes that were inside the melt and directly in contact with it were not studied due to the impossibility to extract the piece from the solidified Si without loosing the cristobalite layer developed on the rod. Thus, the cristobalite formed on the top part of the rod that was studied was representative of a "free" cristobalite development from heat treated quartz. That is different from the used crucibles characterised that were in direct contact with the melt during their holding time at high temperature.

HT2 represented better the CZ conditions encountered in the industry. However, the parameters of the heat treatment were not completely controlled, the heat distribution was not homogeneous and the temperature was approximately 1450°C at the melt surface. That is about 100°C lower than in HT1.

5.3.2 Morphology evolution HT1

A general evolution of the cristobalite morphology between HT1 90 min, 10 h and 24 h is shown on Figures 115, 116, 117 and 118 for A_n, B_n, B_{nc} and Std_{nc} respectively. In fact, this comparison is not possible for A_{nc}, A_n dip and spray coated and B_n spray coated since the information for the 24 h experiment is missing. With a longer time exposure at high temperature, the cristobalite developed further on the surface, the layer densified and became more homogeneous and more brittle (presence of cracks). When comparing the crucible types, it was observed than Std_{nc} seemed to need more time to nucleate cristobalite, as did the non coated A_n crucible. It is B_{nc} that shows the most homogeneous morphology through all the HT1 (90 min, 10 h and 24 h).

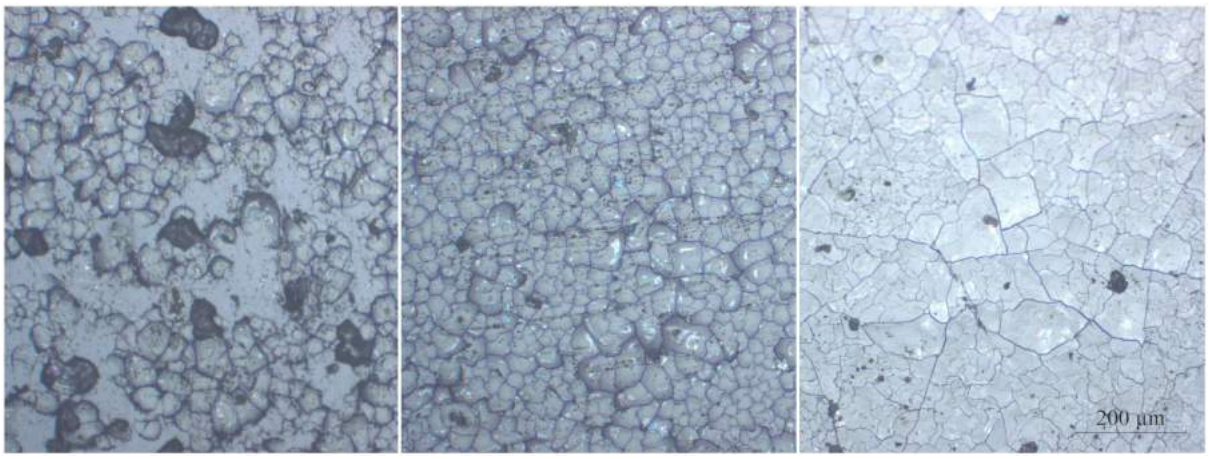

Figure 115: Evolution of the cristobalite morphology of A_n with HT1: From left to right 90 min, 10 h and 24 h

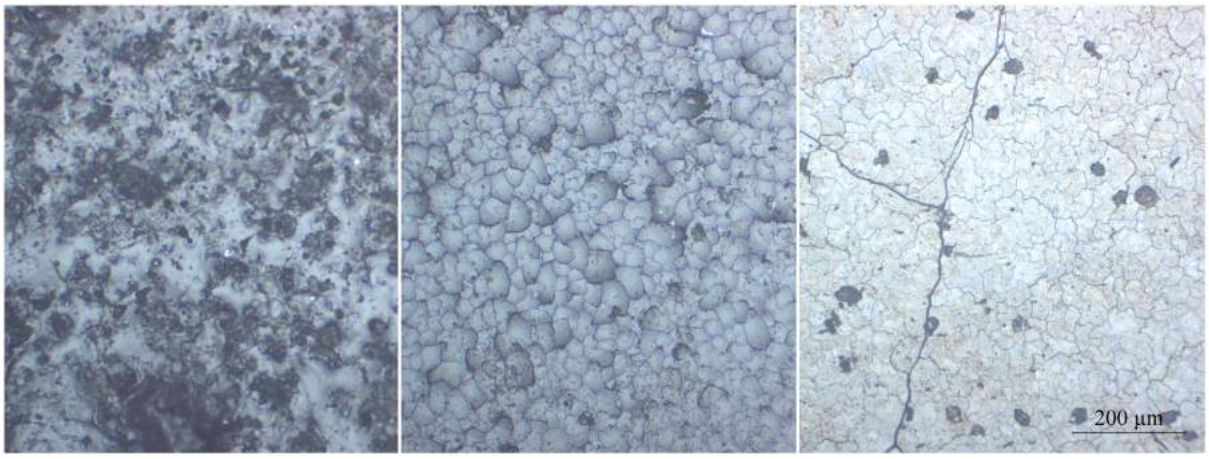

Figure 116: Evolution of the cristobalite morphology of B_n with HT1: From left to right 90 min, 10 h and 24 h

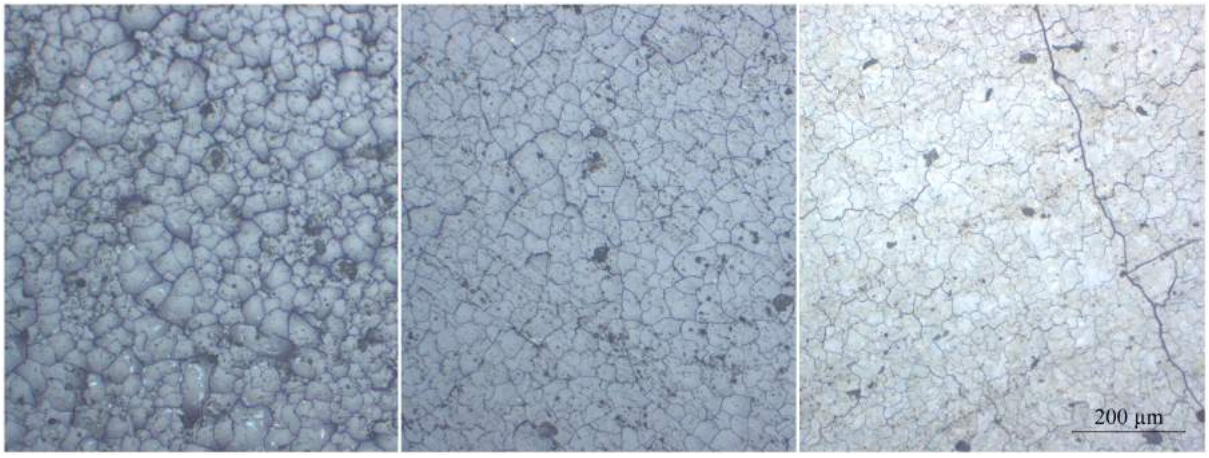

Figure 117: Evolution of the cristobalite morphology of B_{nc} with HT1: From left to right 90 min, 10 h and 24 h

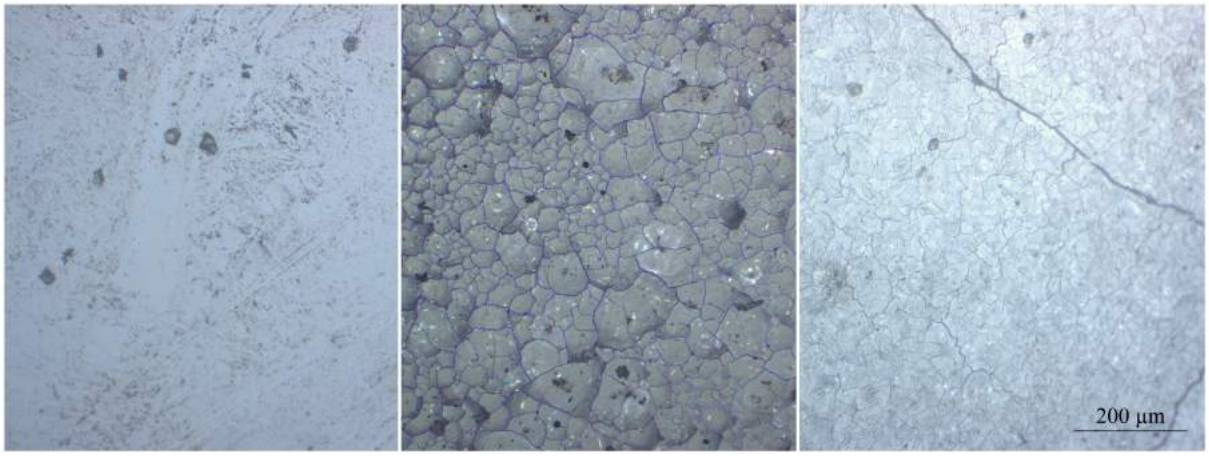

Figure 118: Evolution of the cristobalite morphology of Std_{nc} with HT1: From left to right 90 min, 10 h and 24 h

5.3.3 Thickness evolution HT1-HT3

Concerning the evolution of the cristobalite layer thickness between 90 min, 10 h and 24 h HT1 and HT3 of 100 h, Figure 119 shows that the thickness increased with the exposure time for each crucible type considered in HT1. The growth factor was approximately 1.5 between HT1 of 90 min and HT1 of 10 h and up to 8 between HT1 of 10 h and HT1 of 24 h. The only exception was Std_{nc} on which the layer after 10 h was about 3 μm lower than after 90 min. As already mentioned, after 90 min, only particles of cristobalite were found on the surface of Std_{nc}, so that the thickness measured might not be representative at all. In addition, the measurement uncertainty from the scale on the pictures was about 5 μm so that it might be that the cristobalite layer on Std_{nc} was slightly higher than measured. In terms of coating, it is obvious that the pieces coated at NTNU showed thicker layers at any exposure time than the industrially coated pieces. In addition, the increase in thickness between 90 min and 10 h HT1 is way larger for the pieces coated at NTNU. It might come from the Ba concentration in the coating used at NTNU, the thickness of the coating or its homogeneity, as suggested before.

In general, the coated pieces had thicker cristobalite layers, which was the expected outcome seeing that the coating is supposed to enhance the devitrification of quartz to cristobalite. However, when looking at the results for HT3, it was seen that, for A_u and B_u (40 h and 100 h at high temperature, respectively), lower thickness values than after 24 h in HT1 are obtained. In addition, the difference between coated and non coated pieces in terms of the thickness was way larger and the layer thickness for non coated pieces after 100 h in HT3 was lower than the one observed after 24 h in HT1. The most plausible reason for that observation is that in HT3, the crucible pieces were in contact with the melt during the whole process where the quartz was first dissolved, then cristobalite nucleated (faster for coated pieces) and the cristobalite layer, once formed, was also subjected to dissolution. In fact, in HT1, cristobalite developed freely on the surface, only depending on the atmosphere, the temperature, the quartz surface quality and the coating.

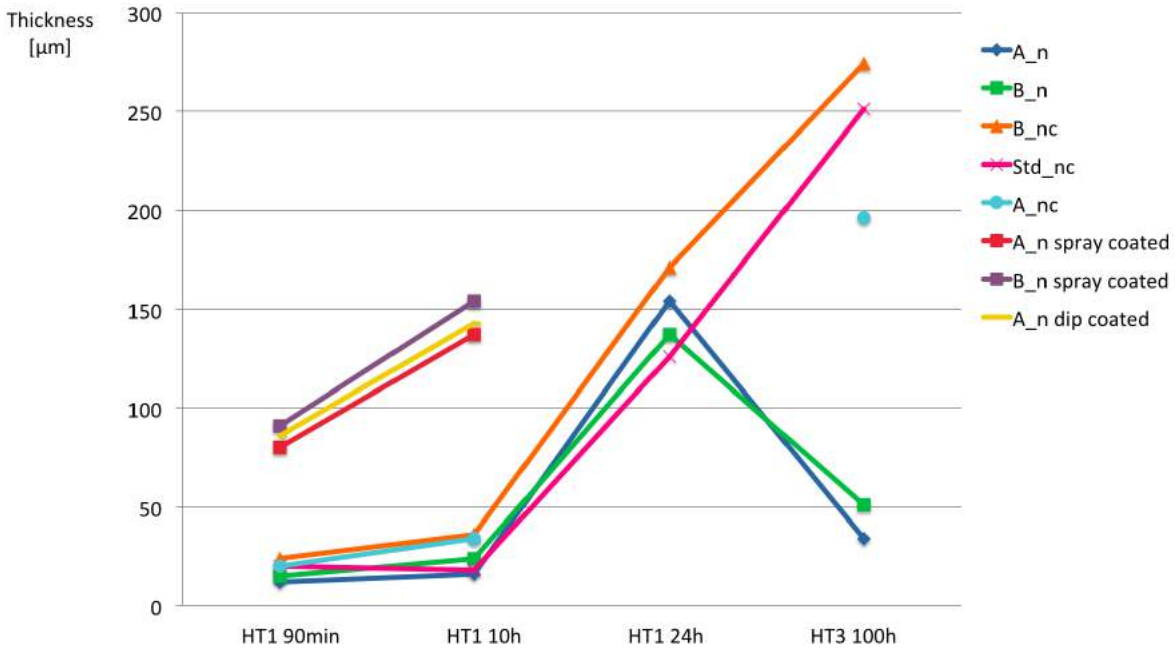

Figure 119: Evolution of the thickness of the cristobalite layer between HT1 of 90 min, 10 h and 24 h and HT3 of 100 h

5.3.4 Thickness comparison HT2-HT1

On Figure 120, a comparison between the thickness of the layers observed on A_{nc} and Std_{nc} after HT2 and HT1 is made. It can be seen that for Std_{nc}, the layers were thicker when developed freely in HT1 in comparison with HT2. However, one has to keep in mind that the results related to Std_{nc} in HT2 were surprising since almost no cristobalite was observed on the two rod pieces studied. Those results are thus considered as not conclusive. Concerning A_{nc}, the thickness of the cristobalite layer after 10 h in HT1 or HT2 is similar. In general, the cristobalite layer was thicker for the piece that was in the melt during HT2, where the temperature was supposedly higher. Those similar values between the 10 h in HT1 and HT2 even for the piece that was in the melt suggested that even if the quartz seemed to have dissolved (see Part 4.1.5), the 10 h were maybe not sufficient to largely dissolve the cristobalite layer formed.

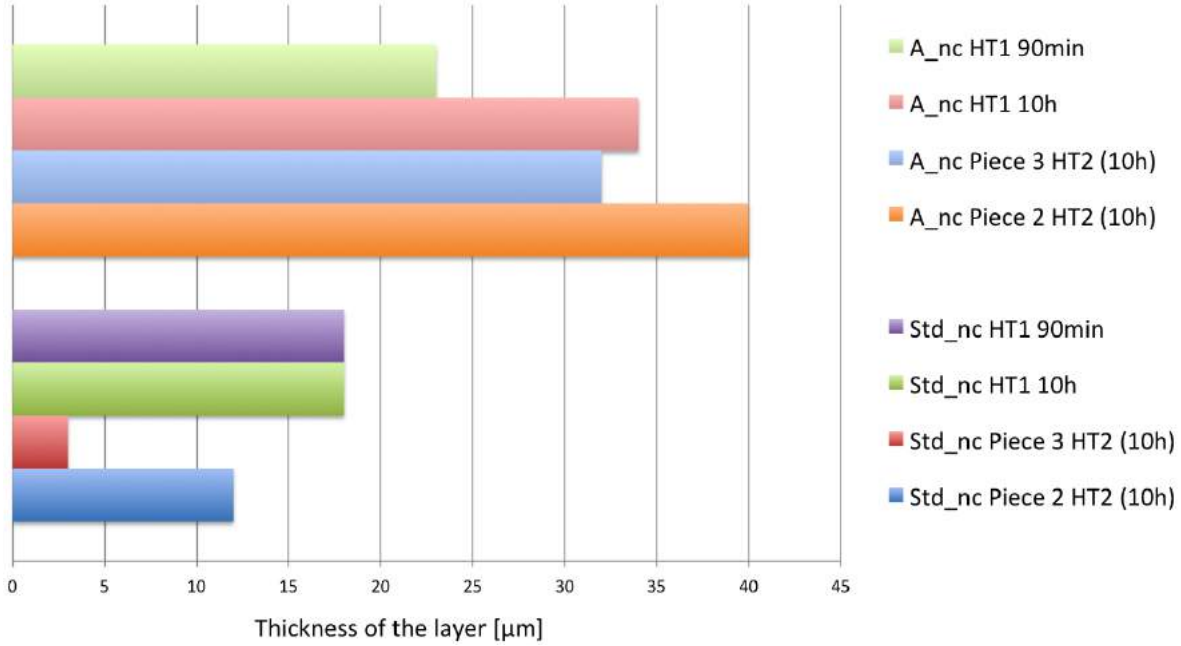

Figure 120: Comparison of the thickness of the cristobalite layer observed on A_{nc} and Std_{nc} after HT2 with the ones observed after HT1 90 min and 10 h

5.3.5 Cristobalite orientation comparison HT1-HT2-HT3

Table 12 shows the main cristobalite orientation observed on each crucible type (with each coating type) in function of the heat treatment. Only two orientations were obtained from the many heat treatments : {101} and {200}. It can be highlighted that on A_n, the same orientation ({101}) was observed for every heat treatment. On the other hand, on the non coated and industrially coated pieces, for each HT1, the orientation ({101}) was also observed. {101} is the orientation observed on randomly oriented cristobalite powders. From those observations, it can be suggested that this orientation corresponds to the early nucleation of cristobalite when the coating is not present in large quantities. For A_{nc} after HT2, A_n spray coated, A_n dip coated and B_n spray coated after HT1 of 90 min and 10 h and B_n, B_{nc}, A_{nc} and Std_{nc} after HT3 of 100 h, the preferred orientation is {200}. This orientation was thus observed on pieces that were coated in a specific way and/or subjected to a heat treatment with contact or close proximity with the melt and long holding time. {200} seems to appear when enough time is given for the growth (i.e. HT3 with 100 h holding time) at high temperature or with a thicker coating on the crucible surface (i.e. the coatings performed at NTNU) for any type of crucibles. The exception of A_n in HT3 might come from the fact that this crucible type was subjected only to 40 h at high temperature in HT3, as mentioned earlier.

In general, many factors influence the cristobalite nucleation direction. Obviously, the coating has an important impact on the orientation but the results suggested that the melt contact, its movements and probably the gas flux movements relative to the heat treatment type were also influencing the nucleation orientation. It is not possible to conclude anything about whether or not a certain orientation of the cristobalite nucleated

has a good or bad impact on the melt quality and the CZ process productivity in general.

Table 12: Comparison of the cristobalite orientation observed on each sample type for each heat treatment performed

Sample type / HT type	**A_n**	**B_n**	**B_{nc}**	**Std_{nc}**	**A_{nc}**	**A_n spray**	**B_n spray**	**A_n dip**
HT1 90min	{101}	{101}	Epoxy	Epoxy	{101}	{200}	{200}	{200}
HT1 10h	{101}	{101}	{101}	/	{101}	{200}	{200}	{200}
HT1 24h	{101}	{101}	/	{101}	/	/	/	/
HT2 10h (piece 2)	/	/	/	Not conclusive	{200}	/	/	/
HT2 10h (piece 3)	/	/	/	Not conclusive	{200}	/	/	/
HT3 100h	{101}	{200}	{200}	{200}	{200}	/	/	/

5.3.6 Repetability

One major drawback of this work is the lack of statistics concerning the results. In fact, many problems related to functioning of the VGF furnace (HT1) were encountered. Those problems prevented the use of the furnace during long periods, reducing the final number of experiments that were conducted in the time allowed for the thesis work. Each crucible type (with every type of coating) was investigated in HT1 of 90 min and 10 h. However, as mentioned earlier, only four crucible types have been subjected to the 24 h HT1. No repetition of the HT1 experiments for the same crucible types was conducted. In addition, from each crucible rod studied in HT1, only one or two small pieces of about 1 cubic centimetre were available for the characterisations. Since this material was used in this work and in the work related to the bubble content, some characterisations could not be conducted to preserve the material for both the studies.

Concerning HT2, the CZ puller was only available for one experiment. Due to a lack of other crucible material, only two crucible types were used in this heat treatment. This limitation depends on the industrial partner that was not able to provide more crucible pieces of the other crucible types (that must have been produced from the same batch) and it reduced the contribution of the results of HT2. However, 3 rods of each crucible types were subjected to HT2, so that the results were verified for at least 3 reproduced samples, increasing the reliability of the results.

The characterisations after HT3 were conducted on two crucible pieces of each type in order to have a confirmation of the observations. Those results are then also more reliable than the results obtained for HT1 even if two pieces are not enough to build good statistics in terms of reproducibility or repetability.

6 Conclusion

The cristobalite formation on fused quartz crucible pieces from the same producer was investigated in this work. Different sand quality crucibles (i.e. A, B and Std) were studied. New pieces, already coated by the crucible manufacturer and non coated were available. In addition, pieces from crucibles used in the CZ process, also coated and non coated, were provided. Some of the new non coated crucible pieces have been dip and spray coated at NTNU. The resulting coatings were observed by SEM, analysed by EDS and XRD and compared to the coatings performed by the crucible manufacturer. After that, the new crucible pieces (non coated, industrially coated and coated at NTNU) were heat treated in a VGF furnace with different holding times (i.e. 90 min, 10 h and 24 h). Some samples were also subjected to a heat treatment in a CZ puller with a 10 h holding time. The used crucibles were considered as a the result of a third heat treatment with holding time 100 h. The cristobalite occurrence on the crucible pieces after those three heat treatments was characterised by light microscopy, XRD and SEM.

The quartz crucibles pieces, new and, had a barium based solid deposited on their surface. The SEM results revealed that the coating performed by the crucible manufacturer or at NTNU was easily removed by the handling procedure. In fact, even if the spray coating pattern (industrial and from NTNU routine) was in general more homogeneously spread on the crucible surface than the dip coating, the industrially coated Std crucible showed almost no coating presence. The XRD analysis confirmed that the barium hydroxide, $Ba(OH)_2$, coating reacted with the carbon dioxide, CO_2, in the air to form barium carbonate, $BaCO_3$, on the quartz surface. This was coherent with the results of a SINTEF study [68]. In addition, the coatings performed at NTNU were thicker than the ones observed on pieces with industrial coating.

From HT1 of 90 min, 10 h and 24 h in the VGF furnace, it was proven that the freely developed cristobalite layer becomes more homogeneous, denser, thicker and more brittle with the holding time at high temperature. This observation was valid for each crucible type investigated, coated and non coated but it was noticed that the development of cristobalite was slower for non coated crucible pieces and Std_{nc} and faster for the pieces coated at NTNU. The most likely reason of this trend was the dependence of the cristobalite growth on the coating presence and thickness. The crystal orientation was found to be {101} on non coated pieces and pieces with industrial coating. The pieces coated at NTNU showed a preferred orientation of {200}.

HT2 of 10 h in the CZ puller was only performed on two crucible types. This lack of data reduced the pertinence of the results. However, it was possible to highlight the corrosive character of the highly reactive silicon melt that dissolved the amorphous quartz surface that was kept in contact with the melt during HT2. The parts dipped in the melt were found to be subjected to higher temperature than the part just above the melt level. This led to a thicker cristobalite occurrence observed on the piece below the melt level despite the dissolution experienced. In addition, it was noticed that the preferred cristobalite

orientation after HT2 was {200} so that, in addition to the coating influence, the heat treatment type and the linked parameters (melt contact and movement, heat and gas flow patterns, etc.) also influenced the cristobalite nucleation direction.

The results of HT3 (used crucibles (100 h)) allowed to furthermore understand the cristobalite growth process when the crucible was in contact with the melt. It was observed that coated crucibles grew the white cristobalite layer faster than the non coated crucibles. Those were more subjected to the dissolution before and after cristobalite growth. When there is a contact with the melt, it was also seen that between 40 h or 100 h exposure at high temperature, for non coated crucibles, there was only a small change in cristobalite layer thickness but the morphology and crystal orientation were very different i.e. brown cristobalite macroscopic occurrence and {101} crystal orientation after 40 h and white cristobalite macroscopic occurrence and {200} crystal orientation after 100 h.

When all the heat treatment results were compared, it was shown that despite the many variables between those heat treatments, some general trends could be recognised. It was observed that the coating promoted the cristobalite growth as expected, even if non coated crucibles also nucleated cristobalite quite homogeneously after a certain time. In addition, the cristobalite layer formed on coated crucibles seemed more resistant to dissolution by the melt so that there is a clear advantage of the use of coating on quartz crucibles in the CZ process. However, the coating process should be controlled. In fact, it was revealed that a thicker coating leads to a thicker cristobalite development. This observation was made by some previous published work but they were more related to the barium coating concentration. More importantly, the coating should be homogeneous in order to help for the development of a dense and widely spread cristobalite layer, nucleating on the quartz surface fast enough to protect the whole crucible surface by reducing the crucible material dissolution in the melt. It was noticed that spray coating, that is used in the industry, was the best technique to meet those coating requirements. Finally, it seemed that with longer exposure time at high temperature or with influence of a thick coating, it is the crystal orientation {200} that remained on the top surface of the crucible pieces covered by cristobalite. In terms of crucible types, it was crucible B that provided, in general, the most homogeneous and coherent results so that it might be the most suitable crucible choice for the production of monocrystalline silicon ingots.

7 Further work

In this work, a practical study method of the cristobalite formation and its influence was established. While some results were coherent with previous works done on the subject, some new observations were made and new perspectives were introduced. For those results to be beneficial to the PV industry, further works should be conducted in order to confirm some of the trends and get more insights about the importance of each individual factor on the formation mechanism.

The results obtained from this thesis were very limited in terms of statistics. A first step of the continuation of this work would be to repeat the experiments performed to assess the repetability of the method and the reproducibility of the results.

In order to have a full picture of the cristobalite development during an industrial process, longer holding times at high temperature should be considered in HT1, e.g. 40 h, 75 h and 100 h. Another interesting feature to study would be the influence of the temperature. The heat treatments could be performed from temperatures just below the theoretical formation point of cristobalite (i.e. 1000°C) to 1550°C with intermediate temperatures also considered. Those two parameters (holding time and temperature), should be investigated separately in order to get an idea of their individual influence.

To better understand the difference between the free cristobalite development and the cristobalite formation when there is a contact with the melt, HT2 should be conducted on the crucible types not investigated in this work and with different holding times and temperatures as well. However, an improvement of the temperature simulation in the CZ puller should be considered so that it better suits the real sample set-up in the furnace.

Another factor that has an influence on the cristobalite formation but that was not studied in this work is the crucible surface quality. It should be investigated prior to the heat treatments for each crucible type in order to highlight possible links.

In addition, it has been seen that the coating has a large influence on the cristobalite nucleation. It would be interesting to highlight the relation between the coating thickness and the cristobalite thickness nucleation but also the influence from the barium concentration in this coating. It is possible that when using a too thick or too concentrated coating, the resulting cristobalite layer formed is of large thickness that might become detrimental for the use of the crucible in the CZ process.

Finally, the growth mechanism of cristobalite should be furthermore studied in terms of crystal orientations. It would be helpful to know if the preferred orientation observed on used crucibles ({200}) is actually profitable for the pulling process i.e. if this nucleation

orientation reduces the dissolution of the quartz material in the silicon melt or allows for a longer use of the crucibles in the CZ process by increasing the structural resistance of the crucibles. If this is not the case, it would be interesting to investigate the impacts of other cristobalite orientations and maybe develop methods to force other orientation growths of cristobalite.

List of Figures

List of Tables

References

[1] . URL https://www.bp.com/content/dam/bp/pdf/energy-economics/statistical-review-2016/bp-statistical-review-of-world-energy-2016-full-report.pdf. Accessed the 17/03/2017.

[2] URL http://www.engineeringchallenges.org/challenges/solar.aspx. Accessed the 22/02/2017.

[3] . URL https://www.perovskite-info.com/perovskite-solar. Accessed the 17/03/2017.

[4] Noritaka Usami Kazuo Nakajima. *Crystal Growth of Silicon for Solar Cells*. Springer-Verlag Berlin Heidelberg, 2009. ISBN 978-3-642-02043-8.

[5] Di Sabatino M. *Solar Cells and Photovoltaic Nanostructures, Impurities and defects in silicon solar cells, Lecture slides, NTNU*. 2016. Accessed the 11/02/2017.

[6] Di Sabatino M. *Solar Cells and Photovoltaic Nanostructures, Silicon solidification, Lecture slides, NTNU*. 2016. Accessed the 14/03/2017.

[7] Picture : "phase diagram of silica" taken from. URL http://www.quartzpage.de/gen_mod.html#F_1.

[8] Hoshikawa Takeshi Xinming Huang and Uda Satoshi. Analysis of the reaction at the interface between si melt and ba-doped silica glass. pages 422–427, 2007. doi: 10.1016/j.jcrysgro.2007.05.020.

[9] Wu Kehui Chen Mingwei Hoshikawa Takeshi Hoshikawa Keigo Huang Xinming, Koh Shinji and Uda Satoshi. Reaction at the interface between si melt and a ba-doped silica crucible. pages 154–161, 2005. doi: 10.1016/j.jcrysgro.2005.01.101.

[10] Di Sabatino M. *Solar Cells and Photovoltaic Nanostructures, Silicon production, Lecture slides, NTNU*. 2016. Accessed the 11/02/2017.

[11] URL https://commons.wikimedia.org/wiki/File:Silicon_purification_processes.svg. Accessed the 11/02/2017.

[12] Gabriella Tranell. Processes for Upgrading Metallurgical Grade Silicon to Solar Grade Silicon grade silicon. 2012. doi: 10.1016/j.egypro.2012.03.011.

[13] URL http://www.google.com/patents/EP2024284A2?cl=en. Accessed the 11/02/2017.

[14] Duffar Thierry. *Crystal Growth Processes Based on Capillarity: Czochralski, Floating Zone, Shaping and Crucible Techniques*. 2010. ISBN 1444320211, 9781444320213.

[15] Hsu Chuck Lan Chung-wen and Nakajima Kazuo. 10 - Multicrystalline Silicon Crystal Growth for Photovoltaic Applications. In *Handbook of Crystal Growth (Second Edition)*, pages 373–411. Elsevier, 2015. ISBN 978-0-444-63303-3. URL http://www.sciencedirect.com/science/article/pii/B9780444633033000109.

[16] URL https://commons.wikimedia.org/wiki/File:Czochralski_Process.svg. Accessed the 12/02/2017.

[17] URL http://meroli.web.cern.ch/meroli/Lecture_silicon_floatzone_czochralski.html. Accessed the 12/02/2017.

[18] URL http://www.tf.uni-kiel.de/matwis/amat/iss/kap_5/advanced/a5_2_2.html. Accessed the 12/02/2017.

[19] URL https://www.tf.uni-kiel.de/matwis/amat/semitech_en/kap_4/illustr/i4_1_6.html. Accessed the 12/04/2017.

[20] P. Rudolph. *Handbook of Crystal Growth: Bulk Crystal Growth*, chapter 2, Czochralski Growth of Silicon Crystals. Handbook of Crystal Growth. Elsevier Science, 2014. ISBN 9780444633064. URL https://books.google.no/books?id=F4BzAwAAQBAJ.

[21] Peter Capper Safa Kasap. *Springer Handbook of Electronic and Photonic Materials*. Springer US, 2007. ISBN 978-0-387-26059-4.

[22] Chetan Singh Solanki. *Solar Photovoltaics : Fundamentals, Technologies and Applications*. PHI Learning, 3rd Edition, 2015.

[23] URL https://www.quora.com/How-are-Sapphire-screens-made. Accessed the 12/04/2017.

[24] Hughes Emma. *High Purity Quartz: A Cut Above*, pages 22–25. Industrial Minerals, Minerals In Motion, 2013.

[25] URL https://www.mindat.org/min-3337.html. Accessed the 12/04/2017.

[26] Mockel R. Gotze J. *Quartz : Deposits, Mineralogy and Analytics*, chapter 2 : Assessment of High Purity Quartz Resources, pages 29–52. 2012. ISBN 9783642221613.

[27] The QUARTZ Corp. High Purity Quartz sand detailed content. (99439):10–11, 2015.

[28] Method of production of quartz crucible : Patent. URL http://russianpatents.com/patent/233/2333900.html. Accessed the 12/02/2017.

[29] Hanna Vaksvik Skarstad. Behaviour of the slip-cast crucible as a contamination source during silicon directional solidification, Master's thesis NTNU, 2016.

[30] D.R. Brown, C.E. Frost, and K.A. White. Method of manufacturing quartz glass crucibles with low bubble content, 1986. URL http://www.google.com/patents/US4632686. US Patent 4,632,686.

[31] R. Bruning and F. Habegger. Method of making quartz glass crucibles, and apparatus carrying out the method, 1983. URL http://www.google.com/patents/US4416680. US Patent 4,416,680.

[32] H. Kishi, M. Fukui, and M. Morikawa. Arc discharge method, arc discharge apparatus, and fused silica crucible manufacturing apparatus, 2013. URL http://www.google.ch/patents/US8416833. US Patent 8,416,833.

[33] K. Kemmochi, L. Baer, and C. Hagstrom. Metal and graphite mold and method of making a crucible, 2013. URL http://www.google.ch/patents/US20130025319. US Patent App. 13/189,897.

[34] Nishi Y. and Doering R. *Handbook of Semiconductor Manufacturing Technology*. Taylor & Francis, 2000. ISBN 9780824787837. URL https://books.google.no/books?id=Qi98H-iTgLEC.

[35] Horioka Yukichi Fujiwara Kozo and Sakuragi Shiro. Liquinert quartz crucible for the growth of multicrystalline si ingots. pages 419–422, 2015. doi: 10.1002/ese3.90.

[36] Capper P. *Bulk Crystal Growth of Electronic, Optical and Optoelectronic Materials*. Wiley Series in Materials for Electronic & Optoelectronic Applications. Wiley, 2005. ISBN 9780470012079. URL https://books.google.no/books?id=ZqTkCF6Ra9kC.

[37] Thorsen Fredrik Winther. Investigation on Quartz Crucibles for Monocrystalline Silicon Ingots for Solar Cells, Master's Thesis, NTNU. 2016.

[38] Hansen Sebastian Holand. Characterization of quartz crucibles for silicon solar cell production, project thesis, ntnu. 2016.

[39] Standford S. Cole. The conversion of quartz into cristobalite below 1000c , and some properties of the cristobalite formed. 1934.

[40] Basic materials division : Tomorrow's innovations spring from 100 years of experience. URL http://www.gmassoc.com/pdf/heraeus-basic-materials-division.pdf.

[41] Olli Anttila. *Handbook of Silicon Based MEMS Materials and Technologies (Second Edition)*, chapter 2 - Czochralski Growth of Silicon Crystals, pages 18–55. Micro and Nano Technologies. William Andrew Publishing, Boston, 2015. ISBN 978-0-323-29965-7.

[42] Schnurre Sophie Marie. Reactions at the liquid silicon / silica glass interface. 2003.

[43] Yamahara Keiji Huang Xinming, Wang Tiefeng. Initial dissolution rate of quartz rods in silicon melts : Influence of quartz surface conditions.

[44] Toshinori Taishi Yamahara Keiji, Xinming Huang. In Situ Observation of the Interfacial Phase Formation at Si Melt / Silica Glass Interface. 2000. doi: 10.1143/JJAP.39.3281.

[45] . URL http://www.solgel.com/articles/Nov00/mennig.htm. Accessed the 22/03/2017.

[46] . URL http://www.nadetech.com/index.php/en/technologies. Accessed the 22/03/2017.

[47] . URL http://plasticphotovoltaics.org/lc/lc-fabrication/lc-coating/lc-spray.html. Accessed the 12/04/2017.

[48] . URL http://www.google.co.nz/patents/CN102336527A?cl=en. Accessed the 22/03/2017.

[49] . URL https://www.researchgate.net/publication/236598204_Process_Optimization_of_Ultrasonic_Spray_Coating_of_Polymer_Films. Accessed the 12/04/2017.

[50] . URL http://www.bmschem.com/servicesaxx$_$en/id/180.html. Accessed the 22/03/2017.

[51] . URL http://www.google.st/patents/US7776155. Accessed the 22/03/2017.

[52] . URL http://russianpatents.com/patent/232/2328562.html. Accessed the 22/03/2017.

[53] K. Kemmochi and Y. Ohama. Silica glass crucible with barium-doped inner wall, 2008. URL http://www.google.com/patents/US7427327. US Patent 7,427,327.

[54] K. Kemmochi, R. Mosier, and P. Spencer. Silica crucible with inner layer crystallizer and method, 2004. URL https://www.google.co.in/patents/US20040040497. US Patent App. 10/654,805.

[55] URL http://www.microbiologyinfo.com/. Accessed the 17/02/2017.

[56] URL https://www.techwalla.com/articles/the-advantages-of-a-light-microscope. Accessed the 17/02/2017.

[57] URL http://www.ruf.rice.edu/~bioslabs/methods/microscopy/microscopy.html. Accessed the 17/02/2017.

[58] URL https://www.jic.ac.uk/microscopy/intro_LM.html. Accessed the 17/02/2017.

[59] URL http://www.nanoscience.com/technology/sem-technology/. Accessed the 19/02/2017.

[60] URL http://www.ammrf.org.au/myscope/sem/background/concepts/interactions.php. Accessed the 19/02/2017.

[61] URL http://www.microscopemaster.com/scanning-electron-microscope.html. Accessed the 19/02/2017.

[62] URL http://serc.carleton.edu/research_education/geochemsheets/techniques/SEM.html. Accessed the 19/02/2017.

[63] URL http://www.mee-inc.com/hamm/energy-dispersive-x-ray-spectroscopyeds/EDS. Accessed the 22/02/2017.

[64] . URL http://www-outreach.phy.cam.ac.uk/camphy/xraydiffraction/xraydiffraction1_1.htm. Accessed the 22/02/2017.

[65] . URL http://prism.mit.edu/xray/introduction%20to%20xrpd%20data%20analysis.pdf. Accessed the 22/02/2017.

[66] Ove Paulsen. Cristobalite formation on quartz glass. 2007.

[67] John Atle Bones. Temperature modelling of the ferrotec czochralski puller with the logiciel cgsim. 2017.

[68] Ryningen Birgit Juel Mari, Paulsen Ove. Characterisation of crucibles tested at norsun. 2015.

[69] S Matsuno, M Kuba, Y Moriyasu, T Morishita, and K Omote. Characterization of surfaces and thin films using a high performances grazing incidence x-ray diffractometer. 2000.

Appendix

A.1 Additional informations for HT1

The temperature profiles for the top and bottom temperatures of HT1 10 h and HT1 24 h can be seen on Figures 121 and 122.

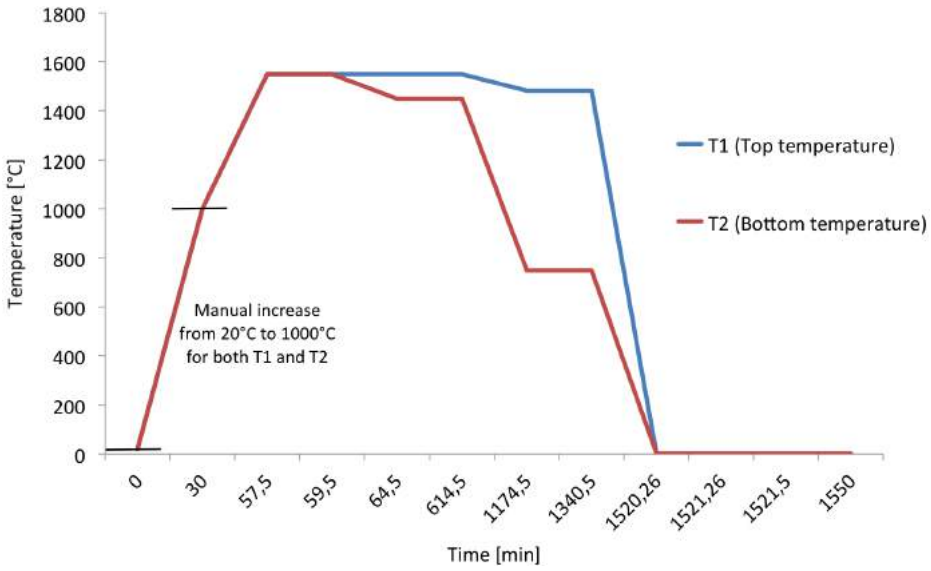

Figure 121: Temperature profile for HT1 in function of the time for the 10 h holding time and total experiment time of 1550 min or 25 h 50 min

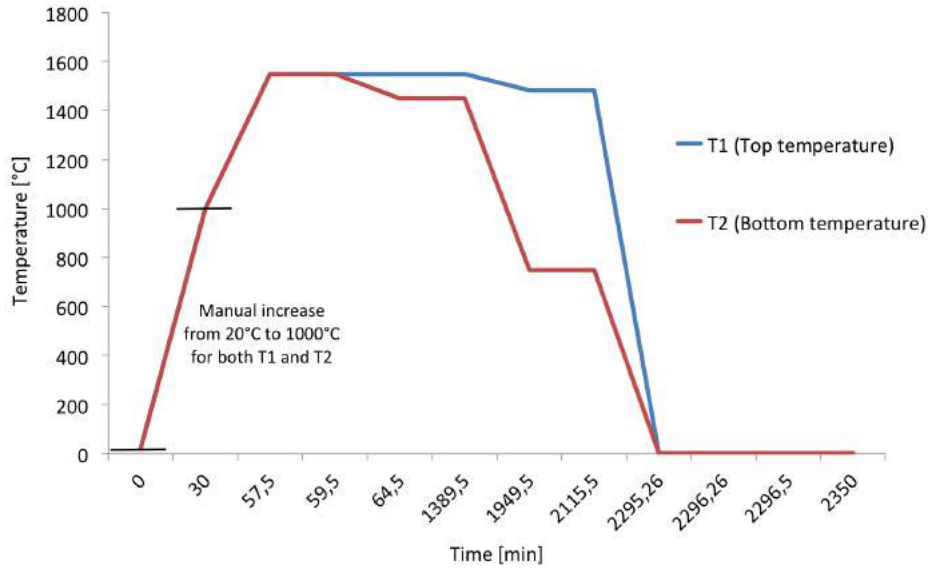

Figure 122: Temperature profile for HT1 in function of the time for the 24h holding time and total experiment time of 2350 min or 39 h 10min

Table 13 contains the information about the sample types and the feedstock weight associated to each HT1 performed.

Table 13: Heat treatments 1 : samples and feedstock weights

Experiment	**Sample 1**	**Sample 2**	**Sample 3**	**Sample 4**
	Feedstock weight 1	**Feedstock weight 2**	**Feedstock weight 3**	**Feedstock weight 4**
HT1a - 90 min	A_n	B_n	B_{nc}	Std_{nc}
	39.92 g	39.98 g	40.07 g	40.07 g
HT1b - 10 h	A_n	B_n	B_{nc}	Std_{nc}
	40.0547 g	40.0442 g	40.0638 g	40.0108 g
HT1c - 24 h	A_n	B_n	B_{nc}	Std_{nc}
	40.0927 g	40.1012 g	40.0792 g	40.1406 g
HT1d - 90 min	A_{nc}	A_n spray	A_n dip	B_n spray
	40.0612 g	40.0128 g	40.0997 g	40.0150 g
HT1e - 10 h	A_{nc}	A_n spray	A_n dip	B_n spray
	40.0631 g	40.1818 g	40.0327 g	40.0718 g
HT1f - 24 h	A_{nc}	A_n spray	A_n dip	B_n spray
	Not performed	Not performed	Not performed	Not performed

A.2 HT1 90 min : Cristobalite layer thickness

On Figures 123, 124, 125, 126, 127, 128, 129 and 130, the most representative cristobalite layers of the samples investigated after HT1 of 90 min are shown.

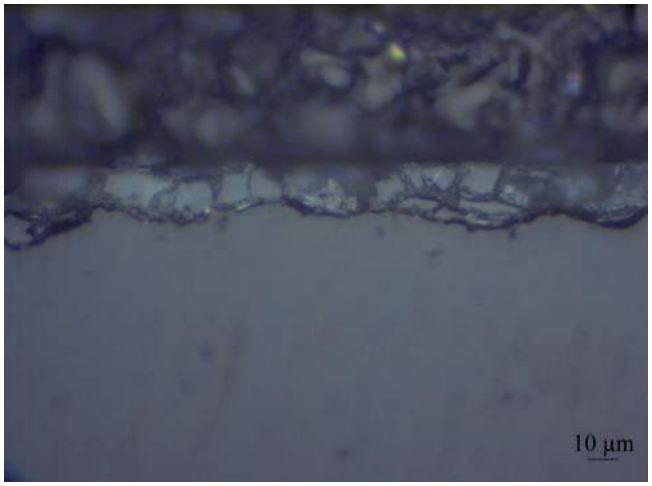

Figure 123: Cristobalite layer observed on A_n after HT1 of 90 min : Thin local occurrence, not homogeneous, hard to focus on due to bad polishing

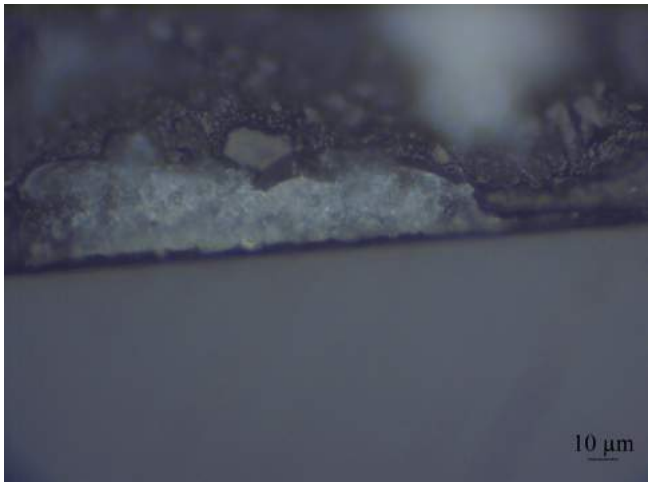

Figure 124: Cristobalite layer observed on B_n after HT1 of 90 min : Thin local occurrence, not homogeneous, hard to focus on

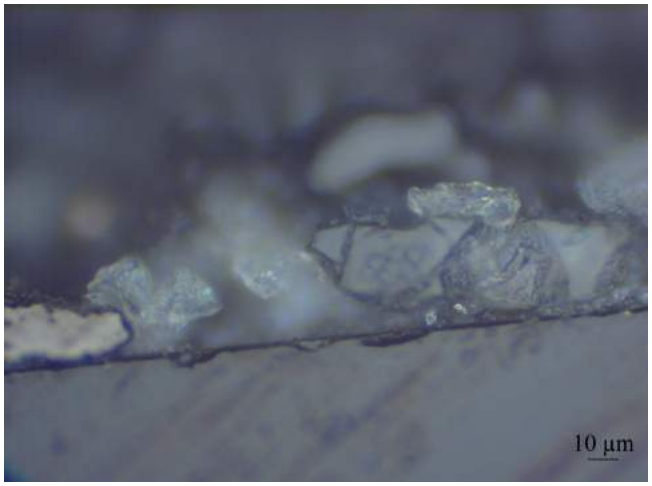

Figure 125: Cristobalite layer observed on B_{nc} after HT1 of 90 min : Thin local occurrence, not homogeneous, hard to focus on

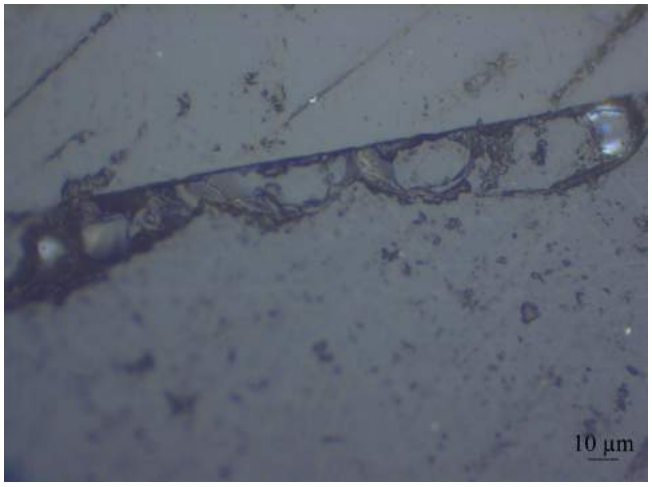

Figure 126: Cristobalite layer observed on Std_{nc} after HT1 of 90 min : Thin local occurrence, quite homogeneous, hard to focus on

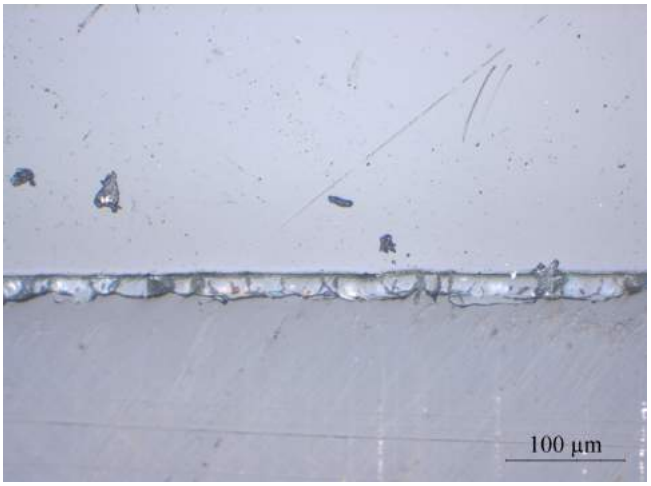

Figure 127: Cristobalite layer observed on A_{nc} after HT1 of 90 min : Thin occurrence, homogeneous, easier to observe

Figure 128: Cristobalite layer observed on A_n spray coated after HT1 of 90 min : Thicker occurrence, homogeneous

Figure 129: Cristobalite layer observed on B_n spray coated after HT1 of 90 min : Thicker occurrence, homogeneous

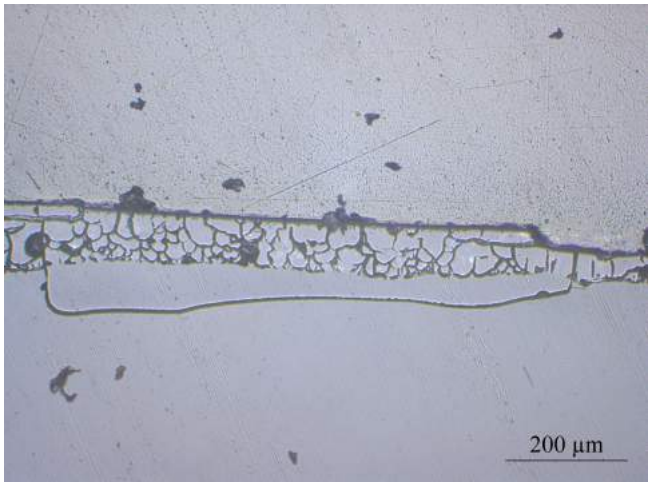

Figure 130: Cristobalite layer observed on A_n dip coated after HT1 of 90 min : Thicker occurrence, homogeneous

A.3 HT1 10 h : Cristobalite layer thickness

On Figures 131, 132, 133, 134, 135, 136, 137 and 138 the most representative cristobalite layers of the samples investigated after HT1 of 10 h are shown.

Figure 131: Cristobalite layer observed on A_n after HT1 of 10 h : Thin occurrence, homogeneous

Figure 132: Cristobalite layer observed on B_n after HT1 of 10 h : Thin occurrence, homogeneous

Figure 133: Cristobalite layer observed on B_{nc} after HT1 of 10 h : Larger occurrence, quite homogeneous

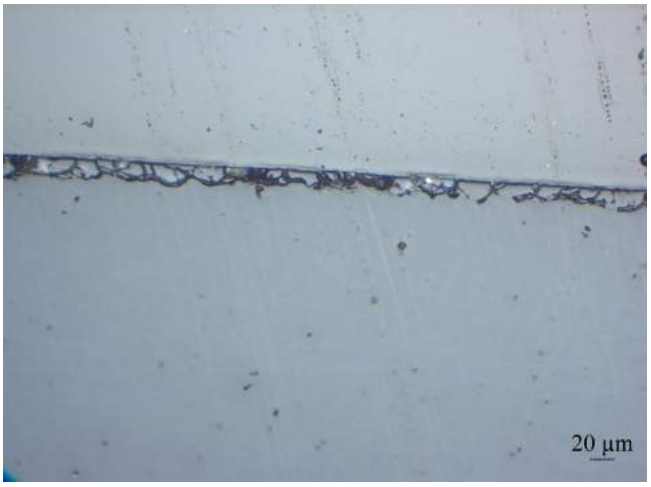

Figure 134: Cristobalite layer observed on Std_{nc} after HT1 of 10 h : Thin occurrence, homogeneous

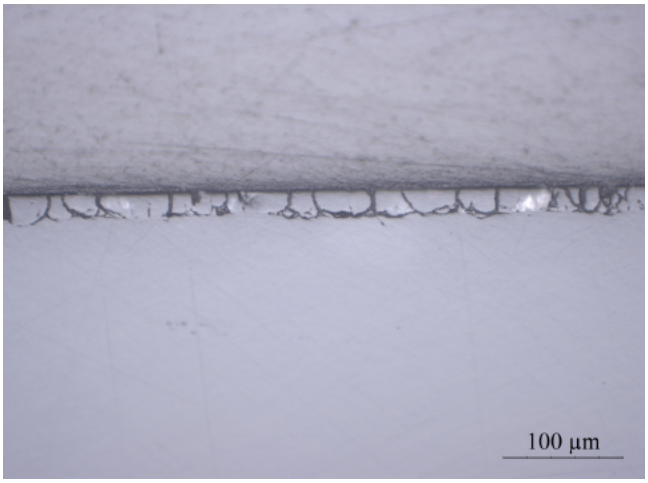

Figure 135: Cristobalite layer observed on A_{nc} after HT1 of 10 h : Larger occurrence, homogeneous

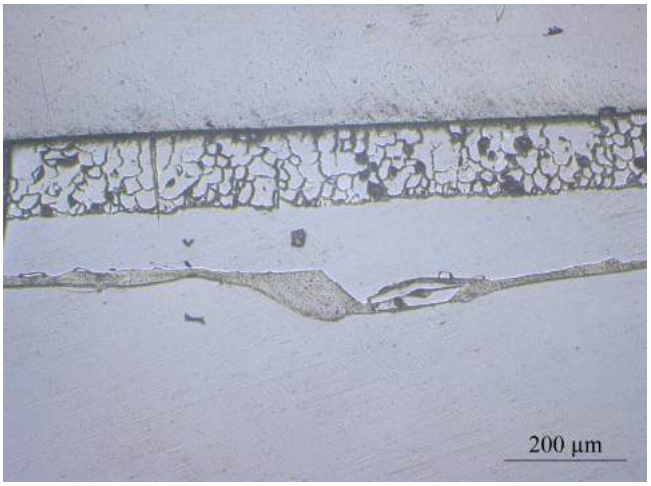

Figure 136: Cristobalite layer observed on A_n spray coated after HT1 of 10 h : Thick occurrence, very homogeneous, presence of cracks in the quartz under the layer

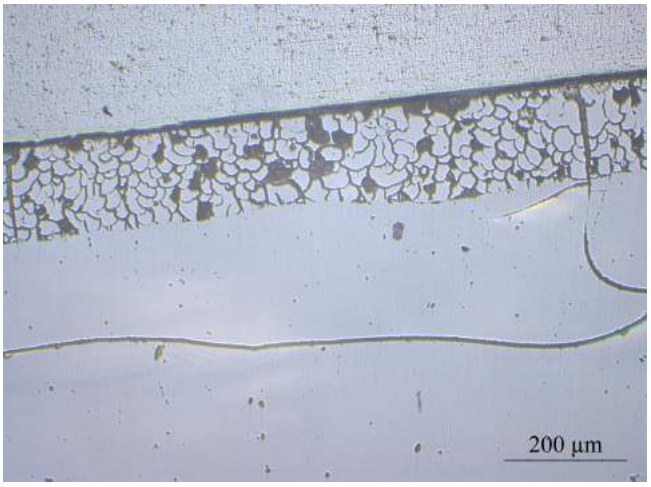

Figure 137: Cristobalite layer observed on B_n spray coated after HT1 of 10 h : Thick occurrence, very homogeneous, presence of cracks in the quartz under the layer

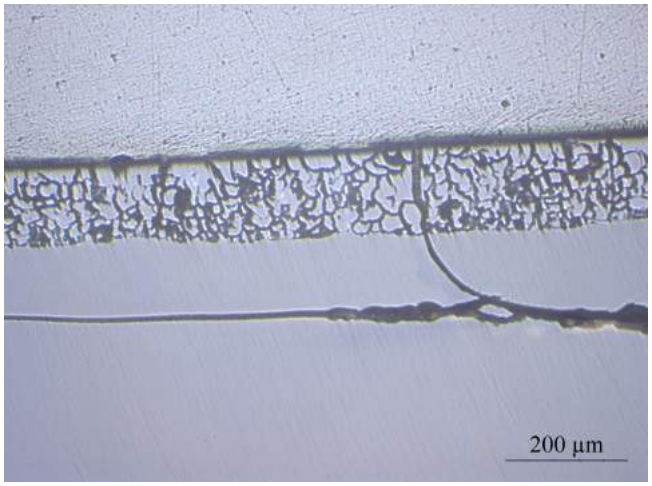

Figure 138: Cristobalite layer observed on A_n dip coated after HT1 of 10 h : Thick occurrence, very homogeneous, presence of cracks in the quartz under the layer

A.4 HT1 24 h : Cristobalite layer thickness

On Figures 139, 140, 141 and 142, the most representative cristobalite layers of the samples investigated after HT1 of 24 h are shown.

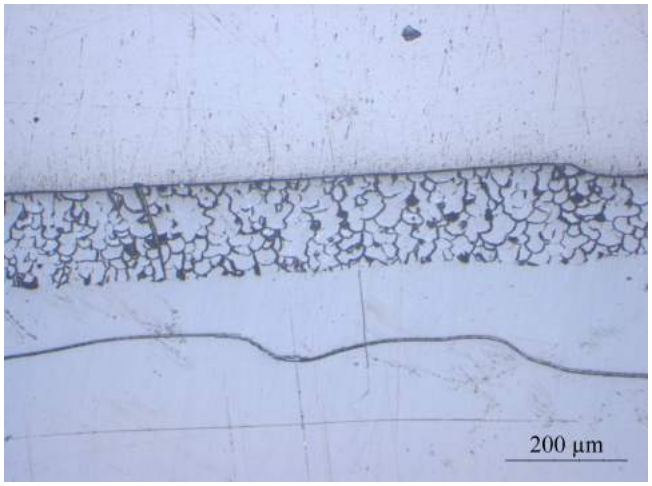

Figure 139: Cristobalite layer observed on A_n after HT1 of 24 h : Large occurrence, very homogeneous

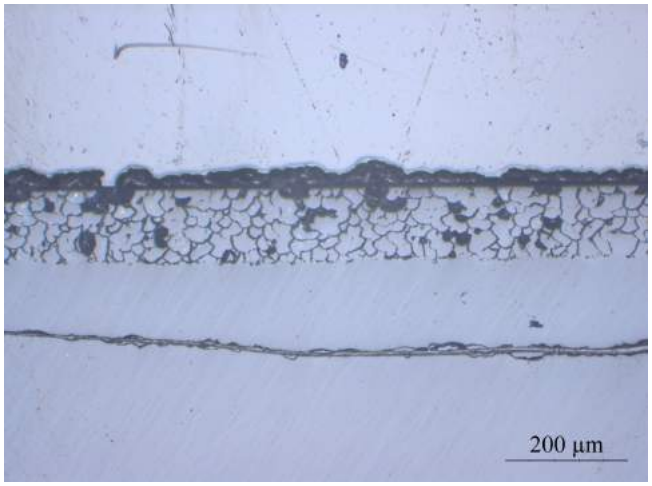

Figure 140: Cristobalite layer observed on B_n after HT1 of 24 h : Large occurrence, very homogeneous

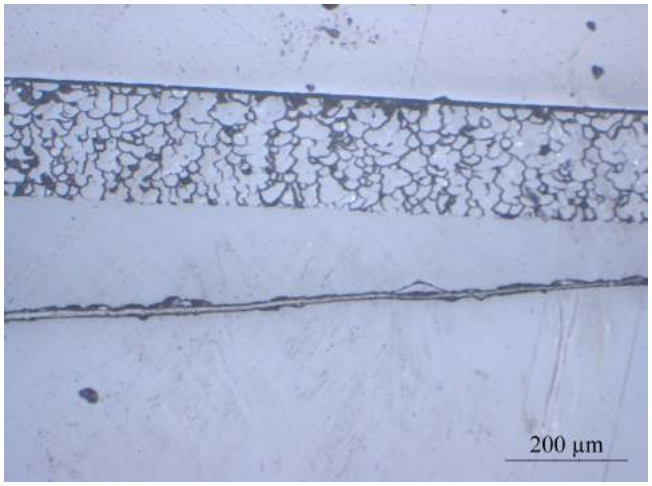

Figure 141: Cristobalite layer observed on B_{nc} after HT1 of 24 h : Large occurrence, very homogeneous

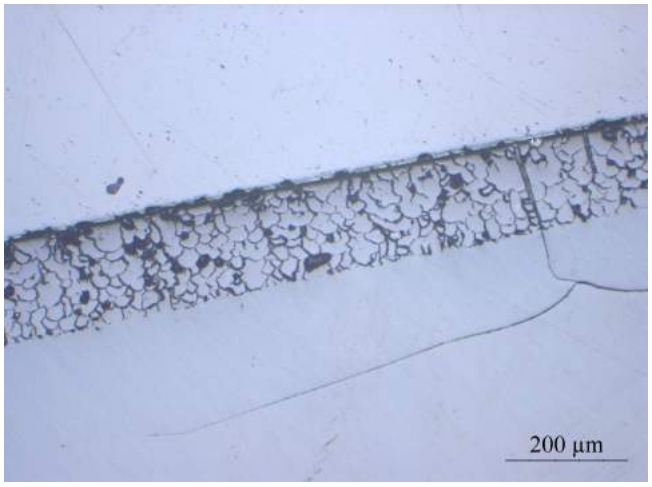

Figure 142: Cristobalite layer observed on Std_{nc} after HT1 of 24 h : Large occurrence, very homogeneous

A.5 HT2 10 h : Cristobalite layer thickness

On Figures 143, 144, 145 and 146, the most representative cristobalite layers of the samples investigated after HT2 of 10 h are shown.

Figure 143: Cristobalite layer observed on A_{nc} Piece 3 (above the melt) after HT2 of 10 h : Thin occurrence, homogeneous

Figure 144: Cristobalite layer observed on A_{nc} Piece 2 (in the melt) after HT2 of 10 h : Larger occurrence, homogeneous

Figure 145: Cristobalite layer observed on Std_{nc} Piece 3 (above the melt) after HT2 of 10 h : Very local, thin occurrence, not homogeneous at all, hard to focus on

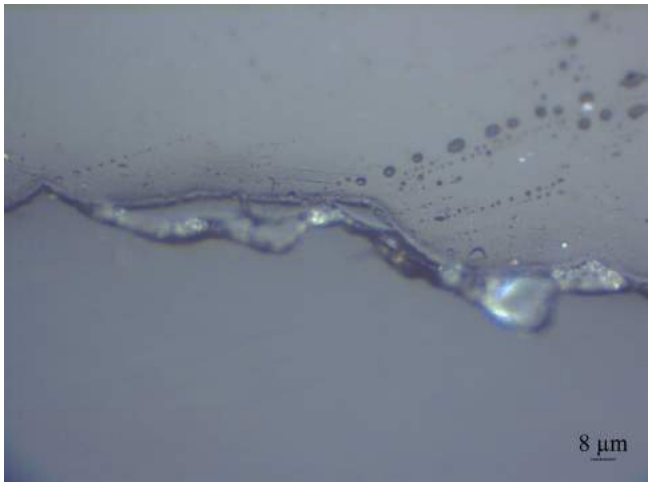

Figure 146: Cristobalite layer observed on Std_{nc} Piece 2 (in the melt) after HT2 of 10 h : Very local, thin occurrence, not homogeneous, hard to focus on

A.6 HT3 100 h : Cristobalite layer thickness

On Figures 147, 148, 149, 150 and 151, the most representative cristobalite layers of the samples investigated after HT3 of 100 h are shown.

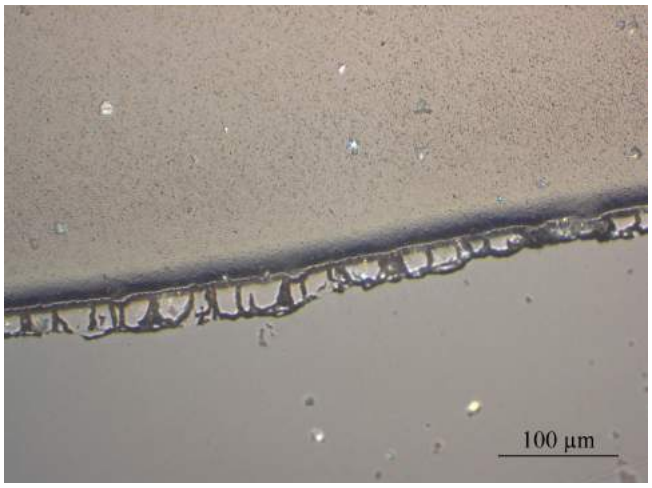

Figure 147: Cristobalite layer observed on A_u after HT3 of 100 h : Thin occurrence, homogeneous

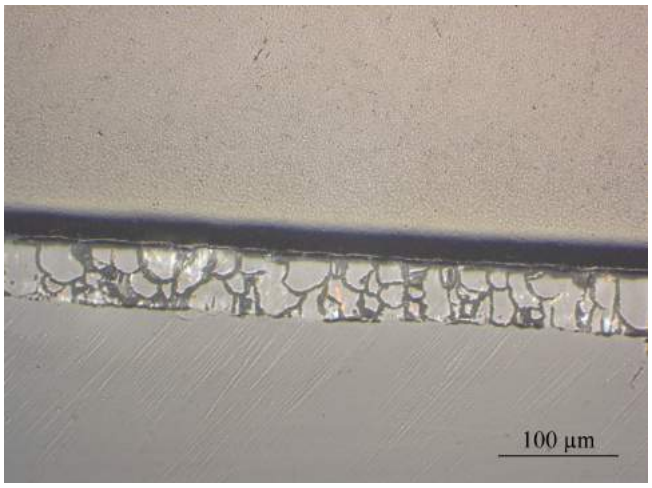

Figure 148: Cristobalite layer observed on B_u after HT3 of 100 h : Thin occurrence, very homogeneous

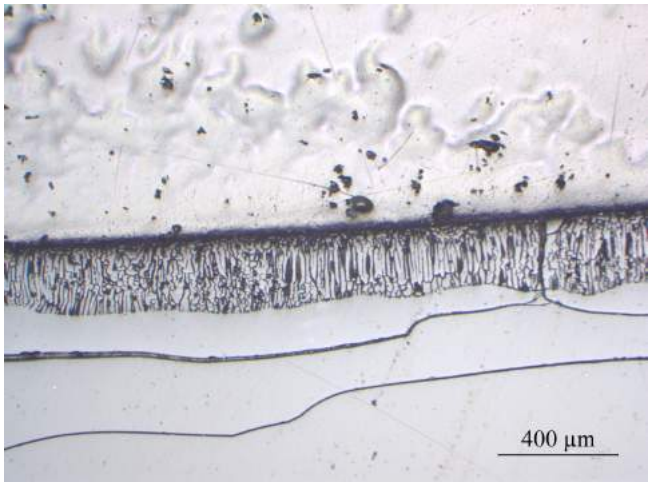

Figure 149: Cristobalite layer observed on B_{uc} after HT3 of 100 h : Large occurrence, very homogeneous and oriented

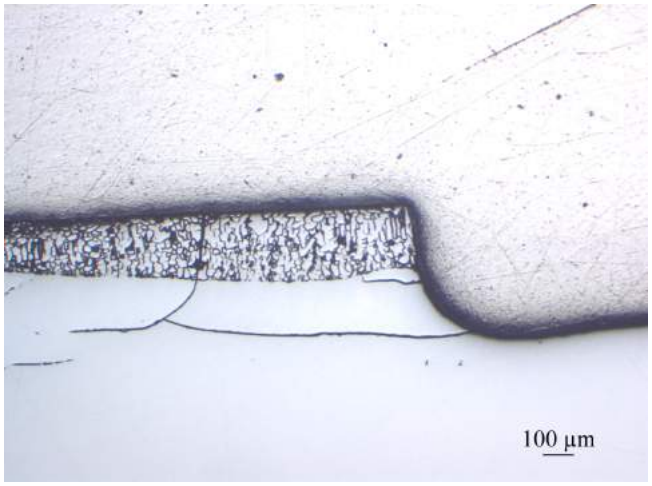

Figure 150: Cristobalite layer observed on Std_{uc} after HT3 of 100 h : Large occurrence, very homogeneous

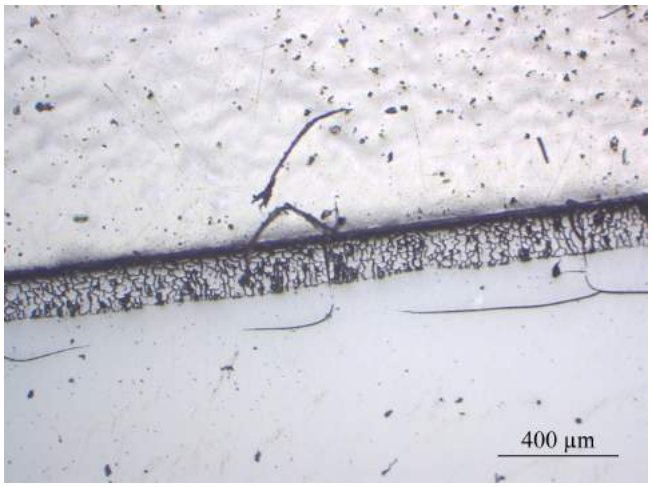

Figure 151: Cristobalite layer observed on A_{uc} after HT3 of 100 h : Large occurrence, very homogeneous